

# Sheffield Hallam University

*A study of zwitterionic adducts of TCNQ.*

BROUGHTON, Richard A.

Available from the Sheffield Hallam University Research Archive (SHURA) at:

<http://shura.shu.ac.uk/19400/>

## A Sheffield Hallam University thesis

This thesis is protected by copyright which belongs to the author.

The content must not be changed in any way or sold commercially in any format or medium without the formal permission of the author.

When referring to this work, full bibliographic details including the author, title, awarding institution and date of the thesis must be given.

Please visit <http://shura.shu.ac.uk/19400/> and <http://shura.shu.ac.uk/information.html> for further details about copyright and re-use permissions.



10483

275818

Sheffield Hallam University  
**REFERENCE ONLY**

ProQuest Number: 10694281

All rights reserved

INFORMATION TO ALL USERS

The quality of this reproduction is dependent upon the quality of the copy submitted.

In the unlikely event that the author did not send a complete manuscript and there are missing pages, these will be noted. Also, if material had to be removed, a note will indicate the deletion.



ProQuest 10694281

Published by ProQuest LLC (2017). Copyright of the Dissertation is held by the Author.

All rights reserved.

This work is protected against unauthorized copying under Title 17, United States Code  
Microform Edition © ProQuest LLC.

ProQuest LLC.  
789 East Eisenhower Parkway  
P.O. Box 1346  
Ann Arbor, MI 48106 – 1346

**A STUDY OF ZWITTERIONIC ADDUCTS OF TCNQ**

by

**RICHARD ANTHONY BROUGHTON BSc**

A thesis submitted to Sheffield Hallam University in partial fulfilment of the requirements for the Degree of Doctor of Philosophy.

Sponsoring Establishment:

Division of Applied Chemistry  
Sheffield Hallam University

Collaborating Establishment:

Health & Safety Executive

February 1993

# CONTENTS

## Synopsis

### CHAPTER 1: ELECTROACTIVE ORGANIC COMPOUNDS

1.1	Historical Introduction	1
1.2	Organic Charge-Transfer Complexes	4
1.3	Conductive Organic Charge-Transfer Complexes	6
1.3.1	Organic Metals	7
1.3.2	Organic Superconductors	12
1.3.3	Some Physical Concepts	14
1.4	Pyridinium and Quinolinium TCNQ Compounds	15
1.5	Organic Materials for Non-Linear Optics - Optical Second Harmonic Generation	23
1.6	Molecular Rectification	27
1.7	References	30

### CHAPTER 2: SYNTHESIS AND CHARACTERISATION OF R(4)Q3CNQ/R(4)P3CNQ

2.1	Experimental	34
2.1.1	Reagents	34
2.1.2	Microanalysis	34
2.1.3	Instrumentation	34
2.1.3.1	Infra Red Spectroscopy	34
2.1.3.2	Ultra Violet/Visible Spectroscopy	34
2.1.3.3	Mass Spectroscopy	36
2.1.3.4	<sup>1</sup> H nmr Spectroscopy	36
2.1.3.5	Differential Scanning Calorimetry	36
2.2	Synthesis	36
2.2.1	Synthesis of the N-alkyl-4-methyl quinolinium bromides	36
2.2.2	Synthesis of C <sub>20</sub> H <sub>41</sub> (4)Q3CNQ	37
2.2.3	Synthesis of LiTCNQ	39
2.2.4	Synthesis of Me(4)P3CNQ	39

2.3	Discussion of Synthetic Methods	41
2.4	Spectroscopic Studies of R(4)P3CNQ/R(4)Q3CNQ	51
2.4.1	Ultra Violet/Visible Spectroscopy	51
2.4.1.1	Solvatochromism in R(4)P3CNQ/R(4)Q3CNQ	61
2.4.2	Infra Red Spectroscopy Studies	65
2.4.3	Mass Spectroscopy Studies	69
2.5	Miscellaneous Studies	84
2.6	References	85

### **CHAPTER 3: LANGMUIR-BLODGETT FILMS**

3.1	Historical Introduction	86
3.2	Molecular Requirements of LB Film Forming Materials	88
3.3	Isotherm Measurement	93
3.4	Deposition and Mono/Multilayer Assembly	98
3.5	Characterisation of LB Films	101
3.6	Applications of LB Films	104
3.7	References	

### **CHAPTER 4: LANGMUIR-BLODGETT FILMS - EXPERIMENTAL**

4.1	The Joyce Loebel Monolayer Coating Unit	111
4.2	The Compression System	111
4.3	Surface Pressure Measurement	113
4.4	Trough Operation	117
4.4.1	Cleanliness	117
4.4.2	Trough Calibration	118
4.4.2.1	Calibration of Surface Area	118
4.4.2.2	Calibration of Surface Pressure	118
4.5	The Subphase	119
4.6	Subphase Surface Cleaning	119
4.7	Monolayer Material Preparation and Spreading	120

4.8	Temperature of Subphase	121
4.9	Compression of the Monolayer	121
4.10	Control of Surface Pressure	122
4.11	Transfer of Monolayer	122
4.12	References	126

## **CHAPTER 5: LANGMUIR-BLODGETT FILMS - RESULTS AND DISCUSSION**

5.1	Langmuir Film Studies on R(4)Q3CNQ	127
5.2	Langmuir-Blodgett Films of R(4)Q3CNQ	144
5.3	Characterisation of LB Films of R(4)Q3CNQ	145
5.4	General Discussion	164
5.5	Change in Film Structure and Absorbance Bands with Time	188
5.6	References	

### **Acknowledgements**

## SYNOPSIS

Chapter 1 gives a general introduction to the field of electroactive organic compounds. The historical development of the field is outlined and then the more specific areas are described in detail. The properties of picolinium and quinolinium TCNQ salts are introduced and the extension of this to the molecules studied in this work developed. Two current areas of interest - second harmonic generation and molecular rectification - are then reviewed and the potential applications of the materials studied in this work highlighted.

Chapter 2 discusses the synthesis of the materials and contrasts the two methods used. A discussion of the reaction mechanisms is given, as well as techniques for monitoring the course of reaction. The characterisation of the materials by a range of spectroscopic techniques is described. The solvatochromic behaviour of the materials is shown to conform with theoretical predictions and the observed mass spectra are shown to have some diagnostic importance.

Chapter 3 gives a general introduction to Langmuir-Blodgett (LB) films starting once again from a historical perspective. The molecular requirements of suitable materials together with pressure/area per molecule measurements and the deposition process are described. The various methods available for the characterisation of LB films are described, as well as the many potential applications proposed within the general field of molecular electronics.

Chapter 4 describes the experimental methods employed when using the Joyce Loebel Langmuir Trough. The importance of parameters such as cleanliness, sample purity and instrument calibration is stressed.

Chapter 5 discusses the behaviour of the materials on the subphase and their resultant fabrication as LB films. The structure of the films is shown to be dependent on the hydrophobic chain length with a definite change in film structure occurring at a 15 carbon chain. Reasons for this are proposed and calculations of chromophore/hydrocarbon chain tilt angles on the basis of the proposed structure are given. A time dependent change in film structure is also discussed, as well as suggestions for future work.

## 1.1 Historical Introduction

The electrical conductivity of most organic materials, when purified, is extremely low ( $\sigma_{\pi} < 10^{-10} \text{ Scm}^{-1}$ ) at room temperature. It was suggested at the turn of the century<sup>1,2</sup> that organic solids may exhibit conductivities comparable with metals. Indeed, today there are two classes of organic solids - polymeric hydrocarbons and charge-transfer complexes - of which certain members may be referred to as organic metals.

Strong  $\pi$ -molecular donor (D) and acceptor (A) molecules can react to produce ion-radicals salts ( $X^+A^-$  or  $D^+X^-$ ), where 'X' is an appropriate anion or cation, or charge-transfer compounds (DA and  $D^+A^-$ ). Such compounds may in some instances exhibit higher conductivities than is normally found in organic materials. A stable charge-transfer complex is formed, as the name implies, by the transfer of an electron from a donor to an acceptor to produce an ionic crystal in which both the anion and the cation are complex chemical units in their own right. The more commonly encountered donors are amines, electron rich alkenes, heterocycles and simple alkali metals. Common electron acceptors include quinones, electron deficient alkenes and heterocycles and the halogen atoms. Examination of the crystal structure of such compounds show that the donor and acceptor molecules stack face-to-face alternately (fig 1.1).

D	A	D	A
A	D	A	D
D	A	D	A
A	D	A	D

**Fig 1.1 Mixed donor-acceptor stacks**

For a more detailed comprehensive review of organic charge-transfer complexes the reader is referred to the excellent text by Foster<sup>3</sup>. In the early 1960's, Melby and his co-workers<sup>4</sup> at duPont reported the synthesis of 7,7,8,8 - tetracyano-p-quinodimethane (TCNQ -fig 1.2), a new, powerful organic electron acceptor.

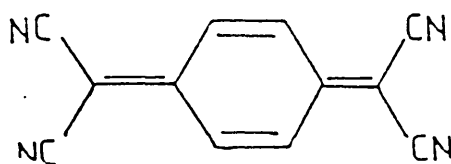


**Fig 1.2 7,7,8,8 - tetracyano-p-quinodimethane (TCNQ)**

A number of complexes were produced between TCNQ and various donors and many were found to be semi conductors ( $\sigma_{\pi} \approx 10^{-5} \text{ Scm}^{-1}$ ), and indeed the quinolinium-TCNQ complex was the best organic conductor known at the time.

This large improvement in conductivity prompted renewed interest in this field, focusing primarily on TCNQ salts.<sup>5</sup> It was soon realised that high conductivity was associated with segregated stacks of donor and acceptor molecules once again packing face-to-face (fig 1.3). The resulting charge transfer and  $\pi$ -overlap between molecules is very strong and thus unpaired electrons are partially delocalised along

the one dimensional stacks. The resultant conduction is therefore highly anisotropic.

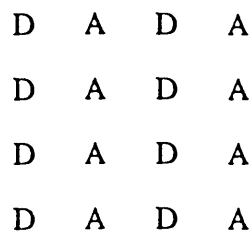


**Fig 1.3 Segregated donor and acceptor stacks**

In 1970,<sup>6</sup> a powerful new donor, tetrathiofulvalene (TTF) (fig 1.4) was synthesised and three years later its TCNQ salt was prepared<sup>7</sup> which was found to be highly conducting at room temperature - ( $\sigma_{rt} \approx 500 \text{ Scm}^{-1}$ )

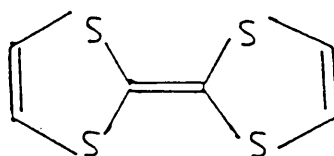


**Fig 1.4 Tetrathiofulvalene (TTF)**

This was the first organic metal - a dramatic increase in conductivity occurring below room temperature, rising as high as  $10^4 \text{ Scm}^{-1}$  at 60K. Below this temperature, a metal-insulator transition occurs, which can be controlled to some extent by the chemical structure.

During this period there was also extensive interest in polymeric hydrocarbons, with extensive  $\pi$ -electron delocalisation leading to a weak conduction band.

Much attention has been focused on a polyacetylene which in its 'pure state' is an insulator ( $\sigma_{rt} \approx 10^{-9} \text{ Scm}^{-1}$ ) due to a relatively large band gap. Heeger and co-workers<sup>8</sup> showed that doping with strong reducing or oxidising agents can increase the conductivity dramatically ( $\sigma_{rt} \approx 500 \text{ Scm}^{-1}$ , for example). Two other classes of one dimensional conductors include polymeric materials of the main group elements, eg  $(\text{SN})_x^9$  and linear chain transition metal compounds<sup>10</sup> where intra chain overlap may include the ligand  $\pi$ -system. The remainder of this introduction will not concern itself with polymeric materials any further; rather it will concentrate upon organic charge transfer salts based on TCNQ.

## 1.2 Organic charge - transfer complexes<sup>3</sup>

The complex formed between iodine and benzene<sup>11</sup> was one of the earliest charge transfer complexes on which much work was carried out. As is typical of such complexes, the ultraviolet/visible (uv/vis) spectrum showed features characteristic of neither the solute nor the solvent. Rather, features characteristic of some form of complex between the two was observed. The explanation of this observation led to an extension of Lewis acid-base theory and thus explanations of many of the phenomena associated with molecular complexes were forthcoming; for example, the very intense absorption bands in the uv/vis region of the spectrum.

In the early 1950's,<sup>12, 13</sup> Mulliken published a series of papers in which he described electron donor-acceptor complexes. By definition, the donor (D) possesses a HOMO (Highest Occupied Molecular Orbital) and the acceptor (A) a LUMO (Lowest Unoccupied Molecular Orbital). From this, therefore, charge

transfer occurs between the HOMO of the donor and the LUMO of the acceptor, as the HOMO is of high energy and the LUMO low. The bonding between the D and A was described<sup>14</sup> by the following wave function:

$$\psi_N(A,D) = a \psi_0(A,D) + b \psi_1(A^-D^+) \quad \text{Eq (1)}$$

where 'a' and 'b' are small integers, and  $a > b$ ;  $\psi_0$  is the "no-bond" contribution and  $\psi_1$  a dative bonding contribution. Thus,  $\psi_N(A,D)$  corresponds to the wave function which adequately describes the resultant combination of two extreme resonance forms. Eq1 also shows that, while the degree to which charge transfer occurs may influence the nature of the complex, it does not dictate the bonding within that complex.

For any electron transfer to take place, the energy levels of the donor and acceptor need to be matched. In solution, this can be achieved by the reorientation of the solvent around both the donor and acceptor, and in the solid state by the reorientation and rotation of bonds. Thus, the energy barrier to electron transfer is the summation of these effects.

The energy of the transition from the donor to the acceptor is dependent on the ionisation energy of the donor ( $I_D$ ) and the electron affinity of the acceptor ( $E_A$ ). Very simply, if a strong donor is in close proximity to a strong acceptor, the energy of the charge transfer is small, the ground state is for all intents and purposes ionic and essentially 100% charge transfer occurs. For weak donors and weak acceptors, the converse is true - the energy of charge transfer is large, the ground state is neutral and the resultant degree of charge transfer is essentially zero.

It has been shown that, if the energy of charge transfer is small (and positive), then partial charge transfer occurs, and the resultant conductivity is high. The reason for this shall be discussed in more detail in subsequent sections.

### 1.3 Conductive Organic Charge-Transfer Complexes<sup>15</sup>

Homomolecular organic materials have extremely low electrical conductivities. At the very best they are wide band-gap semi conductors ( $\sigma_{rt} \approx 10^{-9}$  to  $10^{-14}$  Scm<sup>-1</sup>), though the vast majority are insulators. As was mentioned earlier, the idea of highly conductive organic materials was first suggested many years ago, but only recently has research effort been rewarded in this field. This was partly due to development of the solid state techniques used to study inorganic semiconductors. The realisation that the highly conductive materials were generally charge transfer complexes, coupled with the synthesis of TCNQ at duPont led to an upsurge in interest throughout the 1960's and 70's.

TCNQ is prepared, in two stages, by the condensation of cyclohexane -1,4-dione with malonitrile followed by oxidation in a single step (fig 1.5).

TCNQ readily undergoes a one electron reduction and the resultant anion forms a variety of charge transfer complexes and radical anion salts with suitable donors.<sup>16</sup> For example, stable complexes are produced with quaternary quinolinium and picolinium cations, and these shall be discussed in more detail later. A wealth of structural data has been obtained on TCNQ complexes, and the conductive, charge-transfer species have been shown to crystallise in segregated stacks with the conductivity greatest in the stacking direction. In this structure, the predominant overlap is between molecules of the same type and thus orbitals of similar energy.

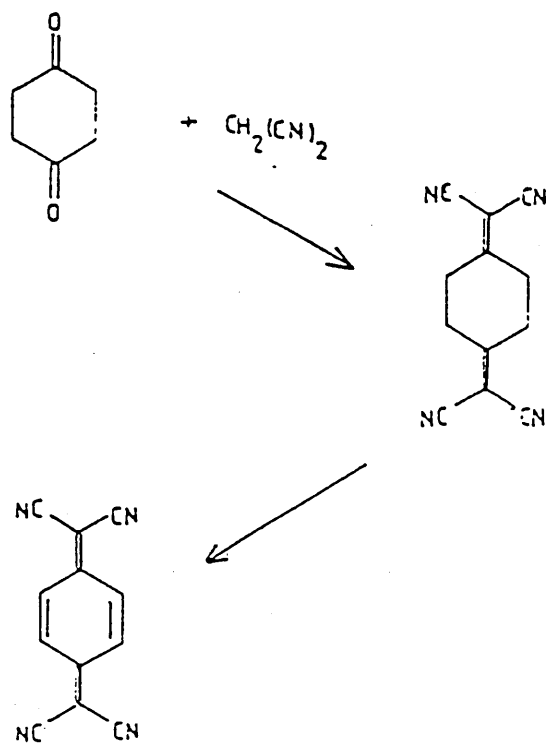


Fig 1.5 The 2-step synthesis of TCNQ

This structure is much more efficient at producing bands than is overlap between different molecules. With the realisation that the TTF - TCNQ complex exhibited metallic conductivity,<sup>7</sup> much work focused on the search for new organic metals and an understanding of their physical properties.

### 1.3.1 Organic Metals<sup>17</sup>

The TTF-TCNQ system has been extensively studied for a number of reasons including:

- i) it is relatively straight-forward to grow good-sized, robust, single crystals.

- ii) its properties are essentially characteristic of the class of organic metals as a whole.

As has already been mentioned, the crystal structure of TTF-TCNQ showed segregated stacks of donor and acceptor molecules, uniformly spaced and interlocking<sup>18</sup>(fig 1.6). It can be seen that, within such stacks, the donor and acceptor molecules do not sit directly on top of each other, rather there is a sideways displacement which leads to a "ring-double bond overlap", in which the exocyclic C=C bond lies above the ring system of the molecule next to it in the stack.

On cooling, the conductivity of the system steadily increases from  $500 \text{ Scm}^{-1}$  at 293K to in excess of  $10^4 \text{ Scm}^{-1}$  at 59K. However, on cooling the system further, three successive phase changes occur, at 59K, 47K and 38K. Eventually, an insulating state is produced with three dimensional order. The many studies that have been carried out on the system interpret the phase transition as a Pierels distortion<sup>19,20</sup>. This is expanded on in Section 1.3.3, though essentially, the Pierels theorem states that any one-dimensional system will become unstable with respect to lattice distortions and long-range order cannot be maintained. Importantly, the period of such lattice distortions is related to the number of electrons in the band and calculations based on this show that partial charge transfer occurs from donor to acceptor, resulting in 0.59 electrons in the TCNQ bands. Hence, both stacks are partially filled and both stacks can contribute to the conductivity.

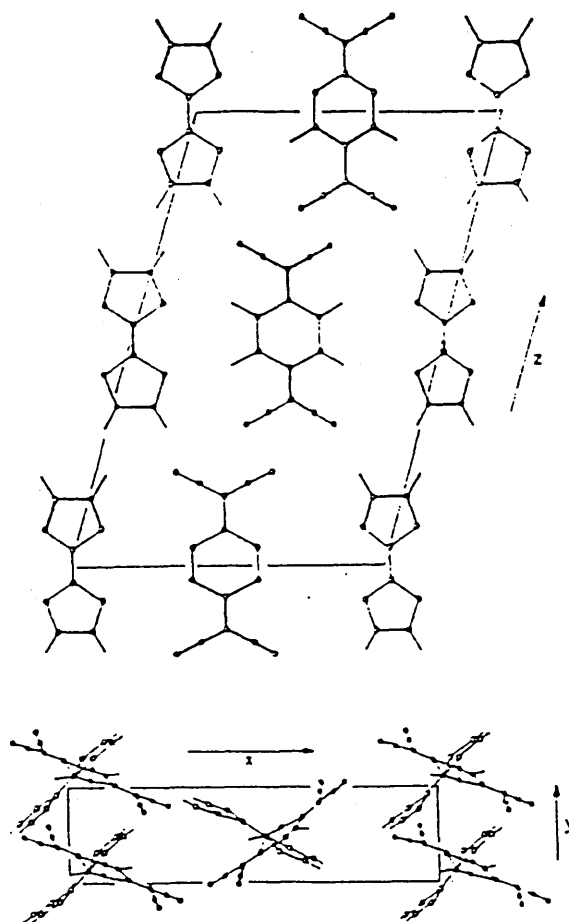


**Figure 1.6** The crystal structure of TTF-TCNQ (from ref 18)  
 The segregated stacks and "ring-double bond" overlap  
 can be seen

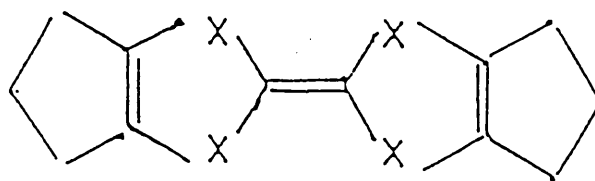
It was soon clear that TTF and TCNQ had certain properties that made them unique amongst the other donor and acceptor molecules available at the time. The ionisation potential and electron affinities were very similar, a condition which was previously shown to favour partial charge transfer and consequent high electrical conductivity. They are planar and, with point group  $D_{2h}$ , have a high degree of symmetry. The  $\pi$ -delocalisation extends throughout the molecule and both are of similar size.

Tremendous effort has gone into the synthesis of new donors with a view to testing the applicability of these factors and also with the ultimate aim of stabilising the metallic state and producing super-conductivity. Most of the synthetic work has concentrated on the search for derivatives of the 1,3-dithiole ring system of TTF. Examples are shown in fig 1.7.

Notice there has been extension of both the  $\sigma$ <sup>21</sup> and  $\pi$ -bond<sup>22</sup> framework. Successful replacement of the sulphur atoms by selenium atoms<sup>23</sup> and tellurium atoms<sup>24</sup> has also been achieved.

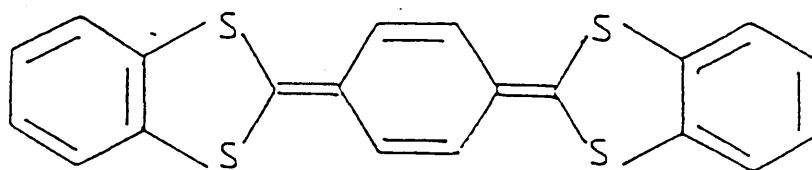
The synthesis of new acceptors has been the subject of very much fewer publications, presumably because the chemistry of producing new TCNQ derivatives is very demanding. However, a series of three early papers<sup>25-27</sup> reported the synthesis of 21 derivatives and also the results of studies on some of the complexes with TTF. From this work several general points can be made and these can be illustrated by a comparison of two salts, HMTSF-TCNQ and HMTSF-TCNQF<sub>4</sub> (the structure of TCNQF<sub>4</sub> is shown in figure 1.8, HMTSF is the selenium analogue of HMTTF shown in fig 1.7).

Fig 1.7 Some derivatives of TTF

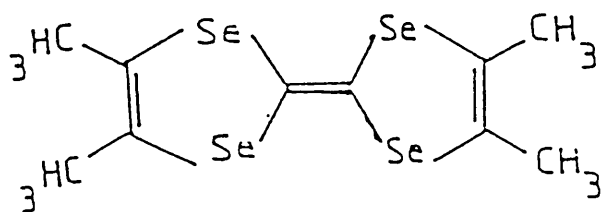


X = S: Hexamethylenetetrathiofulvalene (HMTTF)

X = Te: HexamethylenetetraTellurafulvalene (HMTTeF)



Cyclohexa-2,5-diene-1,4-diylidene-bis-1,3-benzodithiole



Tetramethyltetraselenafulvalene (TMTSF)

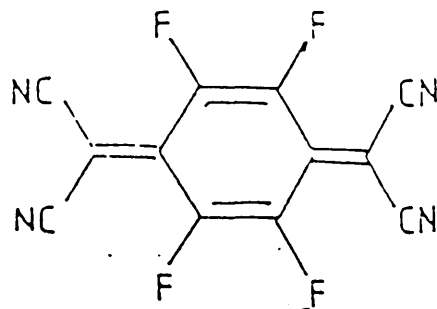


Figure 1.8 TCNQF<sub>4</sub>

HMTSF-TCNQ is an extremely conductive organic charge transfer complex ( $\sigma_{rt} \approx 1500 \text{ Scm}^{-1}$ ) whilst HMTSF-TCNQF<sub>4</sub> has a conductivity many orders of magnitude smaller ( $\sigma_{rt} \approx 10^{-6} \text{ Scm}^{-1}$ ). The key to this lies in the degree of charge transfer. In TCNQ-HMTSF there is partial charge transfer whilst in TCNQF<sub>4</sub>-HMTSF, charge transfer is complete because TCNQF<sub>4</sub> is a much stronger electron acceptor due to the presence of the extra highly electronegative fluorine atoms. This rule has found to be quite general; substitution of the quinoid ring of TCNQ reduces the conductivity of any resulting complex relative to TCNQ itself, with the reduction being particularly marked if the substitution produces a stronger electron acceptor.

In such organic conductors the substitution of selenium for sulphur stabilises the metallic state and the donor stack dominates the transport properties due to the presence of  $d'$ -orbitals.

### 1.3.2 Organic Superconductors

In 1978, the complex TMTSF-2,5 - dimethyl TCNQ was found to conduct electricity under pressure down to 1K; at ambient pressure the now familiar metal-insulator transition occurs at 42K<sup>28, 29</sup>. It was proposed that the conductive state may be stabilised due to the superconducting pairing of electron states. This theory promoted the synthesis of many cation radical salts of the form (TMTSF)<sub>2</sub> X where

'X' is an inorganic anion such as  $\text{PF}_6$ . In 1980 it was shown by Bechgaard<sup>30</sup> that  $(\text{TMTSF})_2 \text{PF}_6$  exhibited superconductivity at 1K under a pressure of 12000 atmospheres. Indeed, many members of the  $(\text{TMTSF})_2 \text{X}$  series exhibit superconductivity, with, for example,  $(\text{TMTSF})_2 \text{ClO}_4$  showing superconductivity at ambient pressure down to 1.4K.

The theory of metallic superconductivity [the well known BCS theory] was first formulated in 1957<sup>31</sup> and was based on the ordered motion of electron pairs - Cooper pairs - and not individual valence electrons. Evidence now suggests that for salts of the  $(\text{TMTSF})_2 \text{X}$  family, Cooper pairing does indeed occur<sup>32</sup>. This pairing is localised along the donor chains - often at temperatures up to 30K. This temperature is well above the onset of bulk superconductivity.

One particularly striking feature of the  $(\text{TMTSF})_2 \text{X}$  salts is the zig-zag stacking arrangement of TMTSF molecules into sheets which are then separated by anions. There are also both inter and intra stack contacts of the selenium atoms<sup>33, 34</sup>, the result of which is a large, two- dimensional sheet of molecules.

This is necessarily only a brief introduction to the field of organic superconductors of which a wealth of data now exists. In recent years, this class of compounds has really been superceded, to some extent, by the ceramic superconductors. For example, claims of superconductivity at temperatures as high as 60K have been made for  $\text{La}_{2-x}\text{Sr}_x\text{CaCu}_2\text{O}_6$ <sup>35</sup>.

### 1.3.3 Some Physical Concepts

The structure of highly conducting organic charge-transfer complexes shown in fig 1.3 leads to the proposal that such complexes are one-dimensional molecular arrays. They consequently have more than their complement of valence electrons required for bonding.

Theoretically, it can be considered that such extra electrons partially fill a conduction band where the interaction between neighbours determines the bandwidth. Pierels,<sup>19</sup> in a classic text, pointed out that such a "quasi" one-dimensional metallic system could not maintain long range order at low temperatures and would become unstable with respect to lattice distortions. The period of the lattice distortion can be related to the number of electrons in the band. Very simply, the conducting chain becomes stretched in one region and contracted in another, thus localising the conducting electrons. The bonding between atoms is much stronger where they are most closely spaced, and the electrons have a lower energy in these regions. There is consequently a localised concentration of electrons along the chain known as a charge density wave which, if in phase with a periodic lattice distortion, results in an energy gap and an insulating or, at best, semi-conductive state. This is a very simple description of the Pierels Theorem.

However, charge-density wave-phonon interactions (ie charge-density waves coupled to underlying lattice vibrations) could enable the wave to travel freely through the crystal generating Fröhlich Superconductivity in a mechanism different to BCS pairing. If the number of electrons in the chain is commensurate with the number of lattice sites, then a metal-insulator transition occurs due to the high potential energy needed to be overcome to enable the electrons to move to new equilibrium positions. If the number of electrons is incommensurate with the lattice

then they will be free to move, as the charge-density wave is not locked to the lattice. Thus, we have a mechanism for high conductivity and for a truly incommensurate system Fröhlich superconductivity would occur.

Electron spin density distortion along a chain provide another possible instability for one-dimensional conductors. Electron spin density may distort along the chain producing in extreme cases an anti-ferromagnetic alignment of spins which can preclude superconductivity. Interactions in one- or two-dimensions are suggested to prevent the onset of spin density waves, particularly in an analysis of the Bechgaard salts.

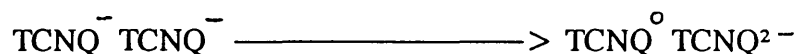
#### 1.4 Pyridinium and Quinolinium TCNQ Compounds

The work documented in this thesis involves the synthesis and preliminary characterisation of  $\pi$ -bonded pyridinium and quinolinium TCNQ systems. The published literature on the properties and structure of radical anion salts of these cations is now discussed.

Melby et al<sup>16</sup> published the first examples of a complex between TCNQ and a nitrogen heterocycle in 1962 - the complex produced when the lithium salt of TCNQ was allowed to react with N-methylquinolinium iodide. Lithium TCNQ is very soluble and is often used in the synthesis of TCNQ complexes for this reason. Along with similar salts of pyridinium cations, the electrical conductivities were very low ( $\sigma_{rt} \approx 10^{-7} \text{ Scm}^{-1}$ ).

The substitution of the pyridinium ring<sup>36</sup> by various alkyl groups did not markedly improve conductivity - these complexes had conductivities in the range  $10^{-6} \text{ Scm}^{-1}$  to  $10^{-8} \text{ Scm}^{-1}$ .

The conduction path in such simple TCNQ salts is dependent on the excitation of an electron from one ionic state to another.



Notice that in this mechanism we are placing two conduction electrons on the same TCNQ site.

An estimation of the band gap can be made by consideration of the Coulombic repulsion energy (U) between electrons on adjacent sites.

So:

$$U = \frac{e^2}{4\pi\epsilon_0 d} \quad \text{Eq.(2)}$$

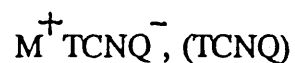
Where 'e' is the electronic charge; ' $\epsilon_0$ ' the relative permittivity of free space and 'd' the charge separation measured in Å.

Thus: for two electrons

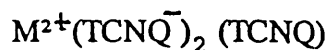
$$U = \frac{14.4}{d} \text{ eV} \quad \text{Eq.(3)}$$

The distance between exocyclic carbon atoms in TCNQ is 5.5Å. The intermolecular interplanar spacing is 3.3Å and the intermolecular distance is 9Å. Thus for two electrons on the same site the repulsion energy is calculated as 2.6eV, and for adjacent sites 1.6eV, if we assume that the conduction electrons localise on the C(CN)<sub>2</sub> groups at opposite ends of the molecule. Thus, the electrical conductivity is low, as placing two electrons on the same TCNQ site is energetically unfavourable.

More complex salts of TCNQ involve various molar proportions of neutral TCNQ with TCNQ<sup>-</sup> and the cation. For example:



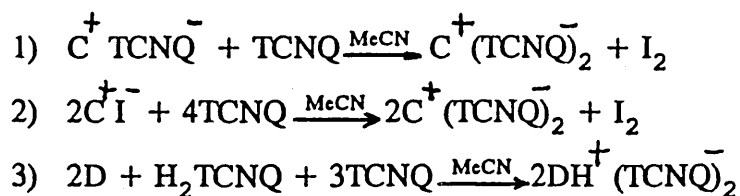
or



The electrical conductivities of complexes of this type are many orders of magnitude larger than those of simple salts, for example -  $10^{-4}$  and  $10^{-1} \text{ Scm}^{-1}$  at  $300\text{K}^{37}$ . This is due to the presence of neutral TCNQ molecules within the chains. In these cases the necessity of placing two conduction electrons on the same site is removed and a corresponding increase in electrical conductivity is observed.

Although the conductivities of simple TCNQ salts is low the long chain N-alkylpyridinium TCNQ salts have been studied as Langmuir-Blodgett films (see Chapter 3) by Barraud and his co-workers<sup>38</sup> in France. Their conductivity has been reported, and the above material has been exposed to gases such as  $\text{Cl}_2$  and  $\text{NO}$ , and its response to these discussed<sup>39</sup>.

Complex salts of quinolinium and pyridinium cations were originally prepared by one of three methods:<sup>17</sup>



Where C is an organic, organometallic or inorganic cation and 'D' is a nitrogen heterocycle.

Addition and substitution reactions of TCNQ have been documented for many years<sup>40</sup>. Substitution at either, or both, of the cyano groups occurs readily with certain amines<sup>41</sup> (fig 1.9).

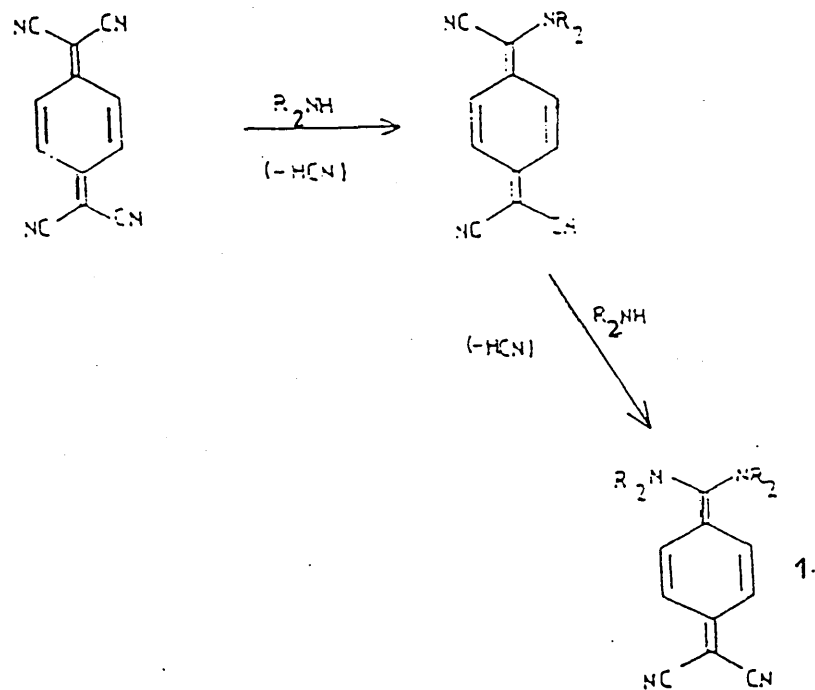
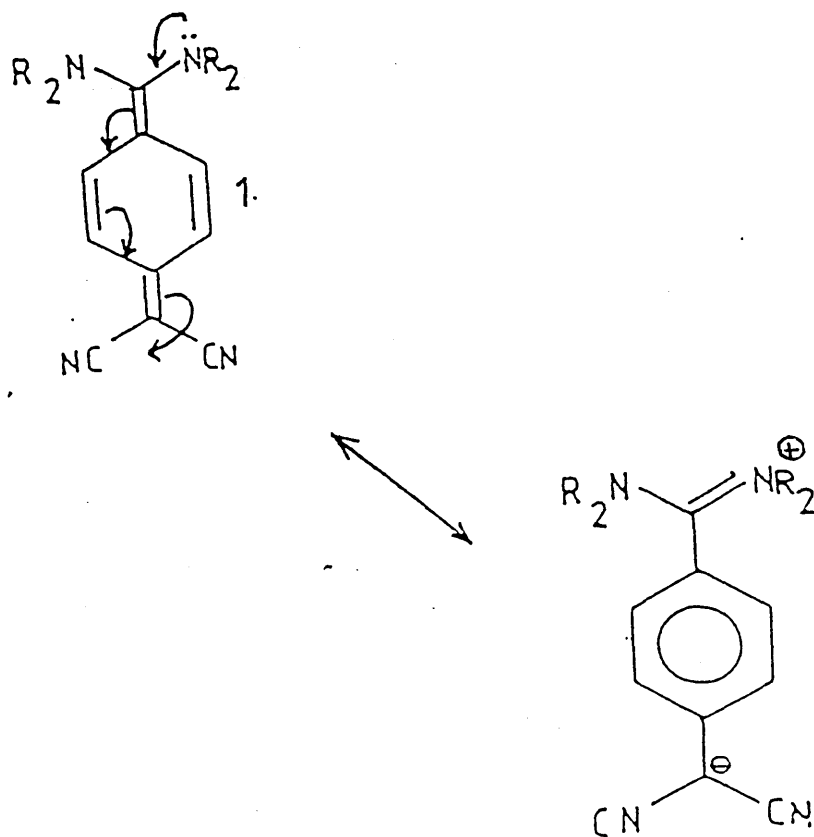


Fig 1.9 Substitution of cyano groups in TCNQ by secondary amines

The structure (1) can be represented by the two resonance structures shown in figure 1.10.



**Fig 1.10 Zwitterionic canonical forms of amino adduct (1)**

The infra-red spectrum of this adduct shows two distinct nitrile stretching frequencies at  $2175\text{ cm}^{-1}$  and  $2130\text{ cm}^{-1}$ , characteristic of a monosubstituted malonitrile anion. The uv/vis spectra of the same species in acetonitrile showed a broad band which was attributed to an intramolecular charge transfer from the donor to the acceptor. In 1984<sup>42</sup>, the zwitterionic donor- $\pi$ -acceptor adduct Z-

(N-methyl-2-pyridinium)- $\alpha$ -cyano-4-styryldicyanomethide (trivial name picolyl-tricyanoquinodimethane) was synthesised in these laboratories in Sheffield. Its structure is shown in fig 1.11 and its molecular geometry in fig 1.12. The bond length between C12 and C15 clearly shows this is a double bond whilst the benzenoid nature of the two rings is also confirmed by bond measurements.

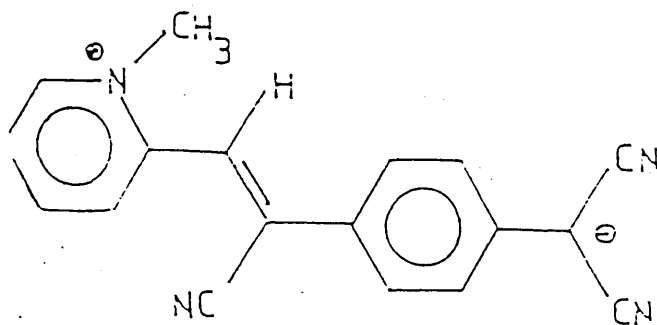


**Fig 1.11 Picolyl-tricyanoquinodimethane**

The molecule is not planar, the pyridinium ring is twisted from the benzenoid ring of TCNQ by  $10.13^\circ$ . The uv/vis spectrum, in acetonitrile, does not show the typical TCNQ band characteristic of the anion radical; rather, a broad band is present, centred on 592 nm. It has been suggested that this is an intramolecular charge transfer transition. Fuller spectroscopic studies of this and related molecules are discussed in more detail in Chapter 2.

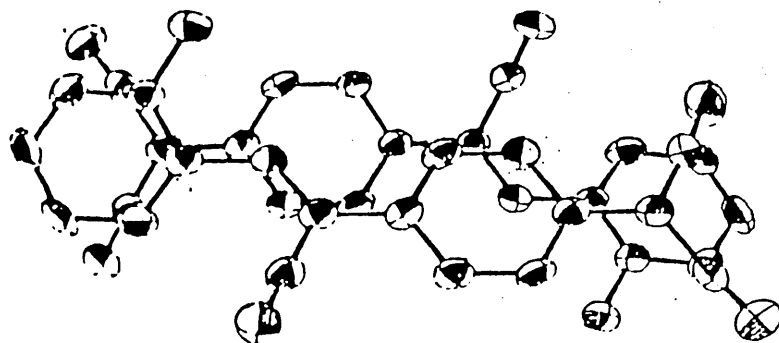


**Fig 1.12** Crystal structure of Picolyl-tricyanoquinodimethane

The charge distribution was shown to be typical of a zwitterion by atom-in-molecule calculations carried out on the structure. Evidence for such a zwitterionic structure was also obtained from the very large computed dipole moment of 26.16D. The molecule has also been studied in its solid state by polarised reflection spectroscopy<sup>43</sup>. An intramolecular charge transition was observed at 537 nm. The stacking of the molecules in the solid state is shown in fig 1.13, clearly showing a head-to-tail arrangement.

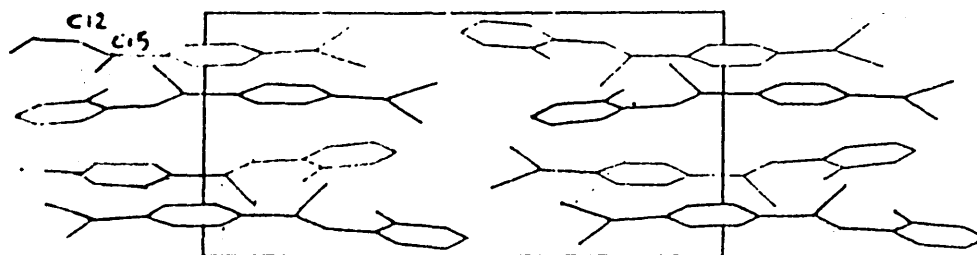


**Fig 1.13** Overlap of two picolyl-tricyanoquinodimethane molecules stacked along the b-axis

Such a head-to-tail arrangement has recently been observed by Miller and Calabrese<sup>44</sup> in the zwitterionic adduct of tetrafluoro TCNQ and tetramethylphenylenediamine,(TMPD) whose structure is shown in fig 1.14.

The structure of such zwitterionic donor- $\pi$ -acceptor adducts opens the door on potential applications in a number of exciting new fields and these are discussed.

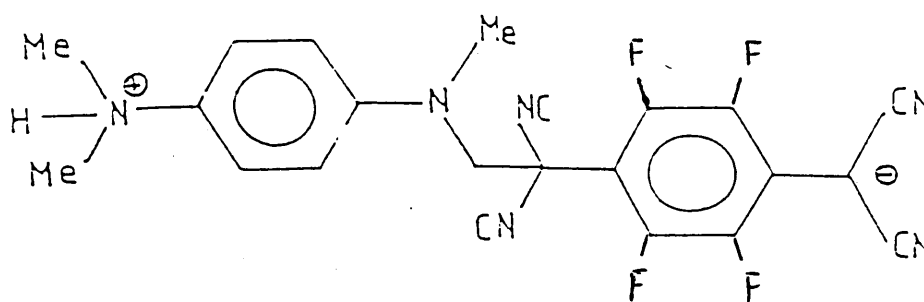


Fig 1.14 The structure of the TMPD-TCNQ zwitterionic adduct

### 1.5 Organic Materials for Non-Linear Optics - Optical Second Harmonic Generation<sup>45</sup>

Traditionally, optics and electronics have relied on inorganic compounds for their various components, though in the future they will no doubt benefit from the vast range of organic materials already known and the many more waiting to be synthesised.

Consider the change in dipole moment which occurs between the ground state  $\mu_g$  and an excited state  $\mu_e$  upon interaction of an electric field - say the electrical component of electromagnetic radiation - with a single molecule. This can be expressed as a power series of the electric field:

$$\Delta\mu = \mu_e - \mu_g = \alpha E + \beta EE + \gamma EEE + \dots \quad \text{Eq (4)}$$

or 
$$P = P_0 + X^{(1)}E + X^{(2)}EE + X^{(3)}EEE + \dots \quad \text{Eq (5)}$$

The coefficient ' $\alpha$ ' is the well known linear polarisability, ' $\beta$ ' and ' $\gamma$ ' are the quadratic and cubic hyperpolarisabilities respectively. As the hyperpolarisability coefficients are tensor quantities, they are symmetry dependent and it can be shown that odd-order coefficients are non-zero for all molecules, but even-order coefficients, such as  $\beta$  are zero for centrosymmetric molecules. The quadratic term is responsible for second harmonic generation (SHG). Note that equation (4) is, in effect, identical to (5) except that (5) refers to the macroscopic polarizability such as may occur in a crystal.

As only about 20% of organic molecules have a non-centro-symmetric structure<sup>46</sup>, so molecules with large predicted values of  $\beta$  may exhibit no SHG.

The Langmuir-Blodgett technique - which will be discussed in detail later - enables us to orientate molecules in a non-centrosymmetric fashion and, indeed, SHG has been observed for such a system<sup>47</sup>.

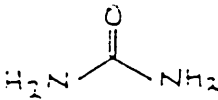
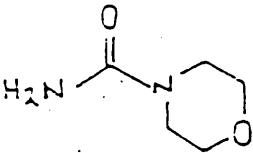
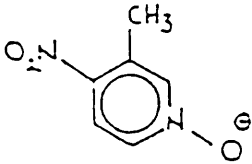
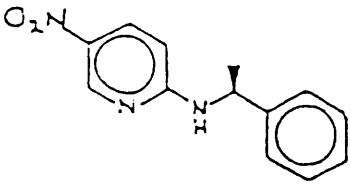
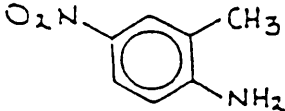
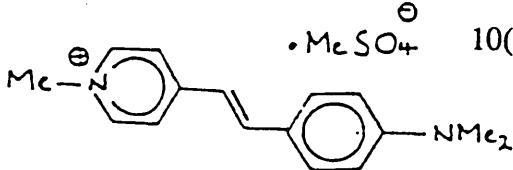
What, therefore are the structural features that would lead us to predict a frequency doubling effect? Consider the selection of molecules shown in table 1. The bracketed numbers give the enhancements in efficiency one might expect if these molecules were optimally aligned in a crystal. The object of the table is not to give any hard and fast data on SHG in organic materials, but just to enable certain trends and points to be noted.

First, active molecules are conjugated and secondly they are polarised, ie they contain both donor and acceptor substituents. Obviously, the presence of a conjugated and polarised system is not mandatory, though materials which are the most efficient appear to exhibit these two criteria.

Thus, on the basis of their determined structure the highly conjugated, donor-acceptor zwitterionic adducts studied in this work may exhibit second harmonic generation if suitably aligned.

TABLE 1

TYPICAL ORGANIC MATERIALS FOR OPTICAL SECOND HARMONIC GENERATION (from Ref 54)

	Structure	Efficiency	$\beta$ ( $\times 10^{-30}$ esu)	Ref
1		1.0(x2.5)	0.45	48
2		0.0	-	49
3		13(x4)	5	50
4		25	-	51
5		22	42	52
6		10(x6.7)	220	53

## 1.6 Molecular Rectification

The construction of a simple, electronic rectifier based on the use of a single organic molecule was discussed by Aviram and Ratner in 1974.<sup>55, 56</sup>

The most common of solid state rectifiers are based on a p-n junction and so for an organic molecule to show rectification properties it must also have the properties of a p-n junction. By altering the substituents on an aromatic system within the organic moiety, it is possible to increase or decrease the electron density in the molecules, thus making the species more electron rich (n-type) or electron poor (p-type). Any electron withdrawing subunits cause an aromatic system to become electron poor in  $\pi$ -density, raising the electron affinity and making the species a good electron acceptor. Conversely, any electron releasing groups increase  $\pi$ -electron density, consequently lowering the electron affinity and producing a good electron donor.

This explanation lacks the rigorous treatment given in any solid state physics course, but is used as a guide as to why the structures chosen for study as potential molecular rectifiers consist of donor and acceptor species.

In a donor-acceptor system, electrons would pass from the cathode to the acceptor and from the donor to the anode, but **not** in the other sense. Interaction of the donor and acceptor must be minimised or a single donor level would exist for the duration of any laboratory experiment.

To insulate a donor and acceptor from each other, a  $\sigma$ -electron bridge to link the two portions was proposed and the following molecule (fig 1.15) suggested as a model.

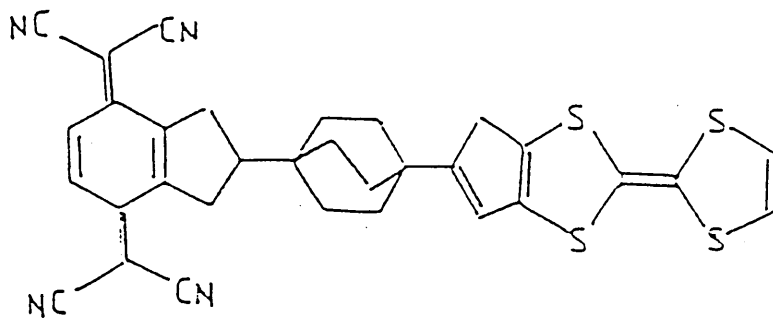


**Fig 1.15 Proposed Molecular Rectifier based on the Aviram/Ratner model.**

A successful synthesis of this molecule has not been achieved but Metzger et al<sup>57</sup> have successfully synthesised a variety of molecules of similar structure (fig 1.16, for example) and have recently reported partial success<sup>58</sup>

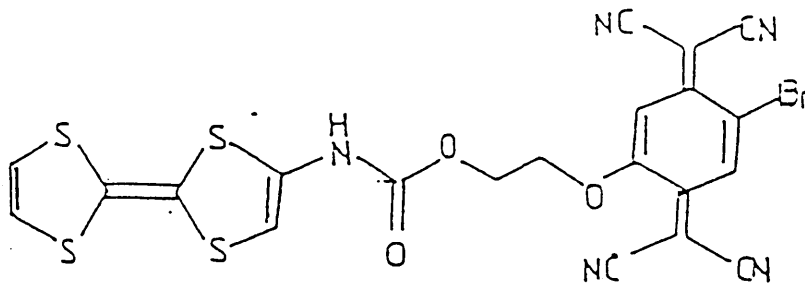


**Fig 1.16 TTF and a TCNQ derivative linked via a urethane unit**

There have been a number of publications recently on the novel Zwitterionic materials documented in this thesis. Ashwell and co-workers have reported on their photochromism<sup>59-61</sup> and possible molecular rectification<sup>62</sup>. Aspects of the LB film-forming properties have recently been reported by Bell et al<sup>63</sup>. For current developments in electro-active organic compounds in general, then the proceedings of the many workshops, conferences, etc provide the necessary background<sup>64</sup>.

## 1.7 REFERENCES

- 1 H N McCoy and W C Moore, *J Am Chem Soc*, 33, 273, (1911)
- 2 C Kraus, *J Am Chem Soc*, 35, 1732, (1913)
- 3 R Foster, *Organic Charge Transfer Complexes*, Academic Press London & New York, 1969
- 4 D S Acker, R J Harder, W R Hertler, W Mahler, L R Melby, R E Benson and W E Mochel, *J Am Chem Soc*, 82, 6403, (1960)
- 5 I F Shegolev, *Phys Stat Sol, (A)*, 12, 9, (1972)
- 6 F Wudl, G M Smith and E J Hufnagel, *J Chem Soc Chem Commun*, 1453, (1970)
- 7 J Ferraris, D O Cowan, V V Walatka and J M Perstein, *J Am Chem Soc*, 95, 948, (1973)
- 8 H Shirikawa, E J Lewis, A G MacDiarmid, C K Chiang and A J Heeger, *J Chem Soc Chem Commun*, 578, (1977)
- 9 M M Labes, P Love and L F Nicholls, *Chem Rev*, 79, 1, (1979)
- 10 A E Underhill and D M Watkins, *Chem Soc Rev*, 9, 429, (1980)
- 11 H A Benisi and J H Hildenbrand, *J Am Chem Soc*, 71, 2703, (1949)
- 12 R S Mulliken, *J Am Chem Soc*, 72, 600, (1950)
- 13 R S Mulliken, *J Am Chem Soc*, 74, 811, (1952)
- 14 R S Mulliken and W B Person, *Molecular Complexes - a lecture and reprint volume*, J Wiley and Sons Inc, London, (1969)
- 15 F Gutman and L E Lyons, *Organic Semiconductors Part A*, R E Kreiger Publishing Company, Malabar, Florida, (1981)
- 16 L R Melby, R J Harder, W R Hertler, W Mahler, R E Benson and W E Mochel, *J Am Chem Soc*, 84, 3374, (1962)
- 17 M R Bryce and L C Murphy, *Nature*, 309, 119, (1984)
- 18 T J Kistenmacher, T E Phillips and D O Cowan, *Acta-Cryst*, B30, 763, (1973)
- 19 R E Pierels, *Quantum Theory of Solids*, Oxford University Press, (1955)
- 20 F Denoyer, R Comés, A F Garito and A J Heeger, *Phys Rev Lett*, 35, 445, (1975)

- 21 R L Greene, J J Mayerle, R Schumaker, G Castro, P M Chaikin, E Etemad and S J Laplaca, *Solid State Commun*, 20, 943, (1976)
- 22 Y Ueno, A Nakayama and M Okawara, *J Chem Soc Chem Commun*, 74, (1978)
- 23 T J Kistenmacher, T J Emge, P Shu and D O Cowan, *Acta-Cryst*, B35, 772, (1979)
- 24 F Wudl and E Aharon-Shalom, *J Am Chem Soc*, 104, 1154, (1982)
- 25 R C Wheland and E L Martin, *J Org Chem*, 40, 3101, (1975)
- 26 R C Wheland and J L Guison, *J Am Chem Soc*, 98, 3916, (1976)
- 27 R C Wheland, *J Am Chem Soc*, 98, 3926, (1976)
- 28 C S Jacobsen, K Mortensen, J R Anderson, and K Bechgaard, *Phys Rev*, B18, 905, (1978)
- 29 A Andrieux, C Dorouré, D Jérôme and K Bechgaard, *J Phys Paris Lett*, 40, L381, (1979)
- 30 K Bechgaard, C S Jacobsen, K Mortensen, H J Pedersen, N Thorup, *Solid State Commun*, 38, 1119, (1980)
- 31 J Bardeen, L N Cooper, and J R Schieffer, *Phys Rev*, 108, 1175, (1957)
- 32 K Bechgaard and D Jerome, *Sci Am*, 247, 50, (1982)
- 33 K Bechgaard, K Carneiro, F B Rasmussen, M Olsen, G Rindorf, C S Jacobsen, H J Pedersen and J C Scott, *J Am Chem Soc*, 103, 2440, (1981)
- 34 N Thorup, G Rindorf, H Soling and K Bechgaard, *Acta Cryst*, B37, 1236, (1981)
- 35 R J Cava, B Batlegg, R V Van Dover, J J Krajewski, J V Warszczak, R M Flemming, W F Peck Jr, L W Rupp Jr, P Marsh, A C W P James and L F Schneemeyer, *Nature*, 345, 602, (1990)
- 36 G J Ashwell, J G Allen, E P Goodings and I W Nowell, *Phys Stat Sol, A*, 82, 301, (1984)
- 37 G J Ashwell, *Pr Nauk Fust Chem Org Fiz (Dr Hab Thesis) - Politech Wroclaw*, 31, 3, (1986)
- 38 A Barraud, J Richard, M Vandevyver, K Hokzer, *J Phys D*, 19, 2421, (1986)
- 39 A Barraud, L Henrion, G Derost and A Ruaudel-Teixier, *Sensors and Actuators*, 14, 251, (1988)

- 40 B P Bespalov and V V Titov, *Russ Chem Rev*, 44, 1091, (1975)
- 41 W R Hertler, H D Hartzler, D S Acker and R E Benson, *J Am Chem Soc*, 84, 3387, (1962)
- 42 R M Metzger, N E Heimer and G J Ashwell, *Mol Cryst Liq Cryst*, 107, 133, (1984)
- 43 S Akhtar, J Tanaka, R M Metzger and G J Ashwell, *Mol Cryst Liq Cryst*, 139, 353, (1986)
- 44 J S Miller and J C Calabrese, *J Chem Soc Chem Commun*, 63, (1988)
- 45 J Zyss, *J Mol Electron*, 1, 25, (1985)
- 46 J Zyss, J F Nicoud and M Coquillay, *J Chem Phys*, 81, 4160, (1984)
- 47 I Ledoux, D Joise, P Frenaux, J P Piel, G Post, J Zyss, T McLean, R A Hann, P F Gordon and S Allen, *Thin Solid Films*, 160, 217, (1988)
- 48 J Zyss, G J Bertier, *J Chem Phys*, 77, 3635, (1982)
- 49 K Jain, J I Cowley, G H Hewig, Y Y Cheng and R J Tweig, *Optics and Laser Technology*, 297, (1981)
- 50 J Zyss, D Chemla and J J Nicoud, *J Chem Phys*, 74, 4800, (1981)
- 51 R Tweig, A Azema, K Jain and Y Y Cheng, *Chem Phys Lett*, 92, 208, (1982)
- 52 G F Lipscombe, A F Garito and R S Narang, *J Chem Phys*, 75, 1509, (1981)
- 53 J L Oudar and R J Hierle, *J Appl Phys*, 48, 2699, (1977)
- 54 R J Tweig and K Jain, *ACS Symp Ser*, 233, 57, (1983)
- 55 A Aviram and M A Ratner, *Bull Am Phys Soc*, 19, 341, (1974)
- 56 A Aviram and M A Ratner, *Chem Phys Lett*, 29, 277, (1974)
- 57 C A Panetta, J Baghdedhi and R M Metzger, *Mol Cryst Liq Cryst*, 107, 103, (1983)
- 58 R M Metzger and C A Panetta, *Synth Met*, 28, 807, (1989)
- 59 G J Ashwell, *Thin Solid Films*, 186, 155, (1990)
- 60 G J Ashwell, E J C Dawnay and A P Kuczynski, *JCS Chem Commun*, 1358, (1990)
- 61 G J Ashwell, E J C Dawnay, A P Kuczynski, M Szablewski, I M Sandy, M R Bryce, A M Grainger and M Hasan, *JCS Faraday Trans*, 86, 1117, (1990)
- 62 G J Ashwell, J R Sambles, A S Martin, W G Parker and M Szablewski, *JCS Chem Commun*, 1374, (1990)

- 63 N A Bell, R A Broughton, J S Brooks, T A Jones, S C Thorpe and G J Ashwell,  
JCS Chem Commun, 325, (1990)
- 64 Synthetic Metals, Vols 41-43, (1991)  
Synthetic Metals, 54, (1993)

## CHAPTER 2: SYNTHESIS AND CHARACTERISATION OF R(4)Q3CNQ/R(4)P3CNQ\*

### 2.1 Experimental

#### 2.1.1 Reagents

All the reagents used were commercially available, and were not purified prior to use. The N-alkyl quinolinium and N-alkyl picolinium donors were all synthesised from commercially available reagents.

#### 2.1.2 Microanalysis

Microanalytical data were obtained from the microanalysis service of the City University, London.

#### 2.1.3 Instrumentation

##### 2.1.3.1 Infra-red spectroscopy

Infra-red spectra were recorded as KBr discs using a Unicam SP1000 series infra-red spectrometer.

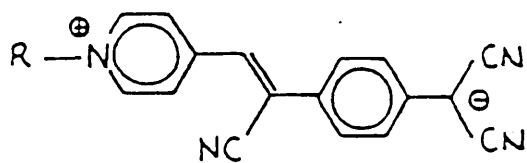
##### 2.1.3.2 Ultra-violet/visible (uv/vis) spectroscopy

uv/vis spectra were recorded using a Perkin-Elmer 550S series spectrophotometer, in the range 190 to 900nm, using a 1cm path length quartz cell.

\* FOR THIS NOMENCLATURE SEE OVERLEAF

## Nomenclature in donor- $\pi$ -acceptor adducts of TCNQ

The following shorthand nomenclature has been adopted for the zwitterions.



R(4) P3CNQ

R - refers to the alkyl chain

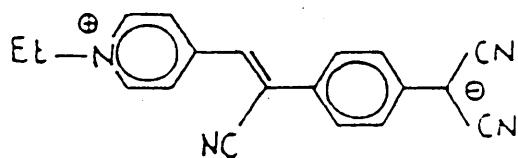
(4) - refers to substitution in the '4'-position of the picolinium ring.

P - refers to picolinium donor. (Q would refer to a quinolinium donor)

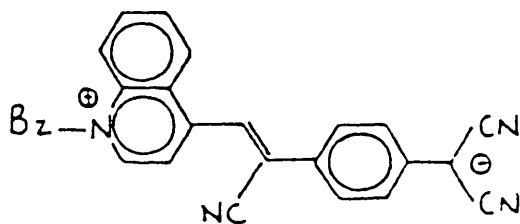
3CN - shows 3 cyano groups present.

Q - refers to TCNQ as the acceptor.

eg:



Et(4) P3CNQ



Bz(+) Q3CNQ

### 2.1.3.3 Mass spectrometry

Mass spectra were recorded using a VG305 series mass spectrometer coupled to a Caslo Erba GC and VG D52050 series data system. A direct insertion probe was used.

### 2.1.3.4 $^1\text{H}$ nmr spectroscopy

$^1\text{H}$  nmr spectra were recorded on a Bruker WP 805Y nmr spectrometer. Samples were dissolved in deuteriated dimethyl sulphoxide with tetramethylsilane as an internal reference.

### 2.1.3.5 Differential Scanning Calorimetry (DSC)

DSC measurements were carried out on a Mettler TA3000 systems in a dynamic nitrogen atmosphere. Scans were made over the range  $-150^\circ\text{C}$  to  $350^\circ\text{C}$  at a rate of  $5^\circ\text{C min}^{-1}$ .

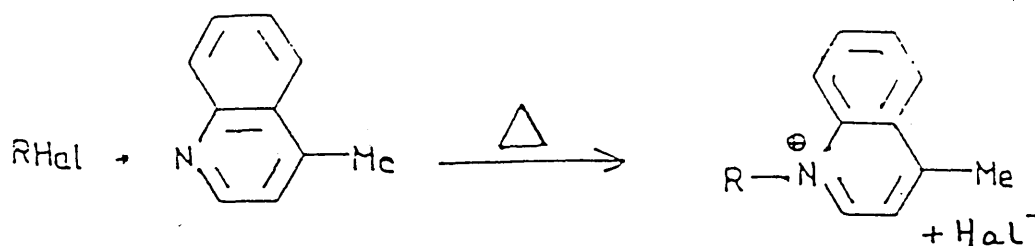
## 2.2 Synthesis

### 2.2.1 Synthesis of the N-alkyl-4-methyl quinolinium bromides

A range of derivatives was synthesised - the methods used being the same in all cases. The synthesis of N-eicosyl-4-methyl quinolinium bromide is described below as representative of the series.

1-Bromoeicosane (13.72g, 0.038 moles) was gently refluxed with 4-methyl quinoline (5.43g, 0.038 moles) for 2½ hours. The initial dark brown liquid became darker in colour and more viscous. On cooling, a dark blue solid was obtained which was recrystallised from hot methanol. Yield 17.5g (91%), mpt 120-122°C,  $\lambda_{\text{max}}$  (MeOH) 604nm.

Equation



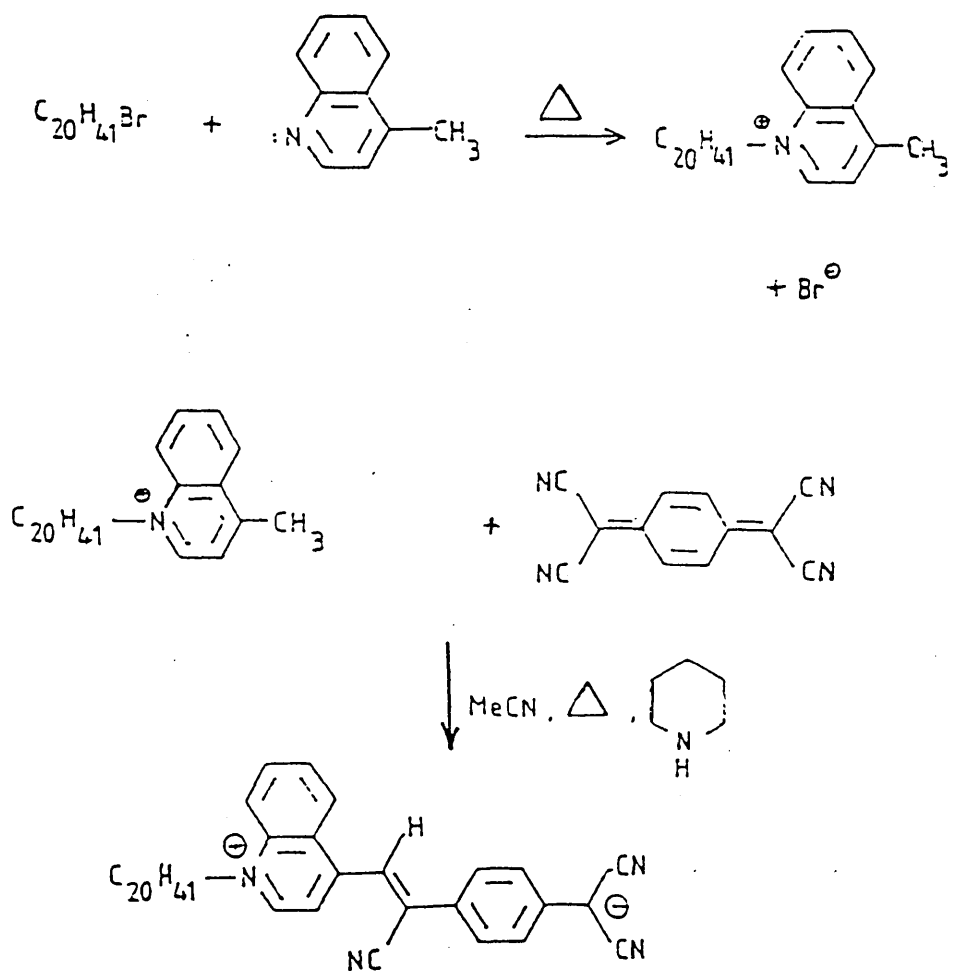
### 2.2.2 Synthesis of $\text{C}_{20}\text{H}_{41}$ (4)Q3CNQ

An examination of the structure of the quinolinium cation showed that the methyl proton is relatively acidic and may be removed by a suitable base. Thus, the following synthetic method was adopted.

Acetonitrile ( $100 \text{ cm}^3$ ) was refluxed with piperidine (3-4 drops) with continuous stirring, for 10 minutes. N-eicosyl-4-methyl quinolinium bromide ( $0.5\text{g}$ ,  $9.8 \times 10^{-4}$  moles) was dissolved in acetonitrile ( $50 \text{ cm}^3$ ) and added dropwise to the refluxing solution. After addition of the cation, TCNQ ( $0.2\text{g}$ ,  $9.8 \times 10^{-4}$  moles) was added and the blue solution was refluxed for a further hour, during which time the colour changed from the intense bright blue to green. After a further 13 hours reflux, the solution turned turquoise and on cooling a fine, black powder was produced. The product was isolated by filtration under suction, and washed with toluene ( $1 \times 10 \text{ cm}^3$ ) and ether ( $2 \times 10 \text{ cm}^3$ ) to remove any unreacted TCNQ. The crude product

was recrystallised from hot acetonitrile, filtered and dried by suction. The product was collected as fine, dark khaki coloured particles. Yield 0.126g (21%); mpt 286-290°C.

### Equation



An alternative synthetic route involves the use of LiTCNQ and a suitable alkylated quinolinium or picolinium species, and is that quoted by Metzger et al<sup>1</sup> in the original paper on Me(2)P3CNQ. This method is described below.

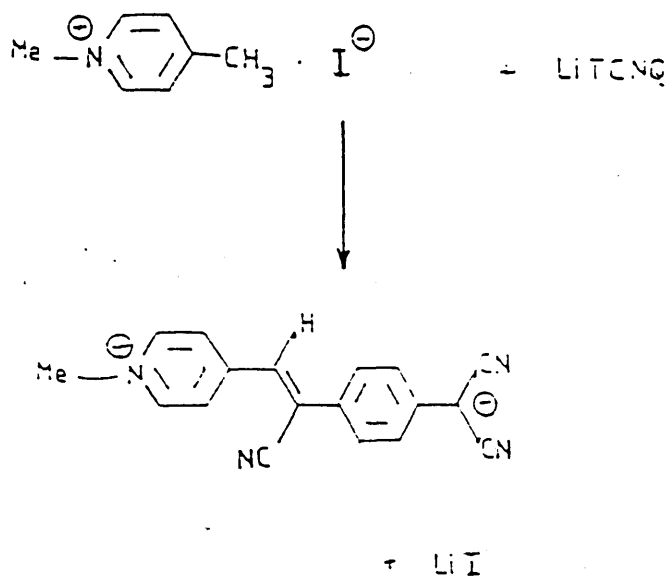
### 2.2.3 Synthesis of LiTCNQ<sup>2</sup>

Lithium iodide (3.3g, 0.024 moles) was added to a solution of TCNQ (0.5g, 0.024 moles) in acetonitrile (100 cm<sup>3</sup>), and was refluxed for one hour. After cooling, to room temperature, filtration gave a purple product of crude LiTCNQ, which was washed with toluene (1 x 10 cm<sup>3</sup>) and ether (2 x 10 cm<sup>3</sup>) to remove the unreacted TCNQ. A dark blue powder was produced in good yield (> 80%).

### 2.2.4 Synthesis of Me(4)P3CNQ

N-methyl-4-picolinium iodide (1g, 4.48 x 10<sup>-3</sup> moles) dissolved in 10 cm<sup>3</sup> of hot water was added slowly to a refluxing solution of LiTCNQ (0.9g, 4.48 x 10<sup>-3</sup> moles) dissolved in 200 cm<sup>3</sup> of MeCN. The reaction mixture was then allowed to reflux until the solution colour changed from the characteristic green of the TCNQ radical ion to blue. On allowing to cool to ambient temperature, green microneedles were produced which were recrystallised from acetonitrile. Yield 0.101g (7.95%), mpt 308 - 310°C,  $\lambda_{\text{max}}$  (MeCN) 644nm.

Equation



A collection of microanalytical data is shown in Table 2.1.

Zwitterion	C% Calc (found)	H% Calc (found)	N% Calc (found)
C <sub>11</sub> H <sub>23</sub> (4)Q3CNQ	80.97 (81.00)	7.21 (7.45)	11.80 (11.72)
C <sub>14</sub> H <sub>23</sub> (4)Q3CNQ	81.20 (80.46)	7.98 (7.75)	10.82 (10.13)
C <sub>15</sub> H <sub>31</sub> (4)Q3CNQ	81.46 (81.26)	7.97 (8.14)	10.55 (10.56)
C <sub>16</sub> H <sub>33</sub> (4)Q3CNQ	81.58 (80.54)	8.14 (8.01)	10.28 (10.08)
C <sub>20</sub> H <sub>41</sub> (4)Q3CNQ	81.95 (81.10)	8.72 (9.11)	9.32 (9.02)

**Table 2.1** Microanalytical data for selected zwitterionic adducts

## 2.3 Discussion of Synthetic Methods

The synthesis of R(4)Q3CNQ and R(4)P3CNQ, where R is an alkyl chain, is a substitution reaction of TCNQ in which a cyano group is substituted by the appropriate quinolinium/picolinium donor. The two alternative methods have differing mechanisms which are shown in fig 2.1 and fig 2.2.

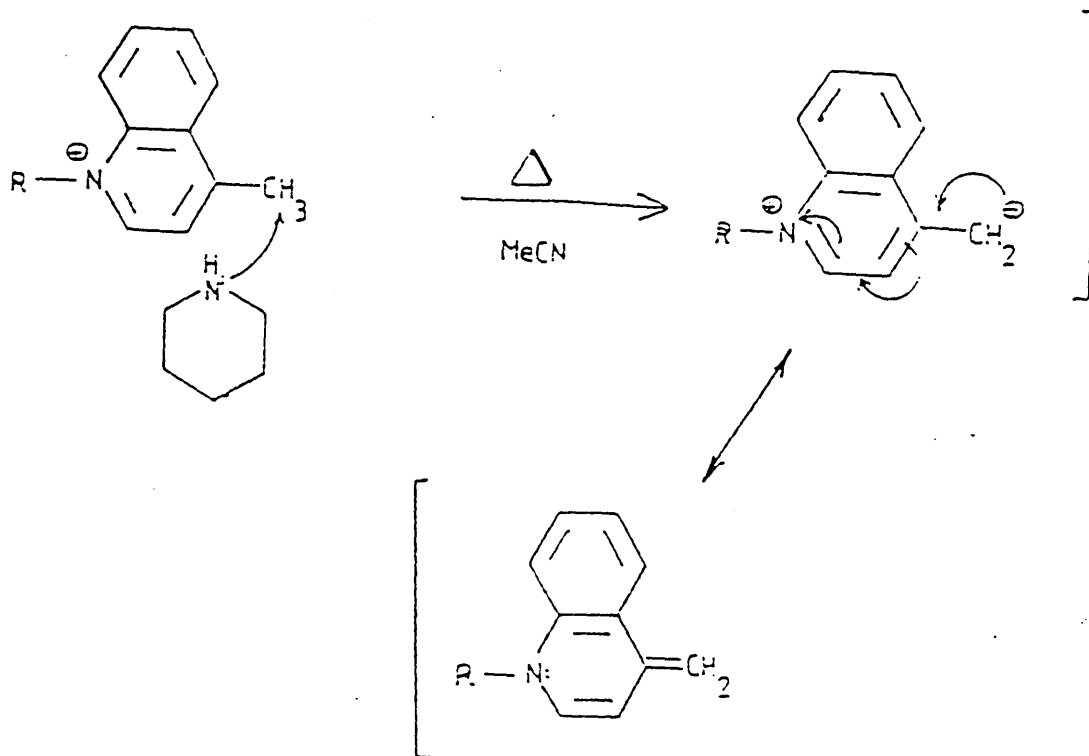
The first method involves the use of piperidine as a base to remove a proton from the 4-methyl group of the N-alkyl-4-methyl-quinolinium ion, a reaction very similar to the preparation of merocyanine dyes using N-alkyl picolinium salts with piperidine again used as a base<sup>3</sup>. The alternative mechanism presumably uses the LiTCNQ as the base, which also removes a proton from the 4-methyl group.

The removal of the proton results in the formation of a stable species which has a resonance structure in which the lone pair of electrons is situated on the electron deficient nitrogen. Such a methyl proton abstraction results in an extremely reactive homo-aromatic base which is highly susceptible to electrophilic addition at the exocyclic carbon. The use of acetonitrile as opposed to a polar protic solvent - say, methanol for example - is preferable as methanol would have a tendency to hydrogen bond to the carbanionic resonance structure.

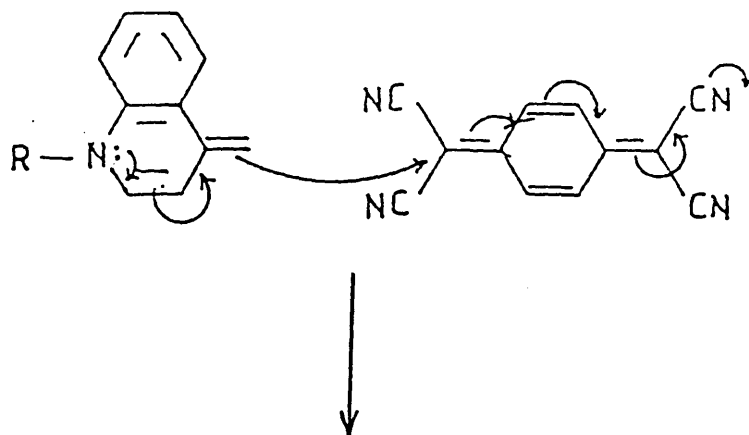
The yields obtained by each reaction type were not particularly large, though using piperidine they were markedly in excess of those using LiTCNQ. This would be expected on the basis of the proposed mechanism, piperidine being a much stronger base than LiTCNQ. Steric factors also increase the rate of reaction, as again would be expected, with a noticeable increase in reaction time occurring as the length of the alkyl chain is increased. This effect is particularly noticeable using LiTCNQ. The preparation of C<sub>10</sub>F<sub>17</sub>H<sub>4</sub>(4)P3CNQ was eventually carried out using this method, but only after heating under reflux for two months. Such a reaction is

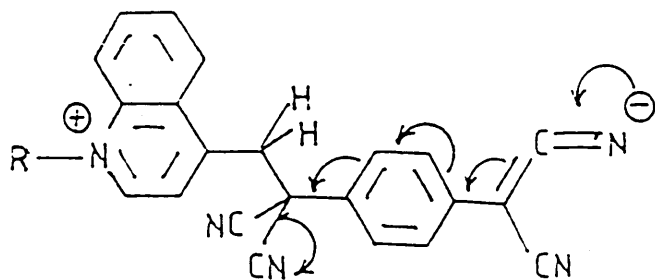
Fig 2.1

Proposed mechanism for the synthesis of R(4)Q3CNQ using piperidine base

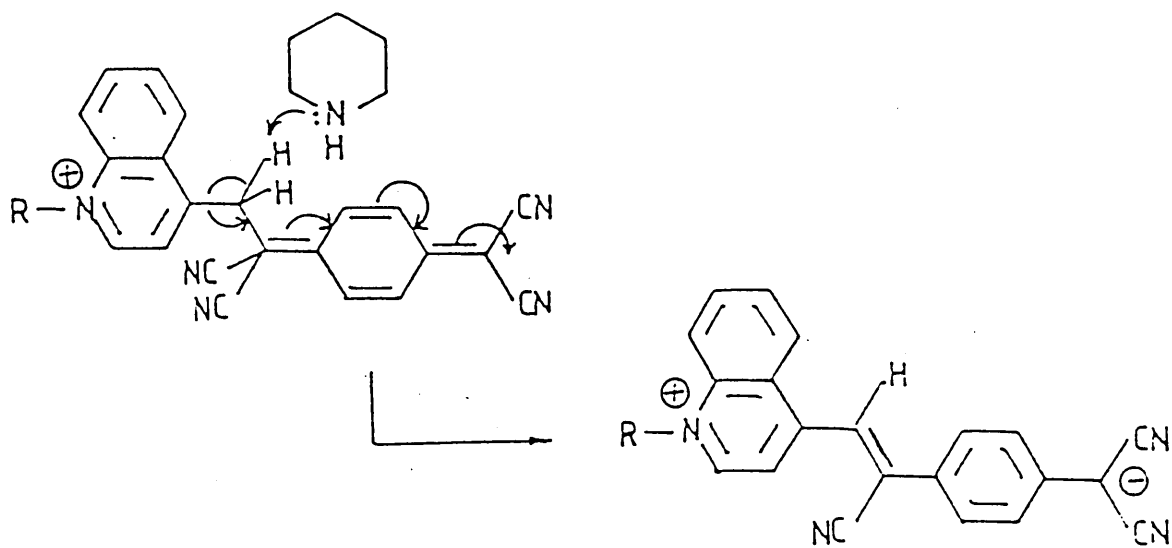


Then:

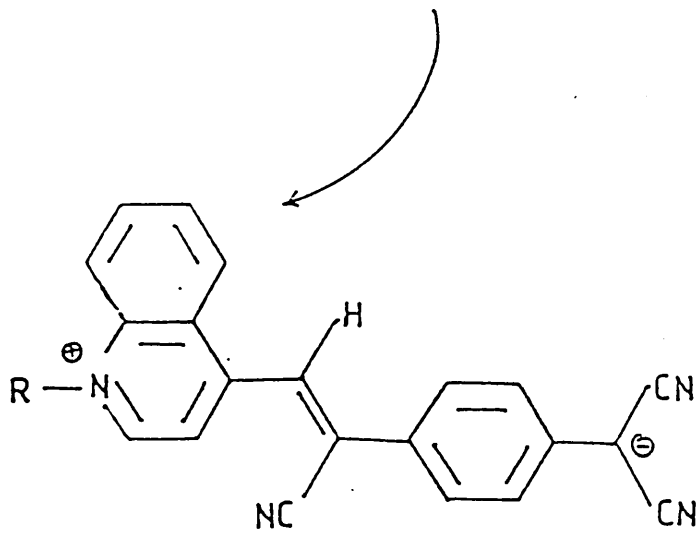
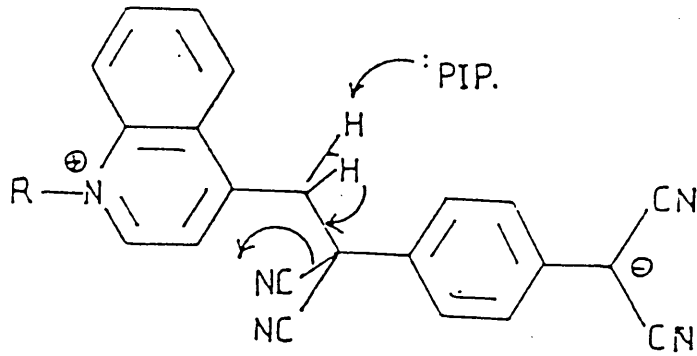
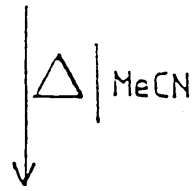
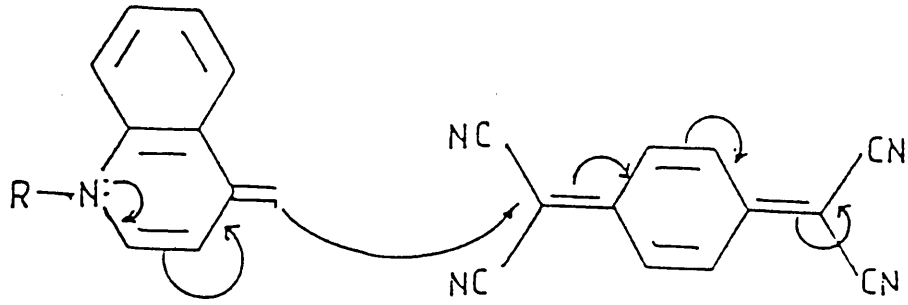




Then :



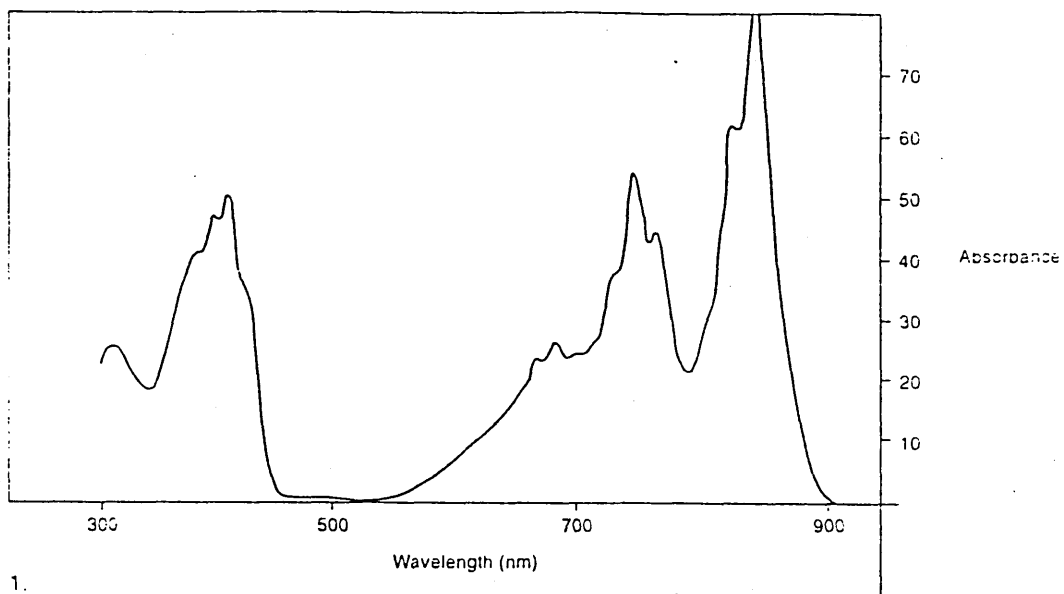
Or :



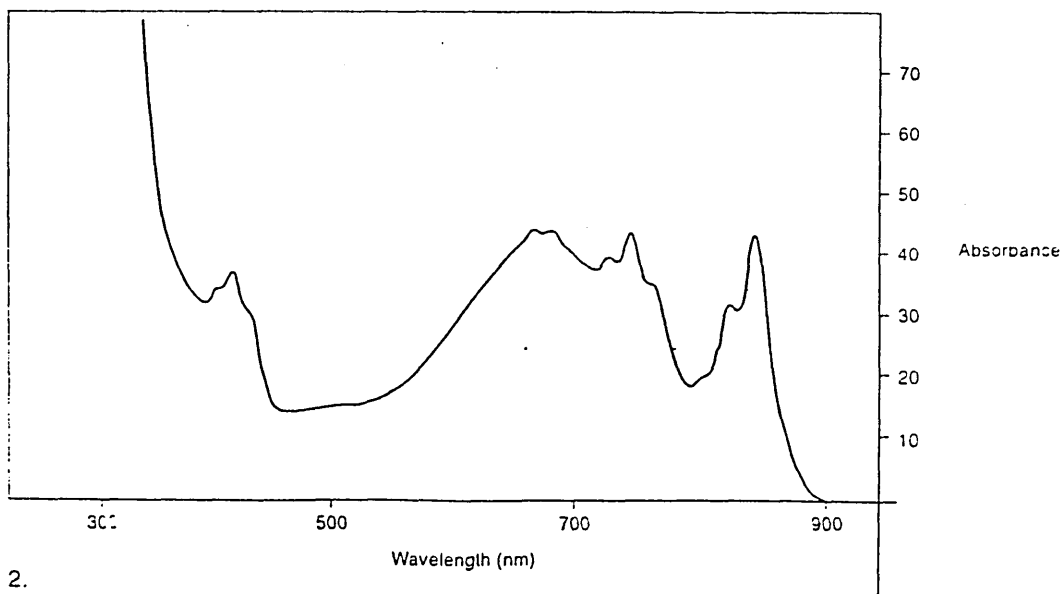


clearly unsatisfactory if the synthesis of long chain analogues is to be carried out on a routine basis. For these reasons, the method described in section 2.2.2 was used in the majority of the synthetic work, even though the problems of additional side reactions can cause the final product to be somewhat impure.

The progress of the reaction could be monitored by observing the uv/vis spectrum of the reaction mixture (for a more detailed discussion of the uv/vis spectra of these materials see Sec 2.4.1). Initially, the spectrum shows bands characteristic of the TCNQ<sup>o</sup> radical anion at ca. 840nm, though as the reaction proceeds, a broad charge transfer band characteristic of the particular zwitterionic adduct can be observed centred around 600-750nm. An example of the change in uv/vis spectrum of the reaction mixture during the course of the reaction for C<sub>10</sub>F<sub>17</sub>H<sub>4</sub>(4)P3CNQ is shown in fig 2.3. The reaction can also be monitored using thin-layer chromatography (TLC). Using a 10:1 methylene chloride:methanol solution as the mobile phase, pure (one-spot) zwitterionic products can be identified having an R<sub>f</sub> value of 2.2. Thus, these two methods, taken together provide adequate means of monitoring the course of the reaction.

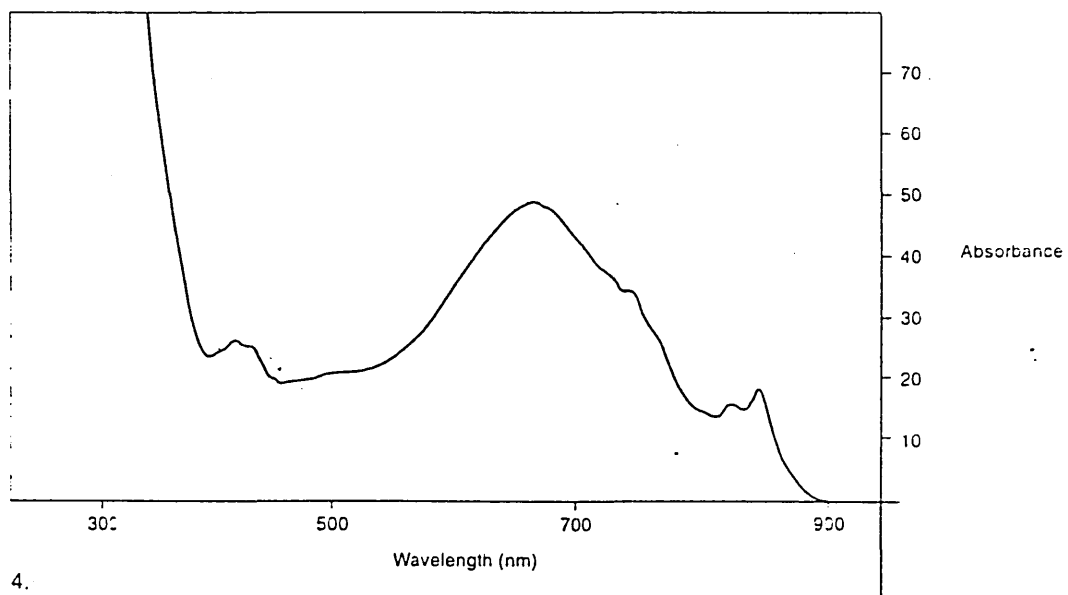
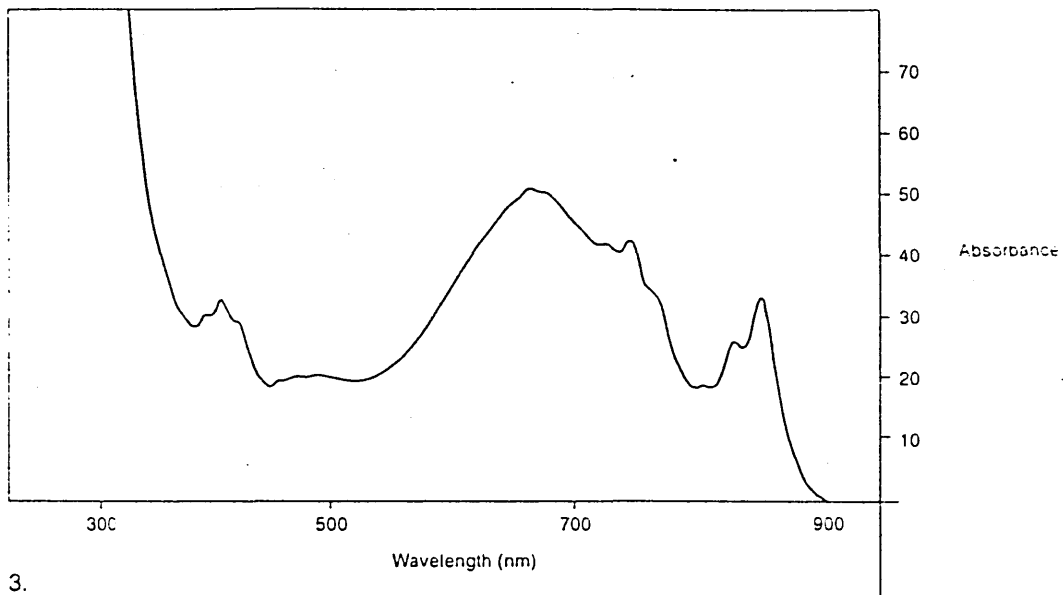


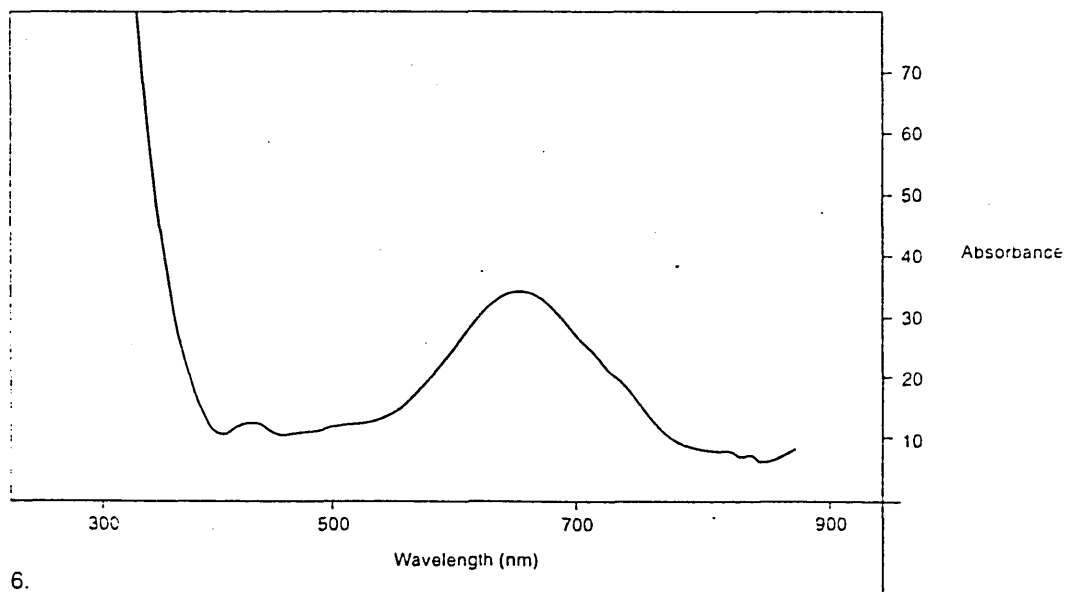
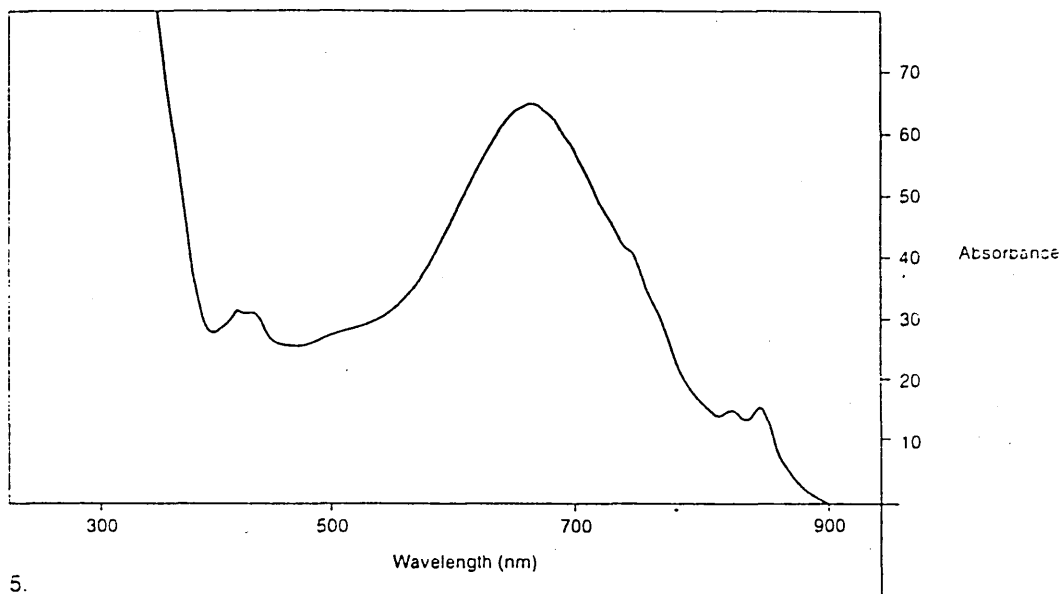
Starting Materials

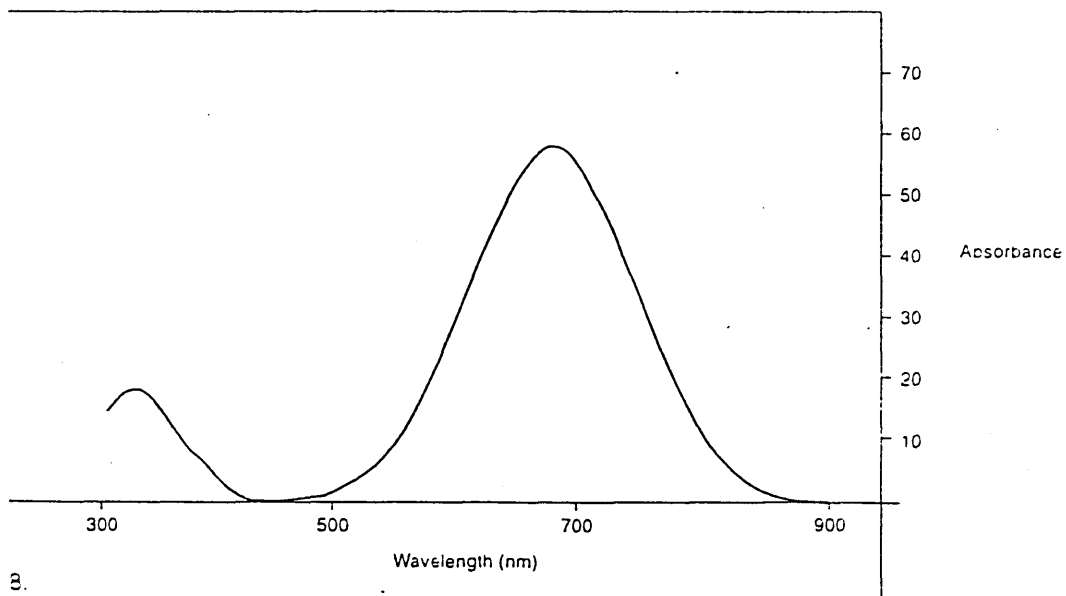
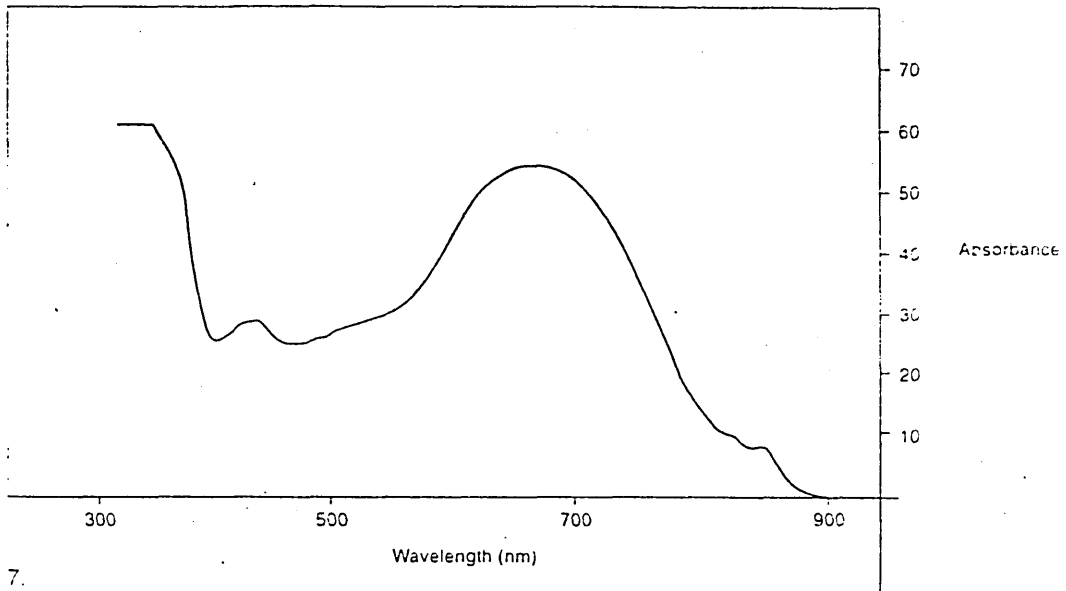


**Fig 2.3**

**UV/VIS spectra showing the course of the reaction between LiTCN(**  
**the  $C_{10}F_{17}H_4$  picolinium cation**







Pure  $C_{10}F_{17}H_4(4)P3CNQ$

## 2.4 Spectroscopic Studies of R(4) or R(2)P3CNQ/R(4) or R(2)Q3CNQ

### 2.4.1 Ultraviolet/visible spectroscopy

All pure adducts show an intense, broad transition centred around 600-750 nm in acetonitrile solution. Two less intense transitions at ca 340 and 378nm are also observed. Typical spectra are shown in fig 2.4 and 2.5. The low energy transition is independent of chain length, and has been attributed to an intramolecular back charge transfer process from the negatively charged dicyanomethanide group to the positively charged quinolinium moiety<sup>1</sup>. This is substantiated by plots of absorbance against concentration<sup>4</sup> which have been shown to obey Beer's Law. As this law is dependent on there being no interaction between absorbing chromophores, such behaviour can be taken as a good indication of an intramolecular process. Table 2.2 shows  $\lambda_{\text{max}}(\text{nm})$  values for a range of quinolinium and picolinium analogues.

As would be expected, the energy of transition is independent of chain length - the active portion of the molecule being the same for each zwitterionic system. However, inductive effects due to increased electron withdrawing character of the alkyl chain, manifest themselves in changes in  $\lambda_{\text{max}}$ . Consider the molecule C<sub>10</sub>F<sub>17</sub>H<sub>4</sub>(4)P3CNQ, where the very electronegative fluorine atoms tend to draw electrons away from the picolinium donor. In this case the "donating" strength of the molecule is diminished slightly. Thus, the intramolecular back charge transfer process from acceptor to donor requires less energy and the absorption maximum is shifted to longer wavelength. This effect is shown in Table 2.3.

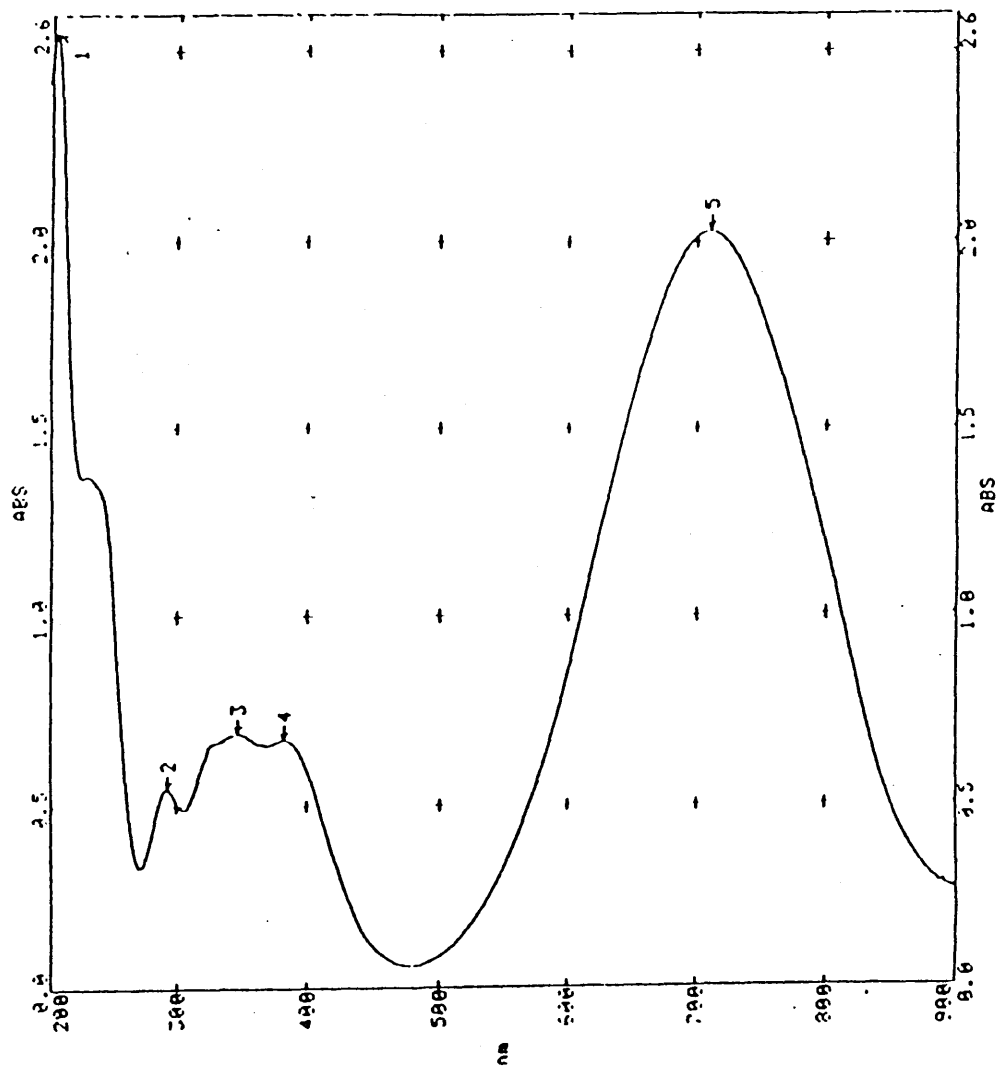


Fig 2.4 UV/VIS spectra of C<sub>6</sub>H<sub>11</sub>(4)Q3CNQ in MeCN

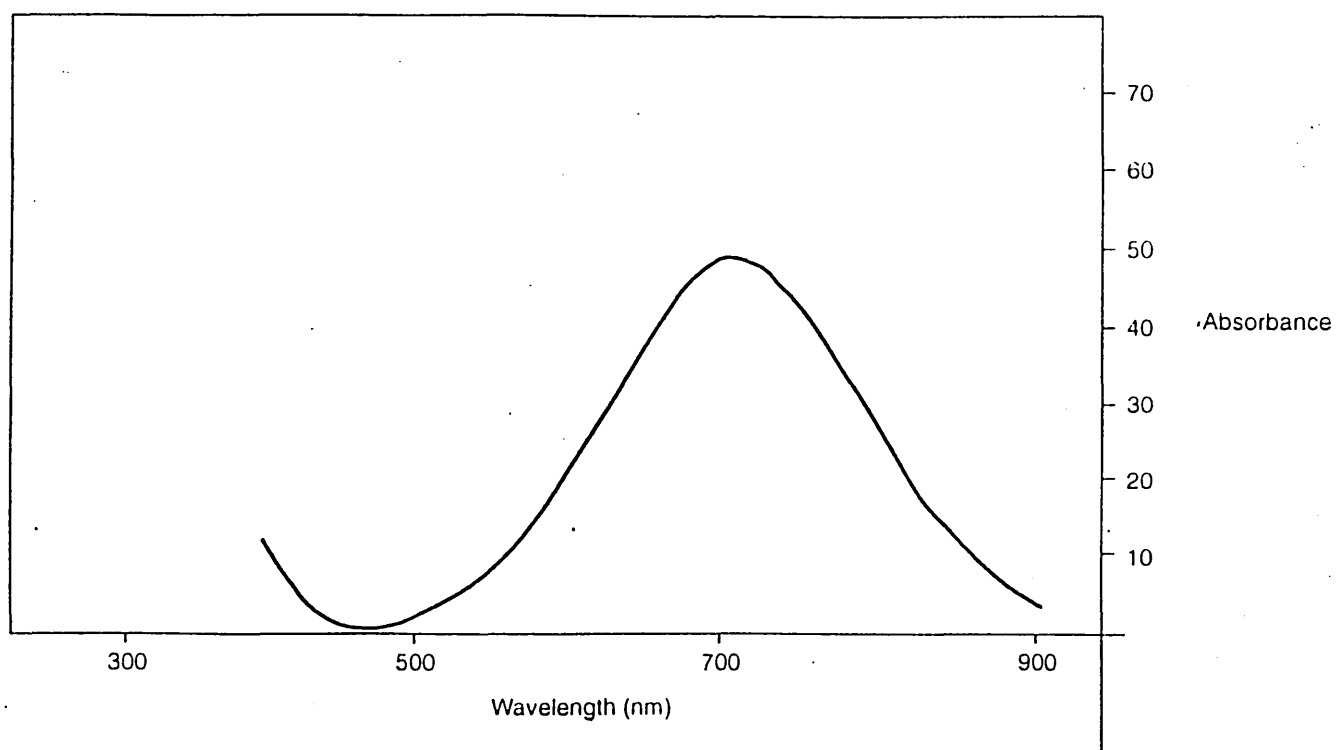


Fig 2.4 (Contd..) UV / Vis spectra of C<sub>11</sub>H<sub>23</sub>(4)Q3CNQ in MeCN

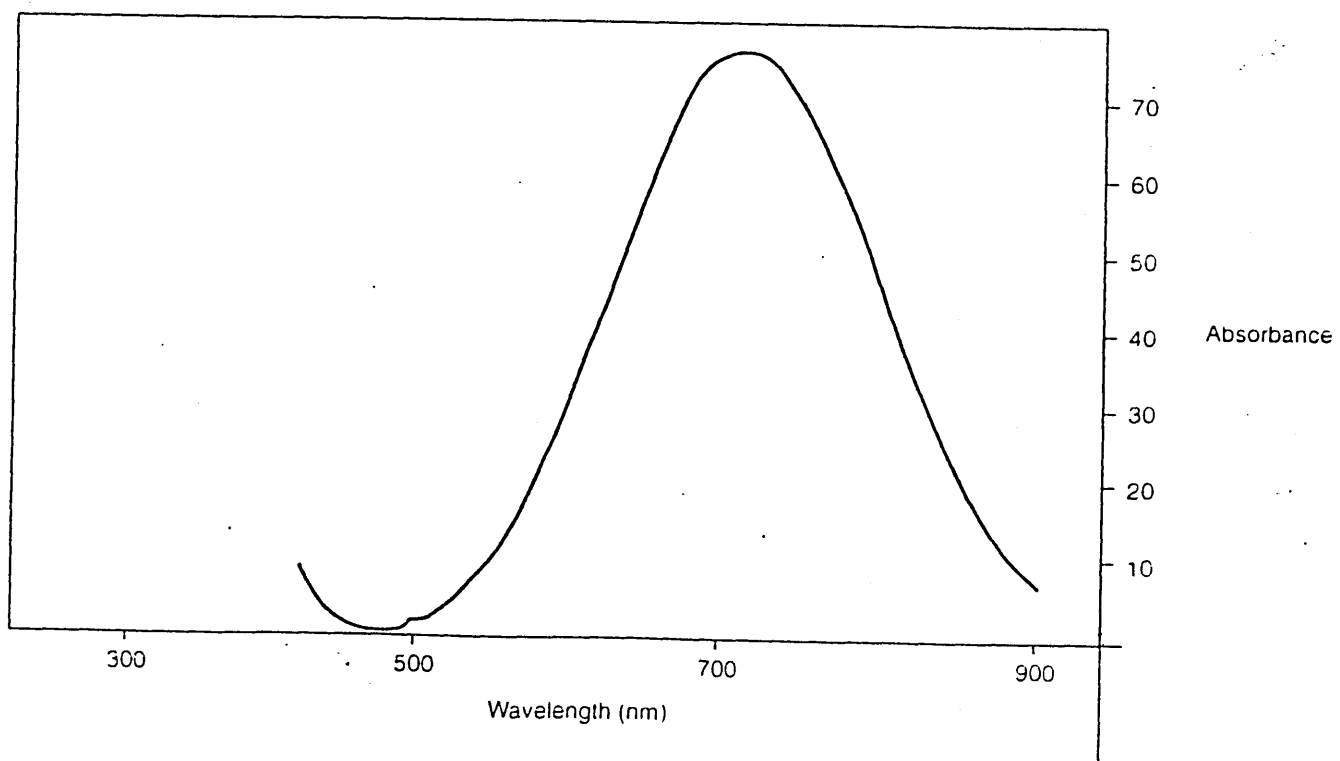


Fig 2.4 (Contd..) UV / Vis spectra of C<sub>13</sub>H<sub>27</sub>(4)Q3CNQ in MeCN

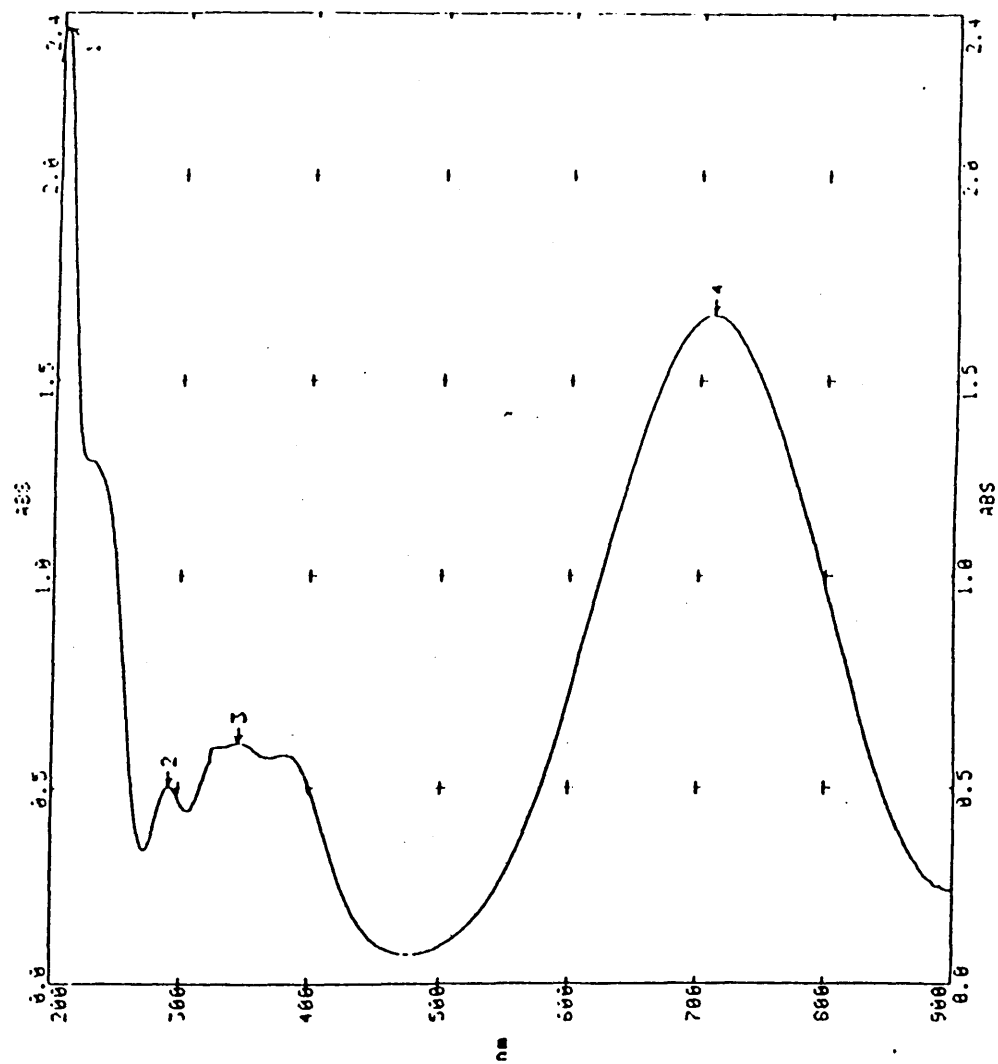


Fig 2.4 (Contd..) UV/Vis spectra of C<sub>14</sub>H<sub>29</sub>(4)Q3CNQ in MeCN

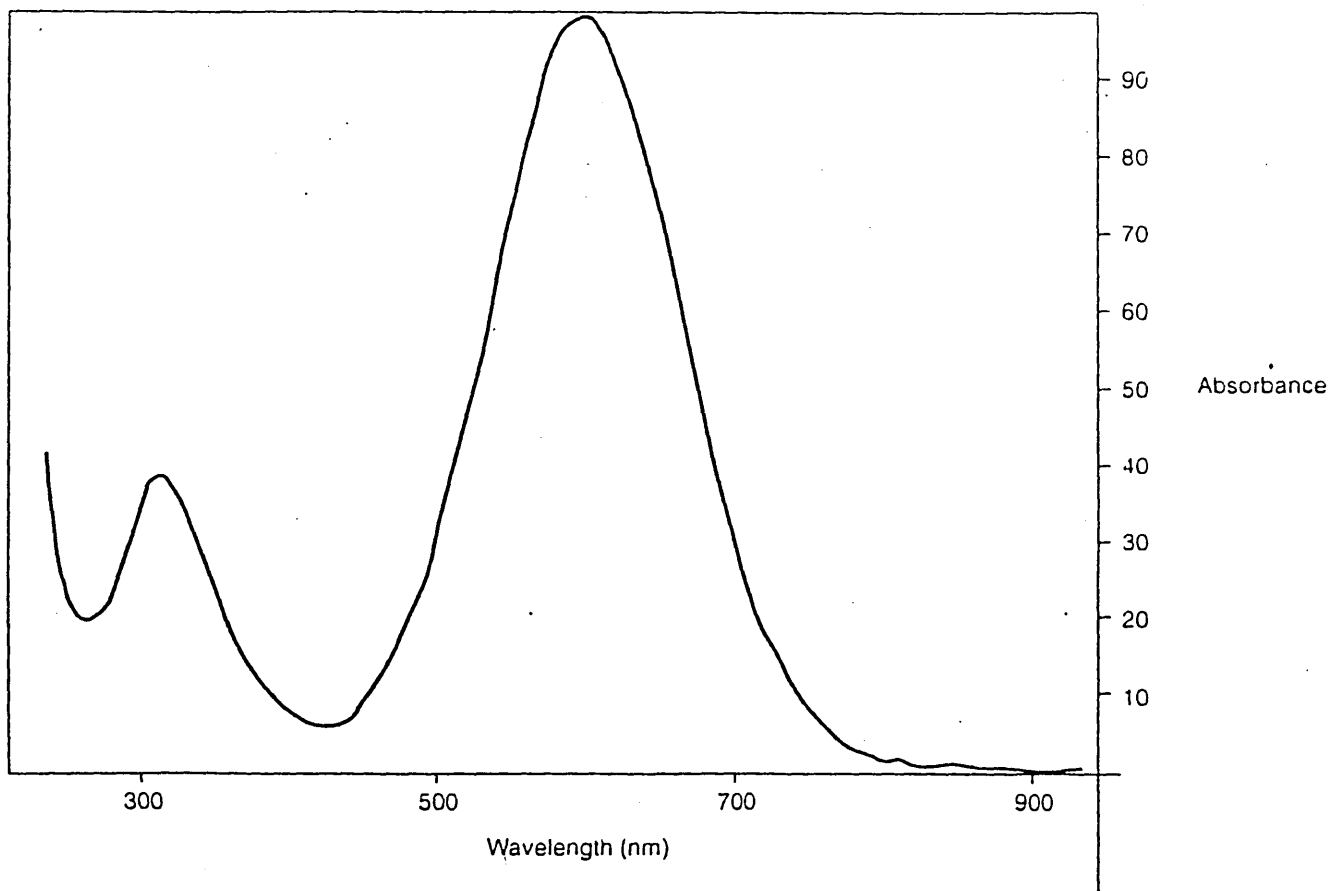


Fig 2.5 UV / Vis spectra of Me(2)P3CNQ in MeCN

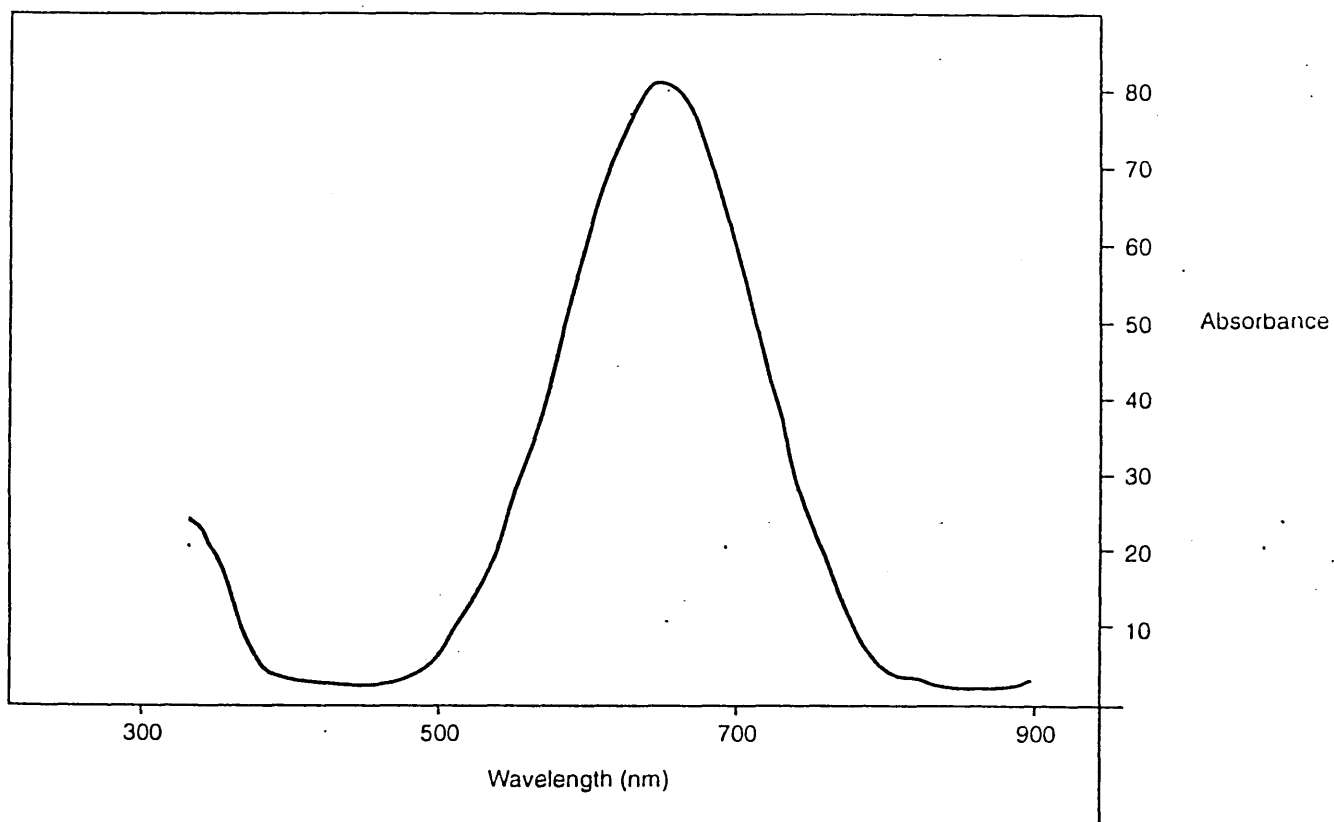


Fig 2.5 (Contd..) UV / Vis spectra of C<sub>8</sub>H<sub>17</sub>(4)P<sub>3</sub>CNQ in MeCN

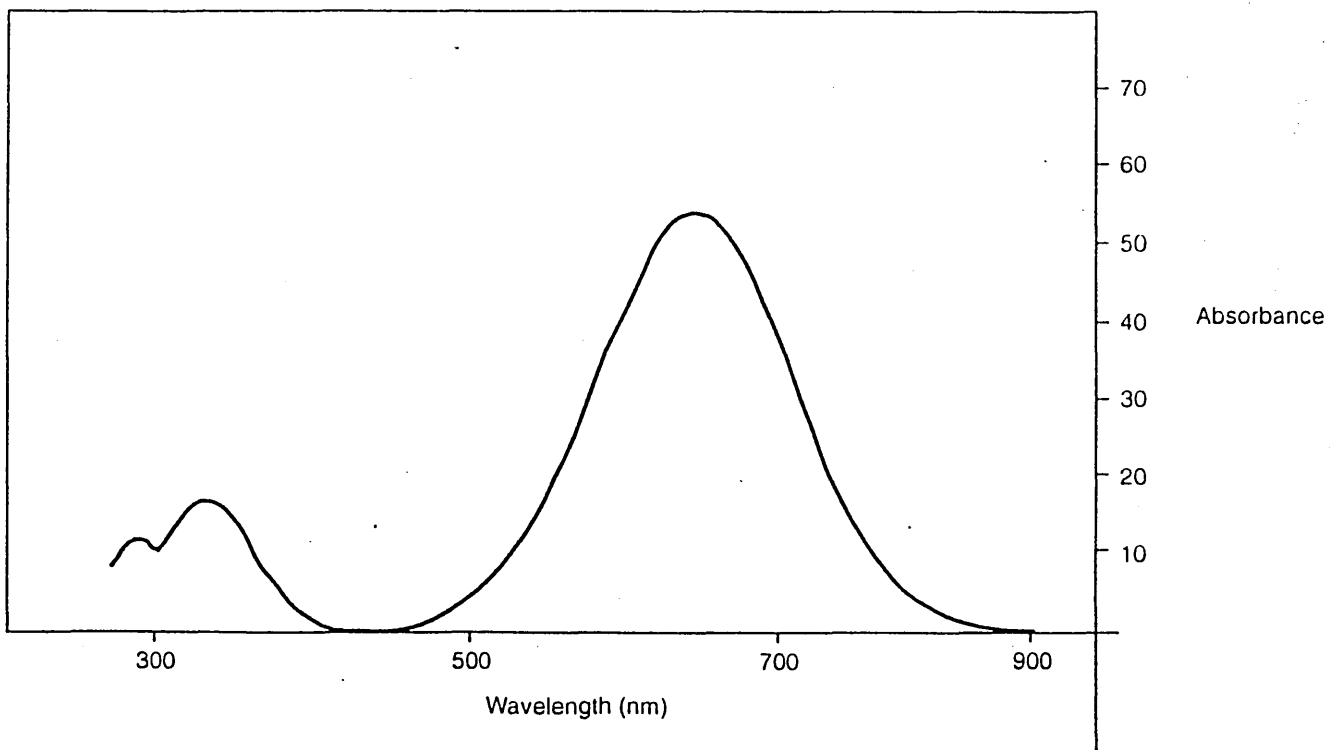


Fig 2.5 (Contd..) UV / Vis spectra of Me(4)P3CNQ in MeCN

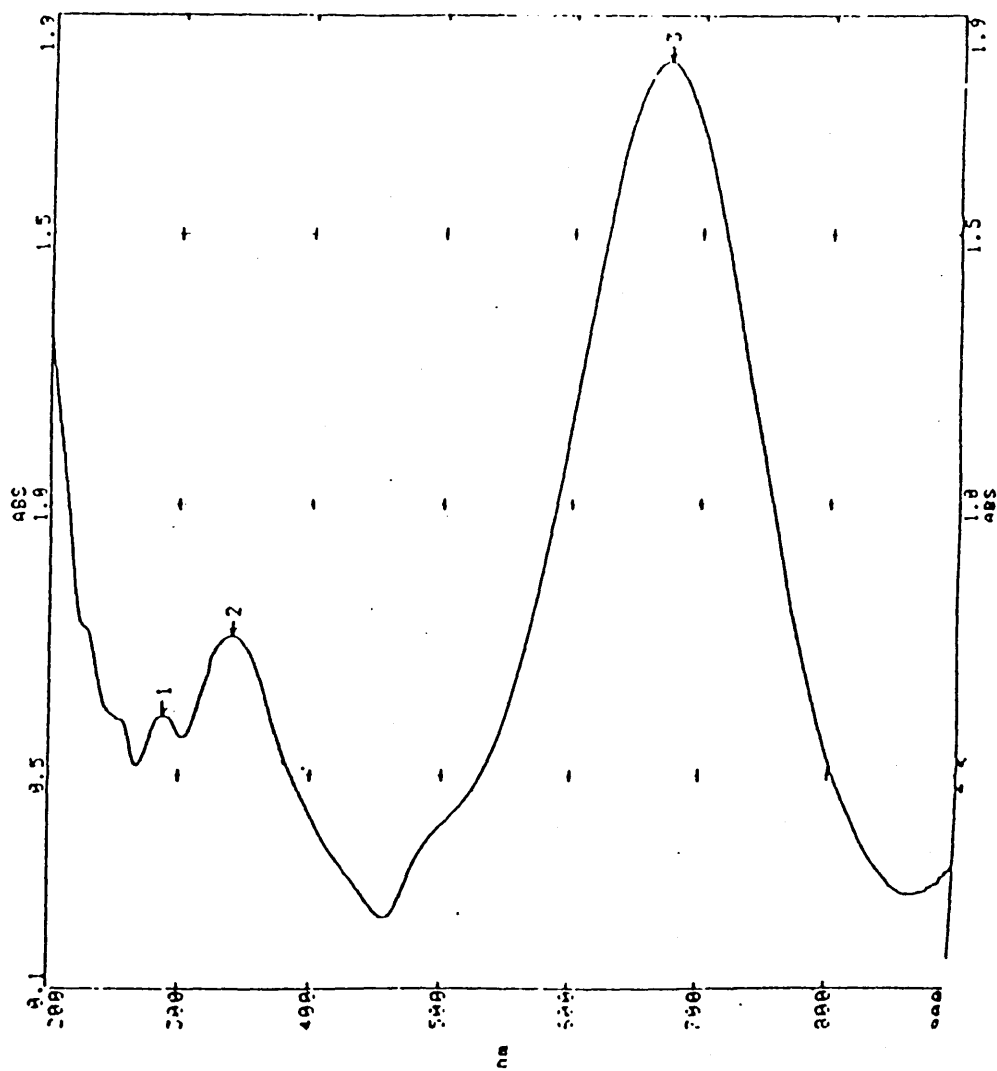


Fig 2.5 (Contd..) UV/Vis spectra of  $C_{10}F_{17}H_4(4)P3CNQ$  in MeCN

ADDUCT	$\lambda_{\text{max}}$ (MeCN, nm)
Me(2)P3CNQ	599
Me(4)P3CNQ	644
Et(4)P3CNQ	649
Me(2)Q3CNQ	696
Me(4)Q3CNQ	698
C <sub>8</sub> H <sub>17</sub> (4)P3CNQ	649
C <sub>10</sub> F <sub>17</sub> H <sub>4</sub> (4)P3CNQ	672
C <sub>8</sub> H <sub>17</sub> (4)Q3CNQ	708
C <sub>10</sub> H <sub>21</sub> (4)Q3CNQ	710
C <sub>11</sub> H <sub>23</sub> (4)Q3CNQ	700
C <sub>15</sub> H <sub>37</sub> (4)Q3CNQ	710
C <sub>20</sub> H <sub>41</sub> (4)Q3CNQ	710

**Table 2.2** Selected spectroscopic (UV/vis) data for zwitterionic adducts of TCNQ

Zwitterion	$\lambda_{\text{max}}$ (nm) MeCN
Et(4)P3CNQ	649
C <sub>8</sub> H <sub>17</sub> (4)P3CNQ	649
C <sub>10</sub> F <sub>17</sub> H <sub>4</sub> (4)P3CNQ	672

Table 2.3 Variation in  $\lambda_{\text{max}}$  with increasing electron withdrawing character of the alkyl chain

#### 2.4.1.1 Solvatochromism in R(4)/R(2)P3CNQ and R(4)/R(2)Q3CNQ<sup>5</sup>

The zwitterionic adducts exhibit solvatochromism, that is, the values of  $\lambda_{\text{max}}$  are solvent dependent. The phenomenon of solvatochromism in related merocyanine dyes has recently been reviewed<sup>6</sup>. Such solute-solvent interactions can be due to a number of factors:

- 1) Dipole-dipole interactions where the solute and solvent are polar.
- 2) Solute dipole-solvent induced dipole interactions where the solute is polar and the solvent is not.
- 3) Solvent dipole-solute induced dipole interactions where the solvent is polar and the solute is not.
- 4) Dispersion interactions.
- 5) Specific interactions such as hydrogen bonding and charge transfer complex formation with the solvent.
- 6) Solvent cage compression effects.

Factors 1-4 are general electrostatic phenomena; however, where 5 and 6 are present, these will predominate. Much work has been done in the past<sup>7-11</sup> - both experimental and theoretical - attempting to explain such interactions. It is not within the remit of this work to discuss this in any great detail. However, the following points are relevant to the following short discussion.

It is predicted that<sup>6</sup> non-polar solutes should undergo a bathochromic (red) shift as the solvent polarity increases. For polar solutes the situation is more complicated in that solvatochromism in such species is dependent on the solute dipole moment in the ground state and its change on excitation.

Expanding on this in more detail, then it has been shown that an increase in dipole moment on excitation should lead to a bathochromic (red) shift. Neutral chromophores may exhibit this behaviour. A decrease in dipole moment (for example charged chromophores) on excitation should lead to hypsochromic (blue) shifts being observed with increasing solvent polarity. The variation in  $\lambda_{\text{max}}$  for various adducts in a variety of solvents is shown in figs 2.4 and 2.5.

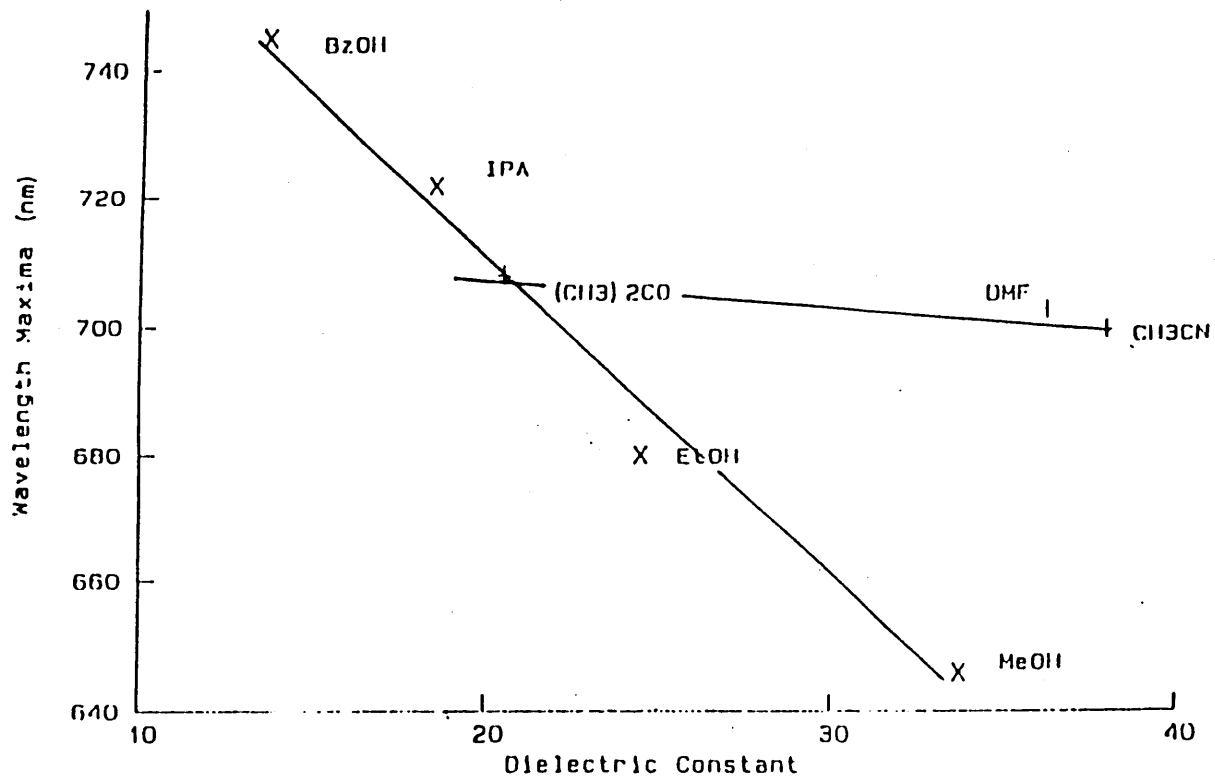


Figure 2.4 Variation of  $\lambda_{max}$  with dielectric constant of solvent for Me(4)Q3CNQ

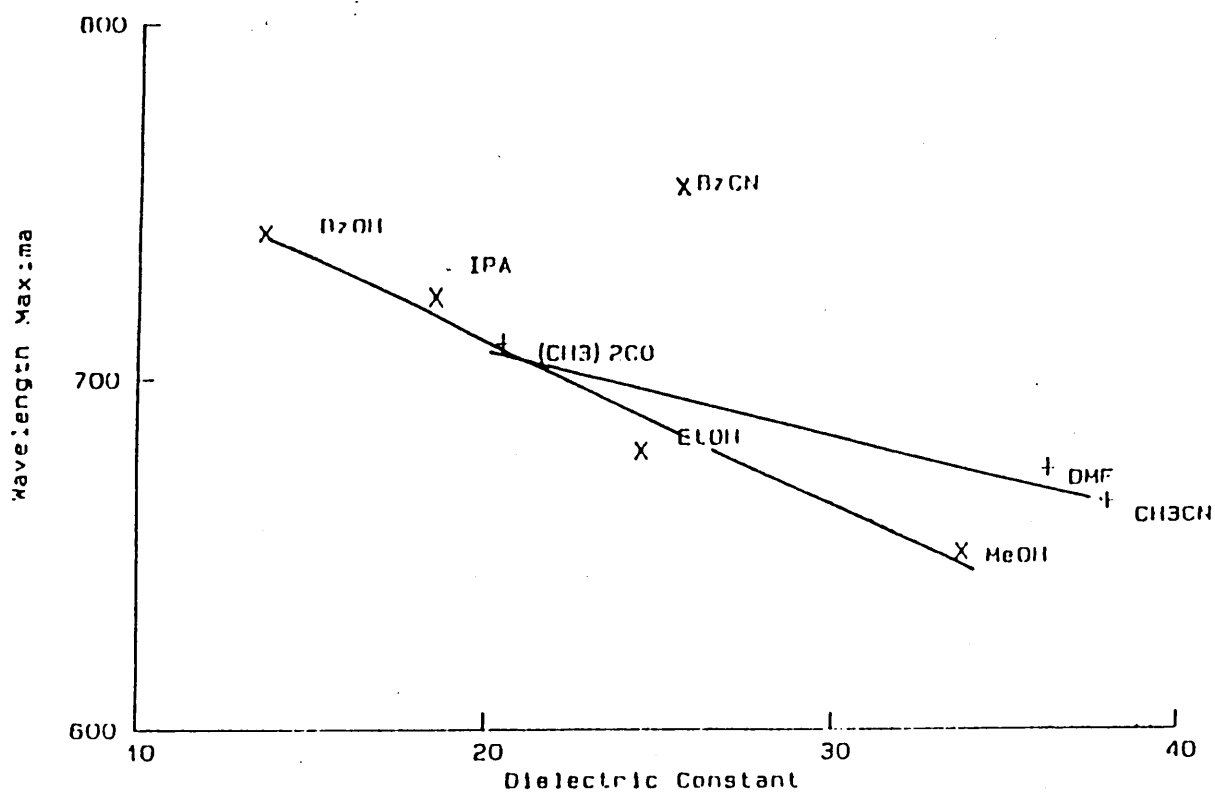


Figure 2.5 Variation of  $\lambda_{\max}$  with dielectric constant of solvent for  $C_{10}F_{17}H_4(4)P_3CNO$

As can be seen, the theoretical predictions are born out by the results obtained. The polar adducts, which undergo a reduction in dipole moment on charge transfer, show clear hypsochromic shifts with increasing solvent polarity. Notice also that the effects of hydrogen bonding appear apparent in both figures - the protic solvents following an independent trend. The  $\lambda_{\text{max}}$  value of C<sub>10</sub>F<sub>17</sub>H<sub>4</sub>(4)P3CNQ in cyanobenzene appears not to follow either trend, though this may be due to some weak charge transfer interaction.

#### 2.4.2 Infra red spectroscopic studies

As expected, all the adducts give similar infra-red spectra. Typical spectra are shown in figs 2.6 and 2.7 with all the relevant frequency assignments in Table 2.4. The important peaks are the two - C $\equiv$ N stretching bands at 2137 cm<sup>-1</sup> and 2177 cm<sup>-1</sup>. Neutral nitriles normally cover the range 2260 cm<sup>-1</sup> to 2200 cm<sup>-1</sup>. The presence of the two cyano stretching frequencies are characteristic of the two distinct cyano environments<sup>12-14</sup>. The band at 2177 cm<sup>-1</sup> represents the neutral environment whilst the band at 2137 cm<sup>-1</sup> is characteristic of the dicyanomethanide 3-carbon unit over which the negative charge is delocalised. Thus this delocalisation of charge reduces the strength of the bond and the stretching frequency is reduced correspondingly.

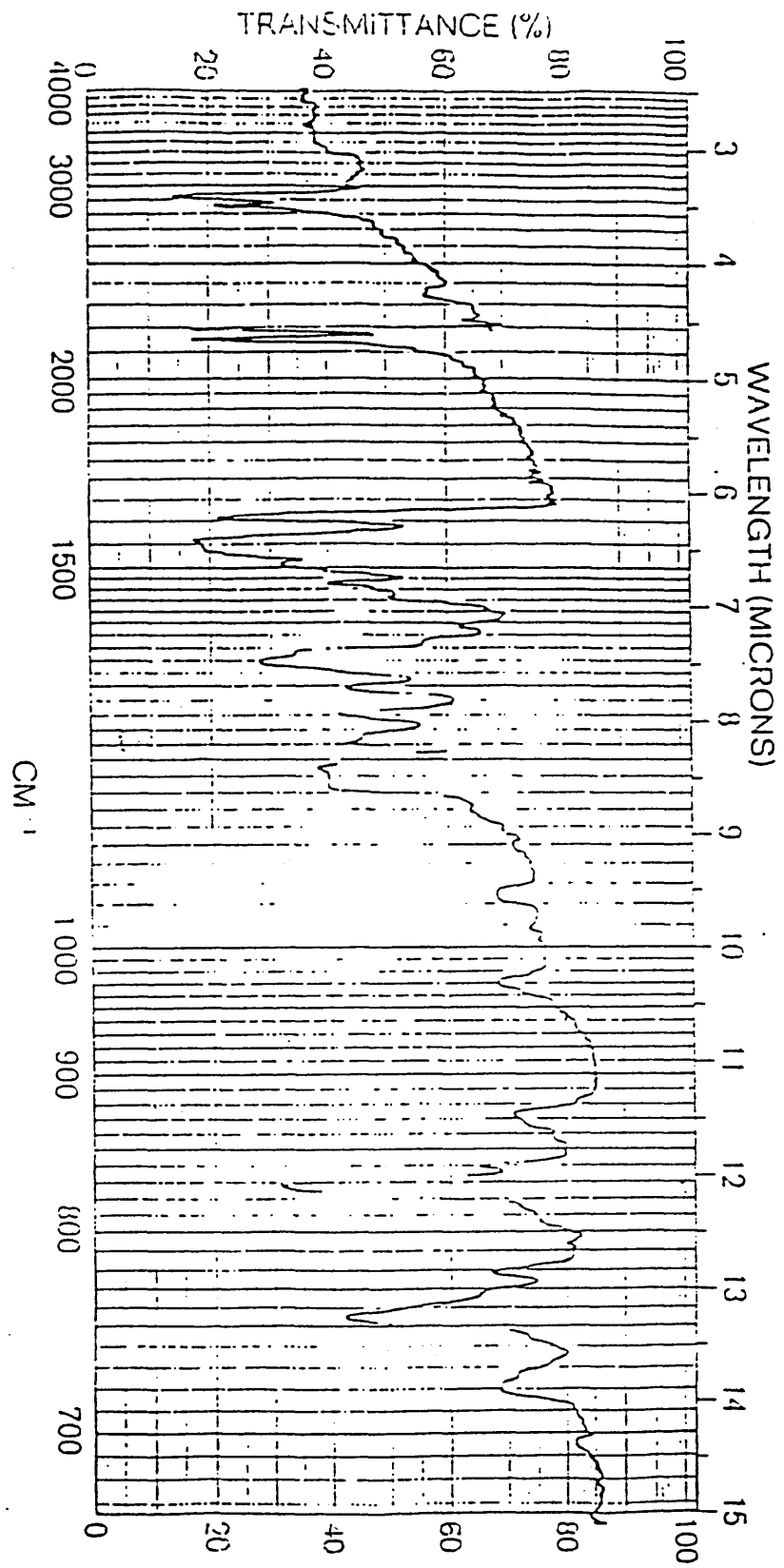


Figure 2.6 Infra red spectra for C<sub>11</sub>H<sub>23</sub>(4)Q3CNQ

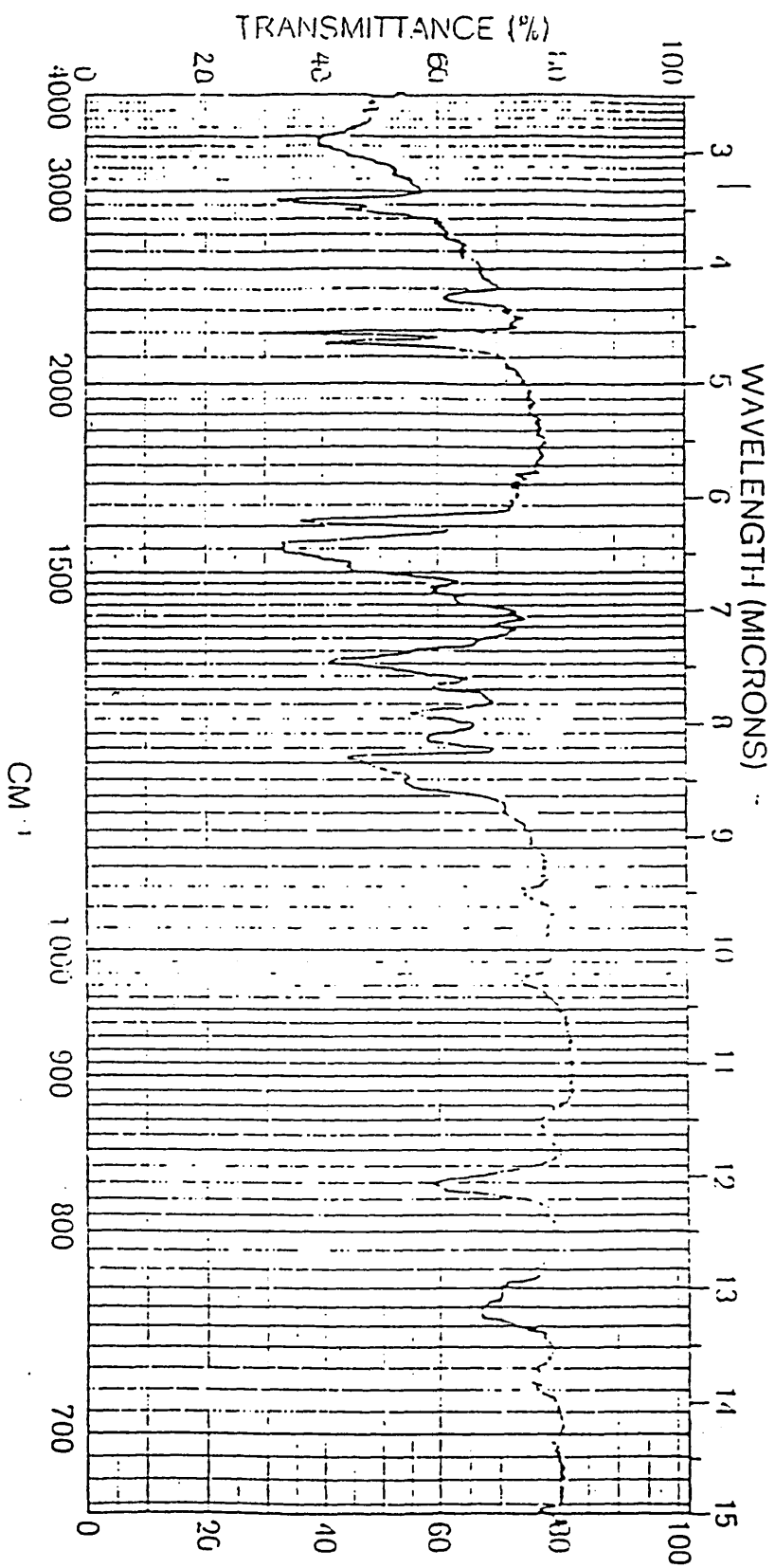


Figure 2.7 Infra red spectra for C<sub>15</sub>H<sub>31</sub>(4)Q<sub>3</sub>CN<sub>Q</sub>

Absorption Band	Assignment
2920 (s)	- C-H stretch
2200 (vs)	- C≡N stretch (neutral)
2150 (vs)	- C≡N stretch (ionic)
1600 (s)	- C=C stretch (aromatic)
1650 (s)	- C=C stretch (neutral)
1500 (s)	- C=C stretch (aromatic)

**Table 2.4** Infra-red spectral bands for an R(4)Q3CNQ adduct  
(s) strong; (vs) very strong

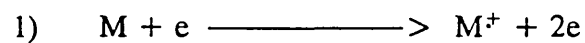
### 2.4.3 Mass Spectroscopy Studies

Mass spectroscopic data for a range of quinolinium and picolinium adducts, substituted in the '2' and '4' position of the donor ring have been obtained and interpreted. Several interesting fragmentation pathways of some diagnostic importance have been identified.

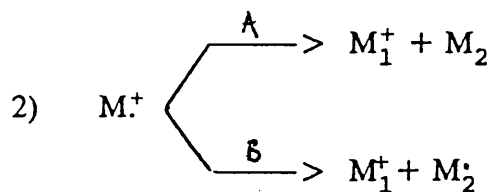
Examples of the spectra obtained are shown in figs 2.8 - 2.14.

The basis of the technique is the production of ions from neutral species.

Bombardment of the molecule with high energy electrons leads to the formation of a positively charged molecular ion. This molecular ion may then break into smaller fragmentation ions. The processes can be summarised as shown below:



ie loss of an electron leads to a radical cation.



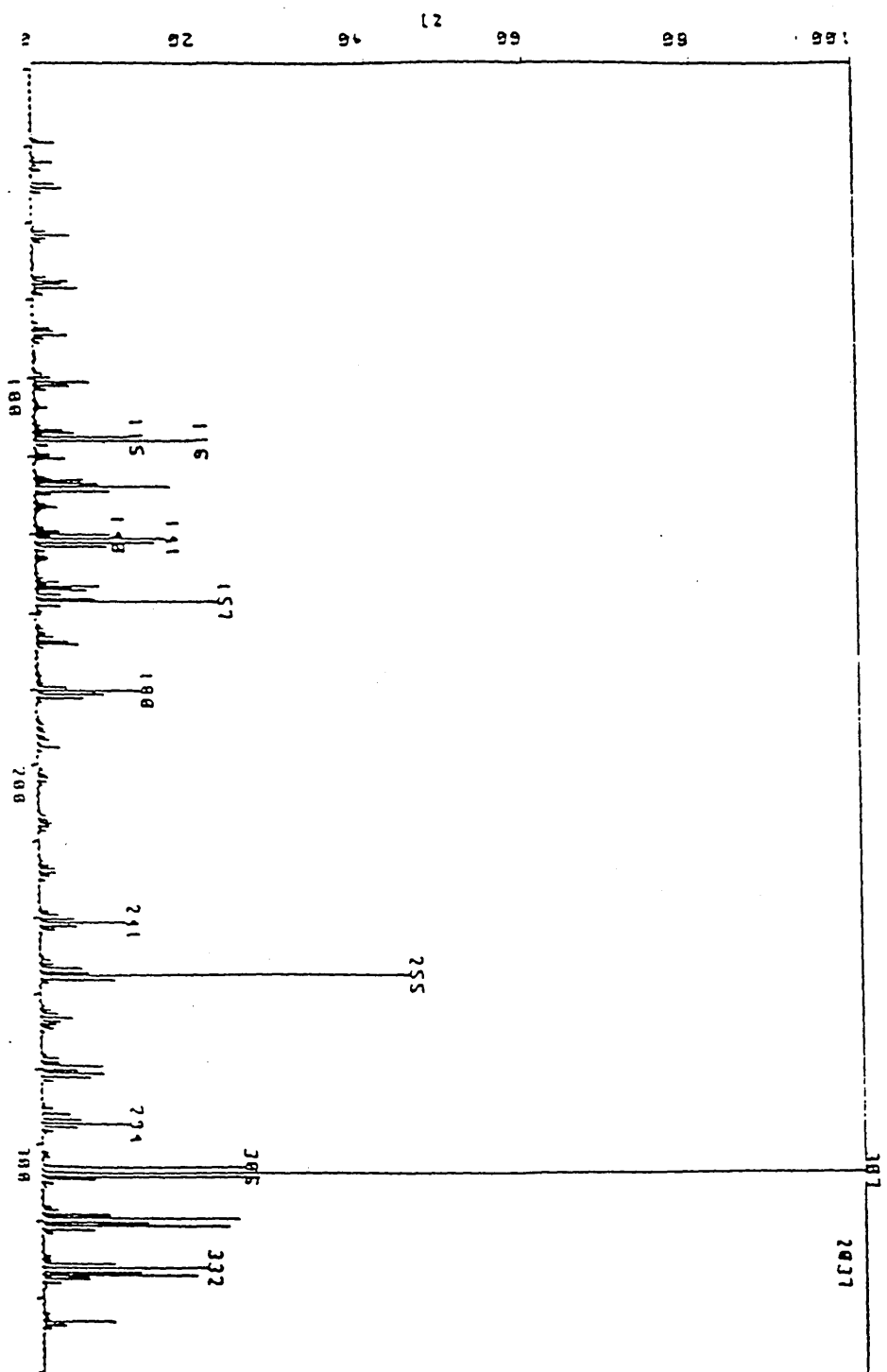


Figure 2.8 Mass spectra of Me(2)P3CNO

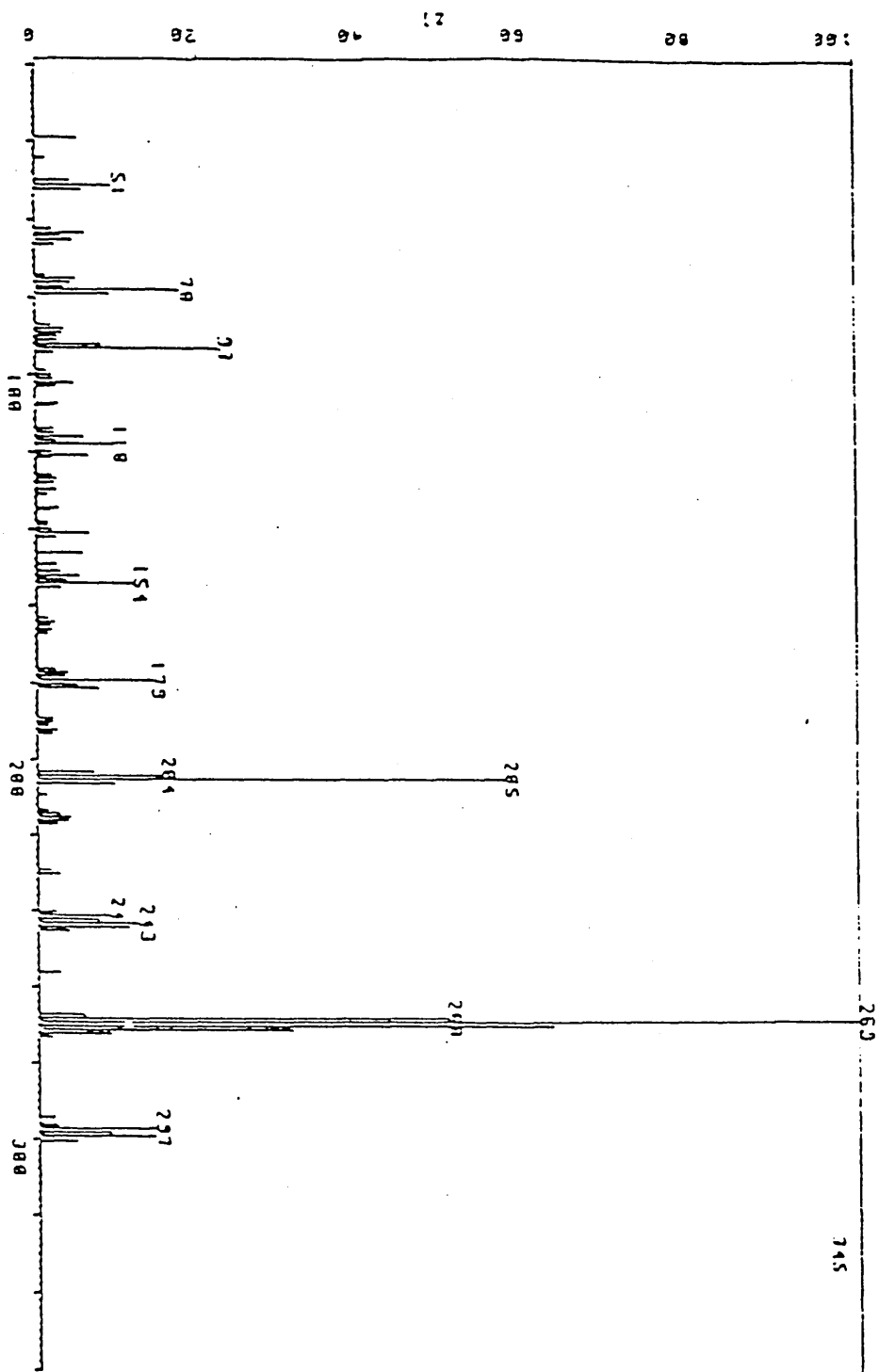


Figure 2.9 Mass spectra of Li(2)P3CNO

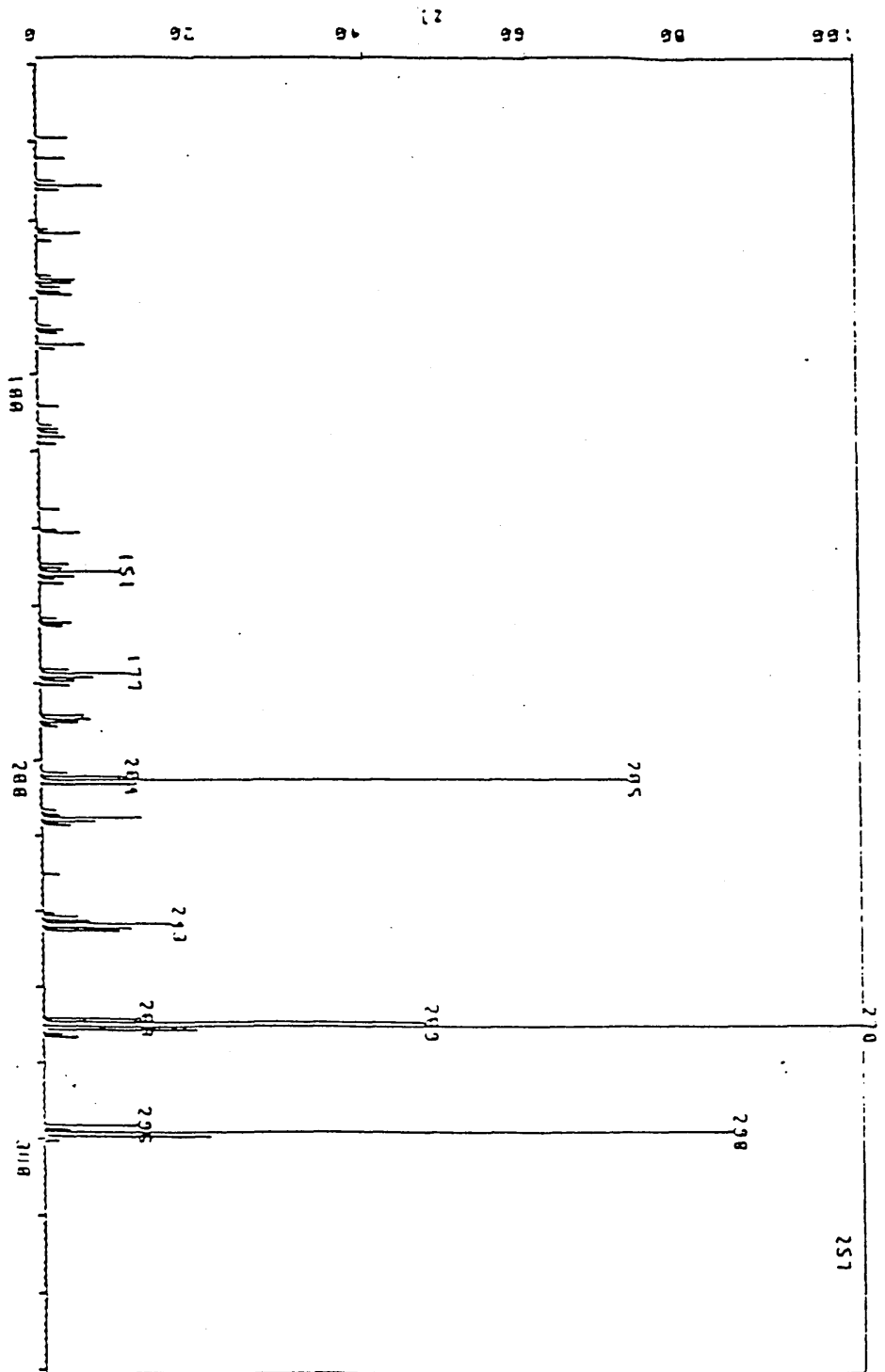


Figure 2.10 Mass spectra of Et(4)P3CNO

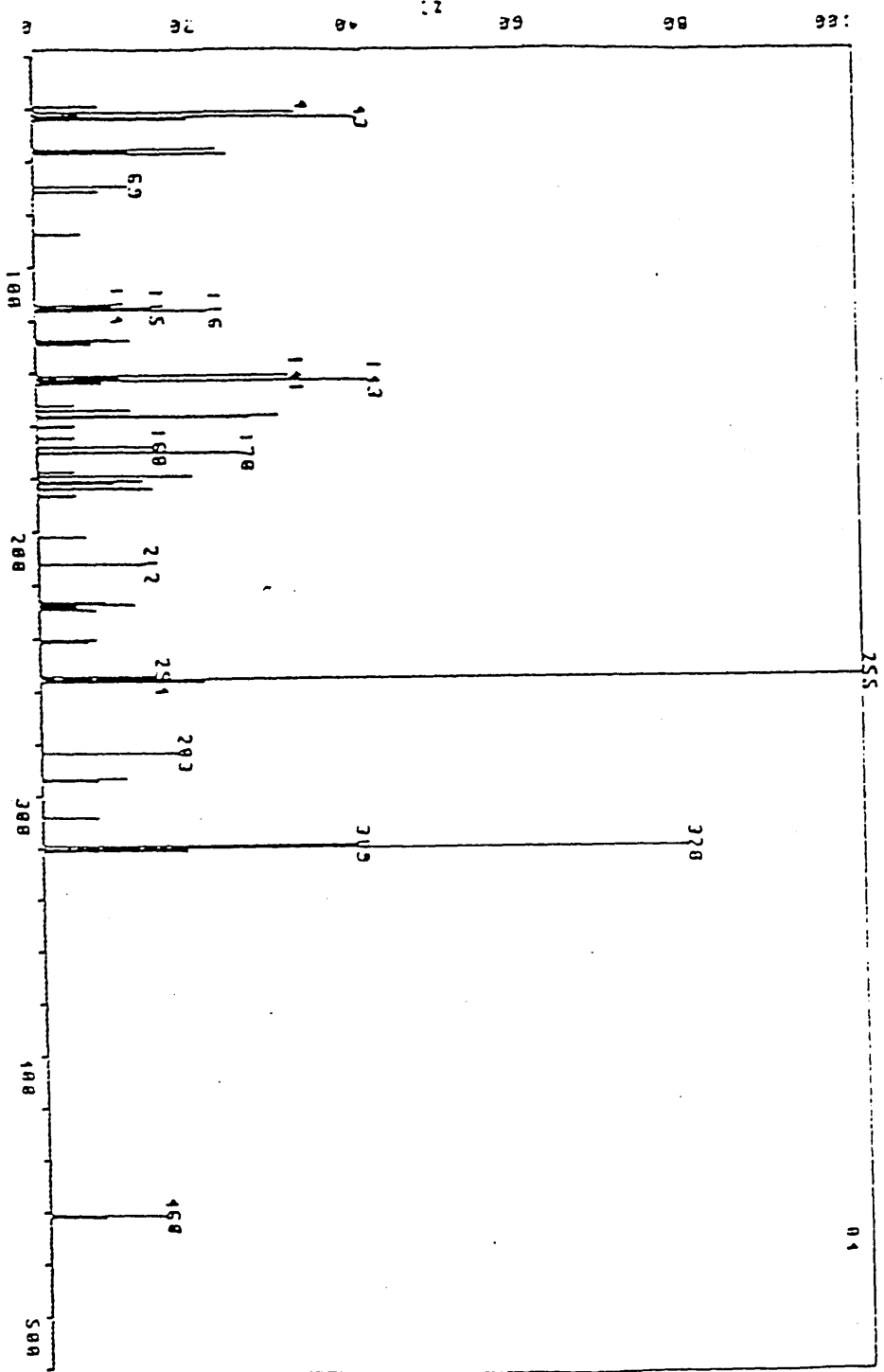


Figure 2.11 Mass spectra of  $C_{10}H_{13}(4)O_3CNO$

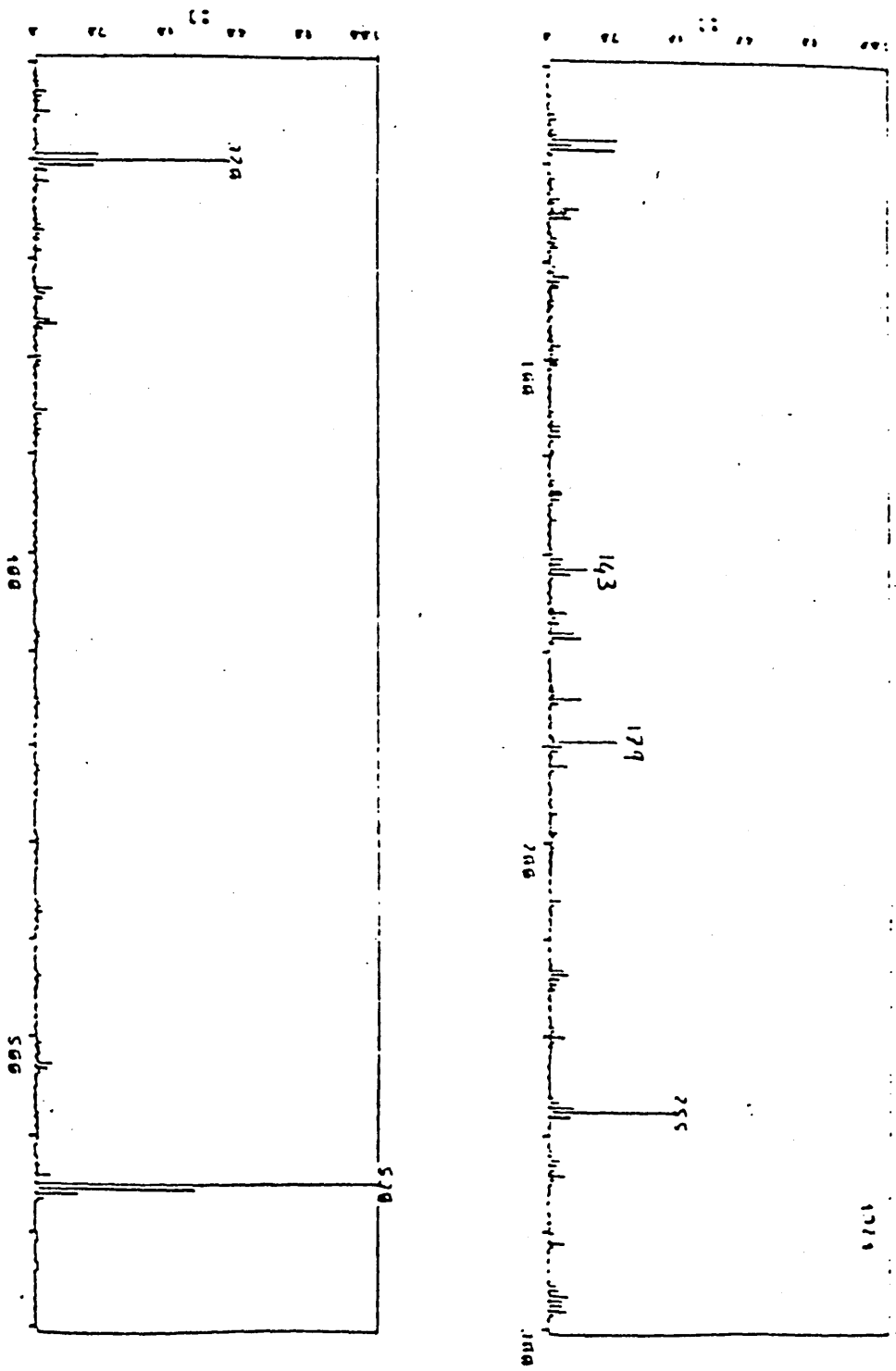


Figure 2.12 Mass spectra of  $C_{15}H_{11}(4)O_3CNO$

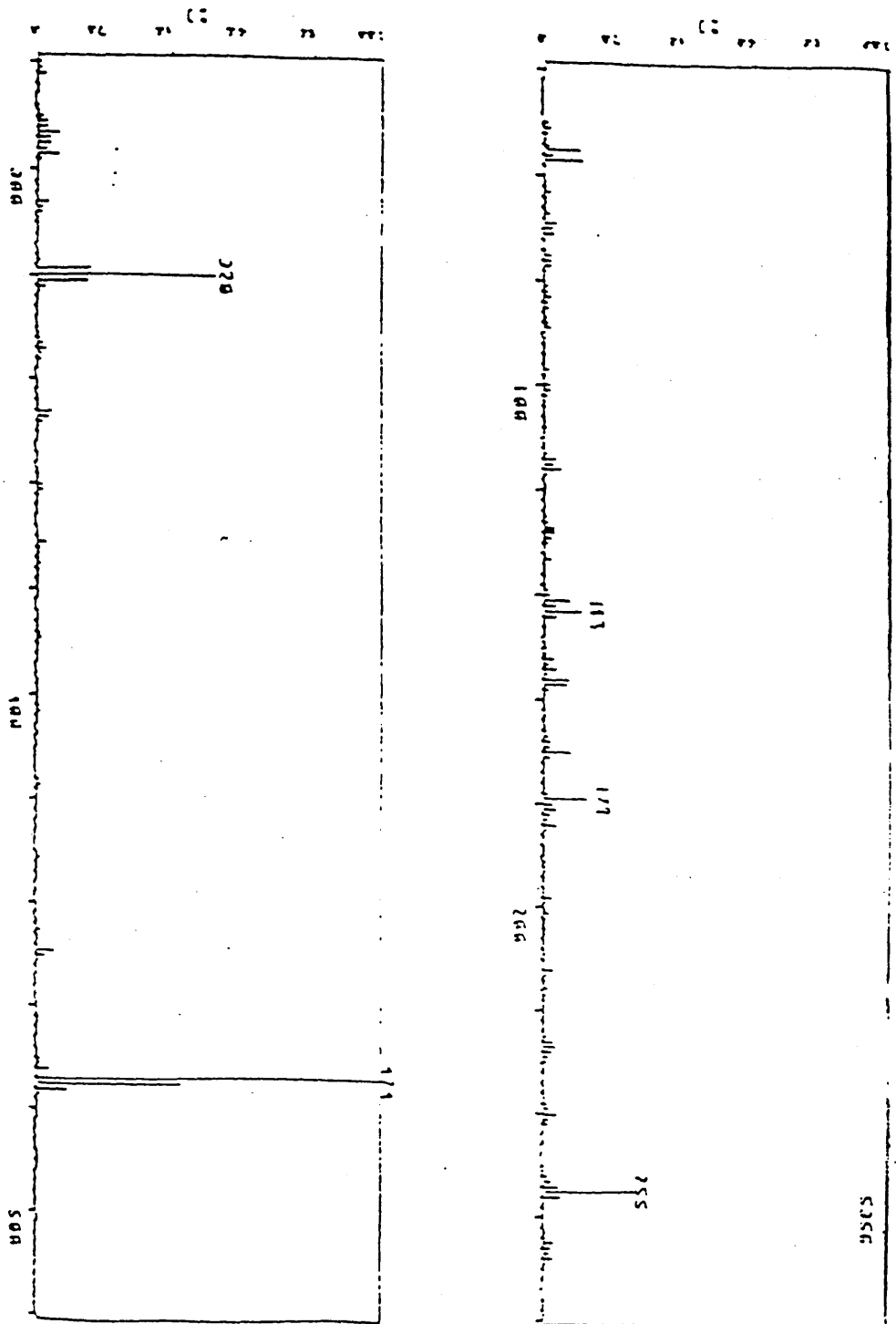


Figure 2.13 Mass spectra of  $C_{11}H_{23}(4)O_3CNO$

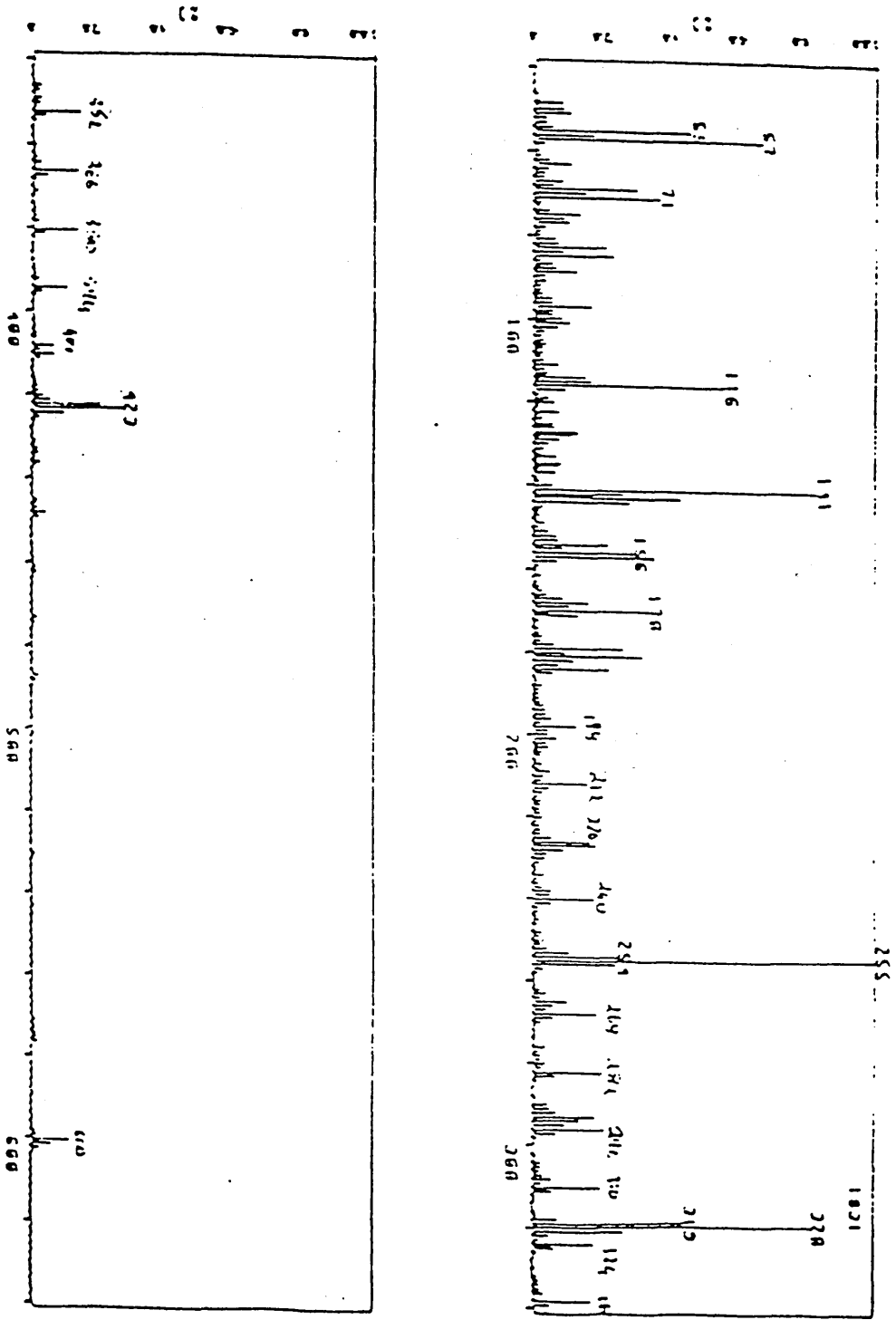
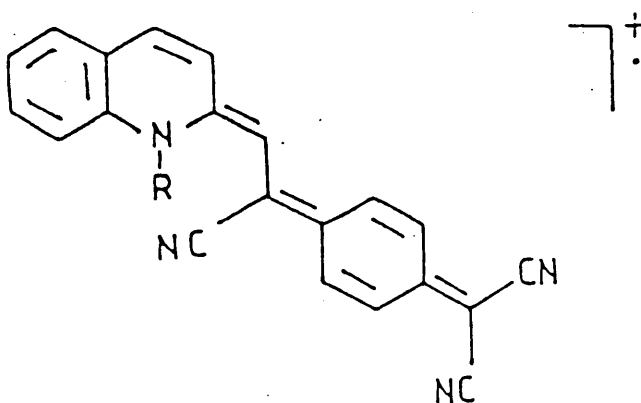


Figure 2.14 Mass spectra of  $C_{20}H_{41}(4)O_3CNO$

Pathway A leads to a new radical cation and a neutral molecule as shown, and B to a cation and a radical.

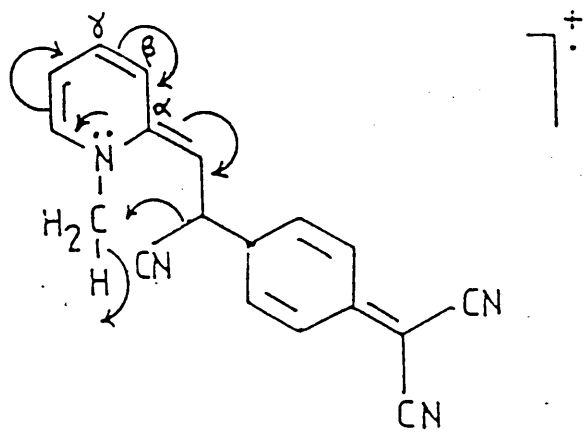
Bearing these principles in mind, the spectra can be analysed. For ease of interpretation, the molecular ion is best regarded as involving the quinoid structure as shown in figure below.



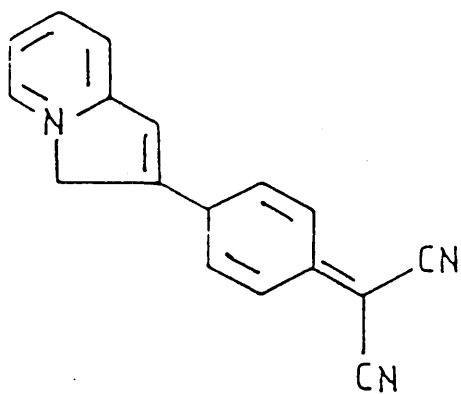
$$RMM = 329 + 'R'$$

Consider the spectra shown in figures 2.8 and 2.9. These quite clearly show the loss of the neutral molecule HCN where the  $\alpha$ -position of the quinolinium/picolinium donor is available. Fig 2.10 shows the spectra of Et(4)P3CNQ and such substitution in the

$\gamma$ -position does not lead to loss of HCN. The following mechanism shows why this is the case:



RMM 284



RMM 257

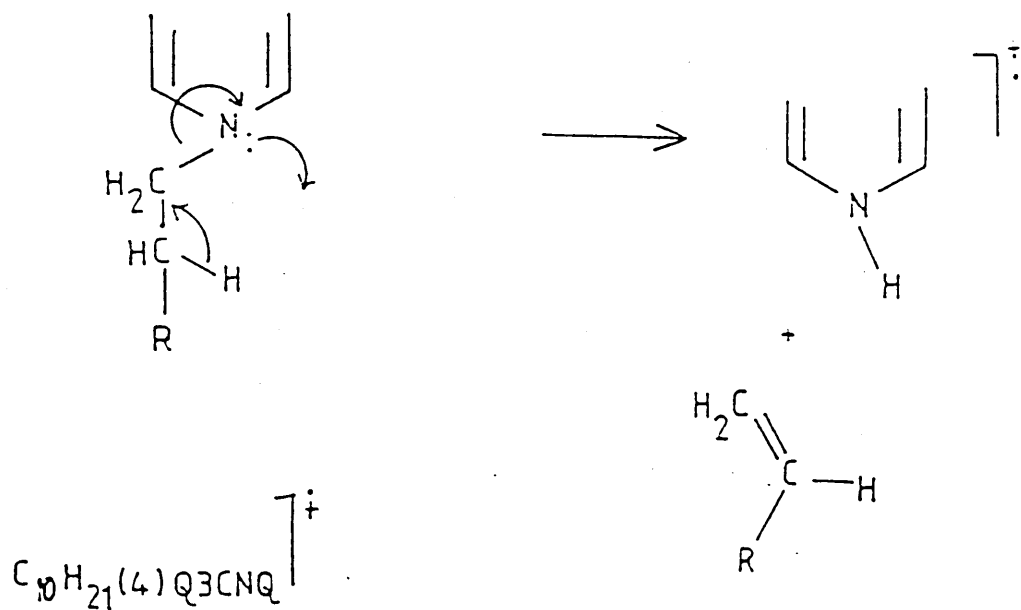
+HCN RMM 27

This mechanism, resulting as it does, in the production of a five-membered ring, can only occur when substitution occurs in the  $\alpha$ -position and not the  $\gamma$ -position. When applicable, such a fragmentation pathway is favourable due to the relative stability of the five-membered transition state and the resulting formation of product ion and neutral HCN.

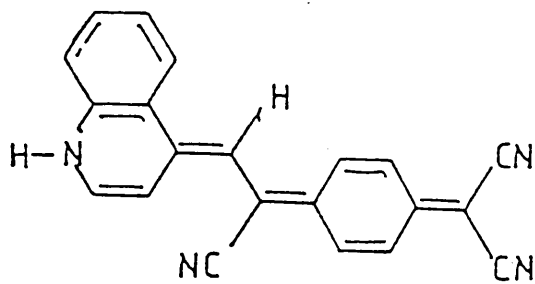
In both picolinium and quinolinium,  $\alpha/\gamma$ -substituted adducts, where the alkyl chain is of 2-carbon atoms or more, then loss of an alkene, as a neutral molecule, occurs. Again, the proposed mechanism involves a cyclic transition state - as shown over page, and these fragmentations are identifiable in the mass spectra of  $C_{15}H_{31}(4)Q3CNQ$  (fig 2.12),  $C_{11}H_{31}(4)Q3CNQ$  (fig 2.13) and  $C_{20}H_{41}(4)Q3CNQ$  (fig 2.14).

All  $R(4)Q3CNQ/R(2)Q3CNQ$  adducts show a strong peak at RMM 255 and  $R(4)P3CNQ/R(2)P3CNQ$  at RMM 205. It is proposed that these fragments correspond to the structures shown in Figure 2.15.

For example, from figure 2.11



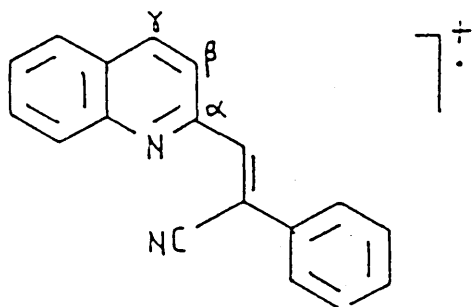
RMM 460



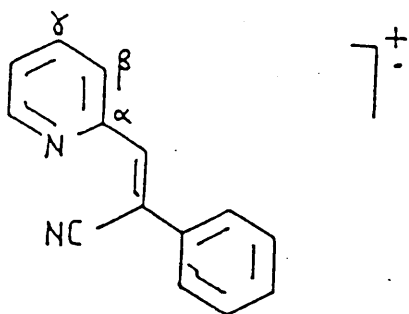
RMM 320

+  $C_8H_{16}CH \equiv CH_2$

RMM 140



RMM 255



RMM 205

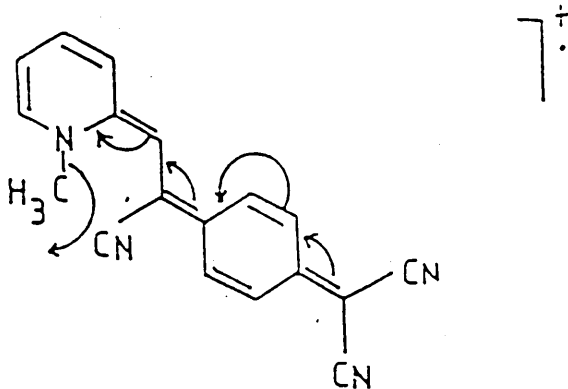
Figure 2.15 Proposed fragmentation structures

The mechanism by which these structures are produced is outlined over the page and involves several fragmentations. Notice that the double bond is shown promoting reactivity - a mechanism which would appear unrealistic in the presence of the generally more reactive cyano groups. However, the mass spectroscopy technique involves such a high energy regime that such reactions cannot be ruled out.

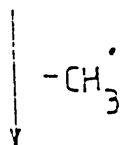
Step `2' involves the loss of a carbene, - a highly reactive intermediate and thus a favoured process. Step `1' involves the loss of the corresponding alkyl chain and is common to all the spectra obtained.

To conclude, distinct differences in the fragmentation patterns are apparent between  $\alpha$  and  $\gamma$  - substituted adducts which can readily be explained by facile mechanisms.

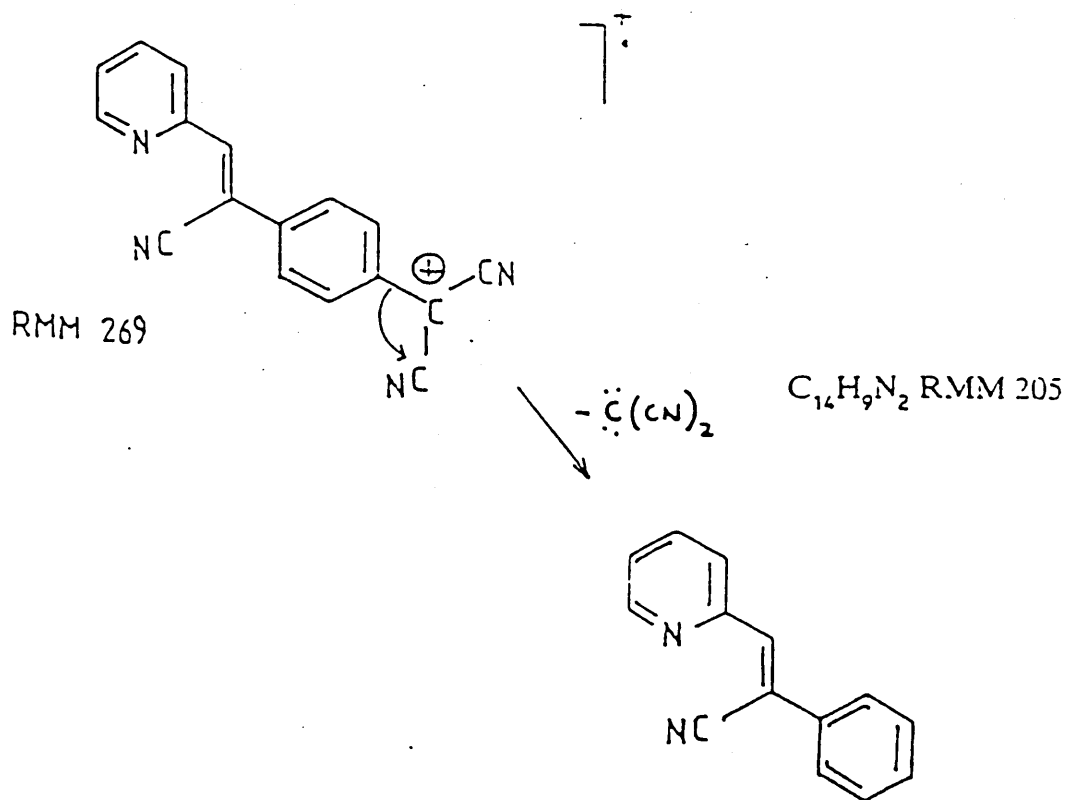
1)



Molecular ion RMM 284



2.)



Thermal analysis of various charge-transfer complexes of TCNQ, using differential scanning calorimetry (DSC), have shown that certain interesting features can be explained by the presence of solvent trapped in the crystal lattice.<sup>15</sup> For the production of good quality LB films for molecular electronic applications, this would be undesirable.<sup>16</sup> Thus, materials were studied using DSC, and no phase changes corresponding to the presence of trapped solvent were observed.

## 2.6 REFERENCES

- 1 R M Metzger, N E Heimer and G J Ashwell; *Mol Cryst Liq Cryst*, 107, 133, (1984)
- 2 D S Acker and W R Hertler; *J Am Chem Soc*, 84, 3370, (1962)
- 3 I R Girling, Personal Communication
- 4 M Szablewski, MPhil thesis, Cranfield Institute of Technology, (1989)
- 5 K M C Davis in "Molecular Association" vol 1, Ed.R Foster, Academic Press (1975)  
W Liptay, *Angew Chem Int Ed Engl*, 8, 177, (1969)
- 6 E Buncel and S Rajagopal, *Acc Chem Res*, 23, 226, (1990)
- 7 C Reichardt, *Solvent Effects in Chemistry*, 2nd Ed, Verlag Chemie, Weinheim, (1988)
- 8 H W Gibson, *Tetrahedron*, 77, 6789, (1977)
- 9 E M Kosower, *J Am Chem Soc*, 80, 3253, (1958)
- 10 L G S Brooker, A C Craig, D W Heseltine, P W Jenkins and L L Lincoln, *J AM Chem Soc*, 87, 2443, (1965)
- 11 A Botrel, A L Beuze and P Jacques, *J Chem Soc Faraday Trans 2*, 80, 1235, (1984)
- 12 J S Chappell, A N Bloch, W A Bryden, M Maxfield, T O Poehler and D O Cowan, *J Am Chem Soc*, 103, 2442, (1981)
- 13 A Terzis, E I Kamitsos, V Pscharis, J S Zambounis, J Swiatek and J Papavassilou, *Synth Met*, 19, 481, (1987)
- 14 *Basic Infrared Spectroscopy*, J H van der Maas, 2nd Ed, Heyden & Son Ltd, (1972)
- 15 G J Ashwell, I M Sandy, A Chyla and G H Cross, *Synth Met*, 19, 463, (1987)
- 16 R A Hann in 'Langmuir-Blodgett Films' Ed G G Roberts, Academic Press, (1990)

### 3.1 Historical Introduction

The phenomenon of oil on water has been known for many years. The Babylonian people, thousands of years ago, apparently observed the spreading of oil on water as a form of divinity.<sup>3</sup> Of perhaps a more practical nature, the Japanese art form *sumo-nagashi* involves the passing of paper through a spread suspension of carbon and protein molecules on a water subphase, to produce a patchwork design of dark and light areas.<sup>4</sup> The calming influence of "oil on troubled water" has also been known to fishermen throughout the ages.

However, the first scientific experiments on monolayers are accredited to the famous American Statesman and scientist, Benjamin Franklin. He reported to the Royal Society way back in 1774<sup>5</sup> that a teaspoon of oil dropped onto the pond on Clapham Common extended to an area of approximately half an acre. In common with the observations of mariners, he also reported on its calming influence. It was Lord Rayleigh,<sup>6</sup> some years later, who deduced that such a volume of oil, spread over such an area would produce a layer one molecule thick.

Concurrent with the work of Lord Rayleigh, a German schoolgirl, Agnes Pockels,<sup>7</sup> carried out a series of experiments determining molecular sizes. Out of this work, developed the apparatus which was the basis of what is now known as the Langmuir trough - although the actual apparatus she used amounted to little more than the kitchen sink.

The true significance of this seminal work by Rayleigh and Pockels went unnoticed for some years until a scientist working at the General Electric laboratories in Schenectady, New York, Irving Langmuir, fully developed the theory of

monolayers, work for which he was awarded the Nobel Prize. In an early communication,<sup>8</sup> he described the design of his film-balance, or trough, and showed how it could be used to deduce the molecular size and orientation of monolayers at the air-water interface.

The first description in detail of the sequential build up of monolayers onto a solid substrate was described by Blodgett<sup>9</sup> and such assemblies are now called Langmuir-Blodgett (LB) films. With the advent of the Second World War, the research interest into LB films ceased, and it was not really until the 1960's that the topic created renewed study. This was due to the work of a German group led by Hans Kahn who published a series of papers<sup>10</sup> on the effect of electron transfer in supermolecular assemblies. Since then, work in this field has continued apace, with five international conferences - in England, America, West Germany, Japan and France having taken place since 1983, and the sixth, in Canada, due later this year.

The microelectronics industry is currently very interested in thin organic films. Currently, the industry relies on inorganic materials for the majority of its needs, and the number of suitable materials is limited. There is a wealth of organic materials already known and countless others waiting to be synthesised. The ability of organic chemists to "tailor-make" molecules fitting a specific molecular requirement opens exciting possibilities - could these molecules be suitably fabricated? This, coupled to the obvious need for very much thinner, defect-free films of a precise order and thickness, is the attraction of LB film research. What, therefore, are the characteristics of those molecules suitable for study as potential LB film materials?

Classically, much of the work done on LB films involved the use of long chain fatty acids - shown schematically in fig 3.1 - of which stearic acid was one of the most widely studied.

In stearic acid there are seventeen carbon atoms constituting a hydrophobic (water-hating) hydrocarbon "tail", and a hydrophilic (water-loving) carboxyl "head" group. Such molecules are said to be amphipathic and it is this amphipathic balance between hydrophobic and hydrophilic moieties that is significant.

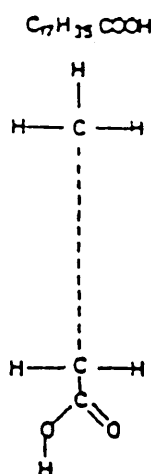


**Figure 3.1 Schematic diagram of a long chain fatty acid**

Other materials of this type have been widely studied including, for example, arachidic acid ( $C_{19}H_{39}COOH$ ) and behenic acid ( $C_{21}H_{43}COOH$ ). Thus from this early work, the key requirement was found to be a hydrophilic and hydrophobic

portion within each molecule. Some more specific structural types are now discussed.

The introduction of double bonds into the hydrocarbon chain has been achieved. For example,  $\omega$ -tricosenoic acid (fig 3.2) has been extensively studied. The presence of the terminal double bond in this material greatly reduces the disruption of the close-packed hydrocarbon chains, which is commonly observed when the double bond is situated mid-chain.

LB films of this material have been extensively studied due to their polymerisation when exposed to an electron beam.<sup>11</sup>

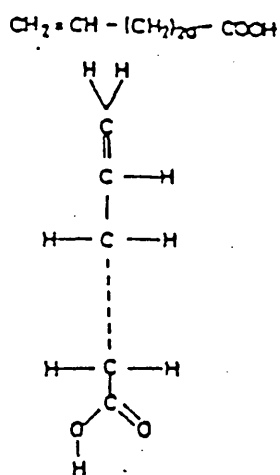


Figure 3.2  $\omega$ -tricosenoic acid

As well as being easily polymerised, such films exhibit excellent thermal and mechanical stability. The very similar alkyne derivative (fig 3.3) also readily undergoes polymerisation.

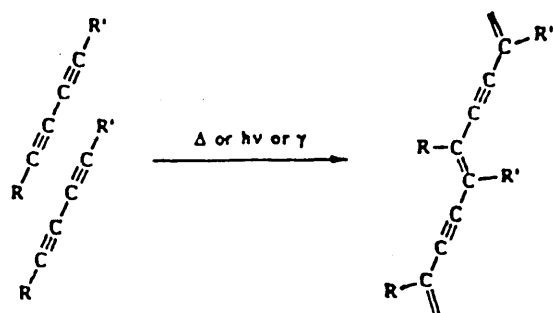
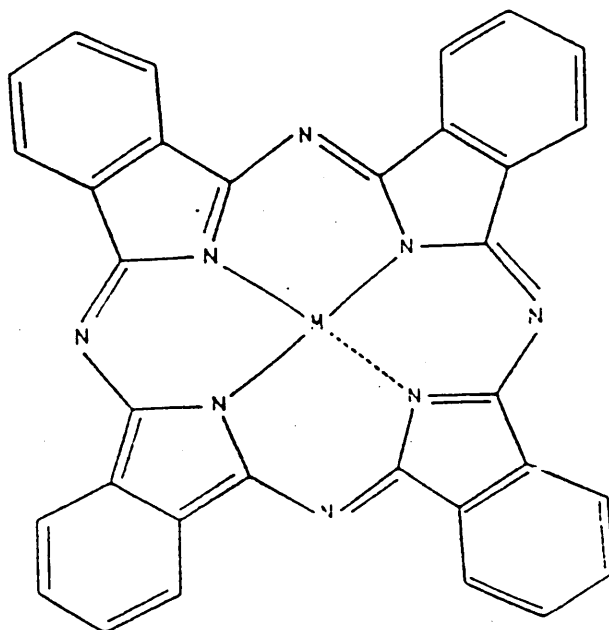


Figure 3.3 An alkyne derivative

It is a relatively straight forward task for the organic chemist to attach such long hydrophobic tails to many of the suitable hydrophilic head groups and then spread the material as a monolayer. Indeed, the number of film forming materials now known is vast and increasing steadily. These include variations upon the hydrophilic portions, including, for example, cyano<sup>13</sup> and sulphur<sup>14</sup> containing materials. The ability of preformed polymers to produce stable films is also well documented, both in early work<sup>15</sup> and more recent studies.<sup>16</sup> It has also been shown that many of the organic charge-transfer complexes described in Chapter 1 can produce LB films, in particular TCNQ-pyridinium salts<sup>17</sup> and TCNQ-TTF,<sup>18</sup> the first organic metal.

The attachments of long hydrophobic groups severely restricts any practical applications. Two factors may explain this: firstly, the presence of such large hydrophobic groups can introduce a large degree of instability and, secondly, the more interesting properties of the organic molecule can be severely diluted by the long aliphatic chain. Recently, therefore, more robust molecules containing much less aliphatic character have been fabricated as LB films. These include the phthalocyanines (fig 3.4), first studied at Durham<sup>19</sup> and porphyrins<sup>20</sup> (fig 3.5).



**Figure 3.4 Basic structure of a Phthalocyanine molecule**

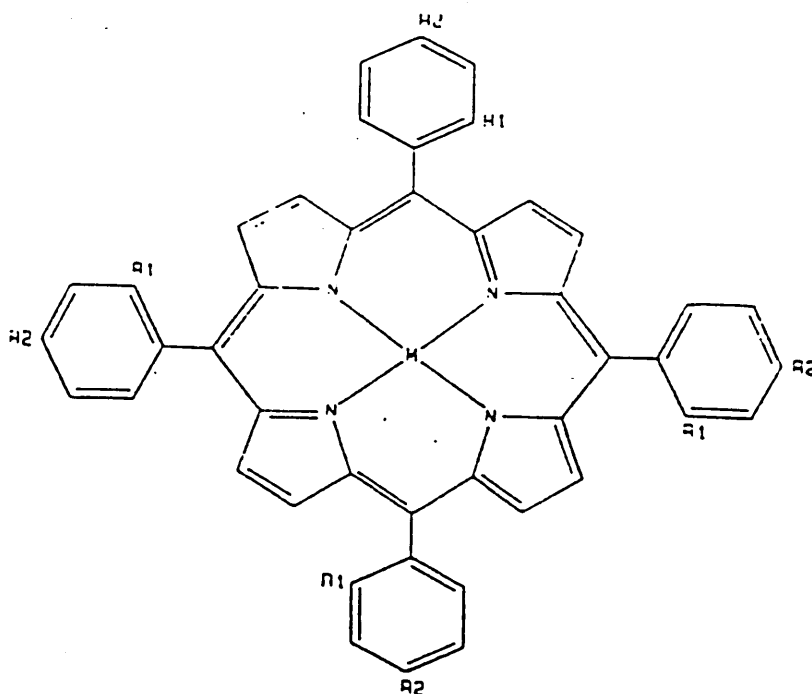


**Figure 3.5 A Porphyrin derivative**

Study of such species have shown that the films produced have a generally imperfect structure when compared to the long chain fatty acids, though this is perhaps the price to be paid as a consequence of greater mechanical and thermal stability.

Recently the ad hoc nature of the search for new materials has been somewhat superseded by more coordinated work on structure property relationships. Perhaps the first schematic study of this type was carried out on anthracene derivatives by scientists at Durham and ICI.<sup>21</sup> It was shown that systematic alteration of the hydrophobic and hydrophilic portions could enable molecules of the structure shown in fig 3.6 to be fabricated as LB films. Here R' is a carboxylate group and R can be as short as four carbon atoms.

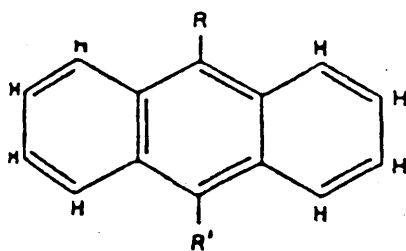


**Figure 3.6** A C-4 anthracene derivative suitable for fabrication as an LB film

Thus, one conclusion from this work was that the size of the aliphatic chains could be reduced if a polycyclic aromatic system was incorporated.

To conclude, therefore, the number of suitable materials is now extensive and work is now following a more systematic path as regards the often subtle external changes needed to effect gross changes in film behaviour.

### 3.3 Isotherm Measurement

Amphipathic molecules, dissolved in an appropriate solvent, may be spread upon a suitable subphase. The solvent then evaporates and the remaining molecules are compressed by means of a barrier. The resultant plot of surface pressure against area per molecule (an isotherm) obtained during the compression of a long chain fatty acid is shown in fig 3.7.

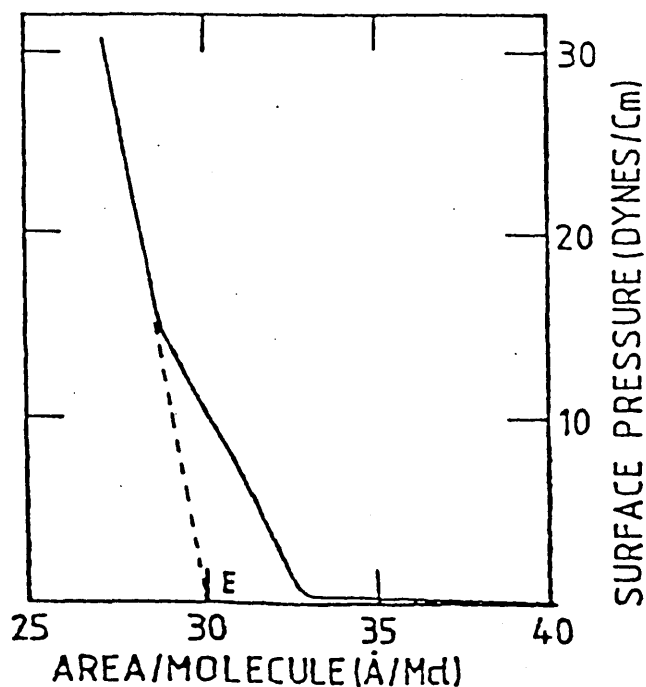


Figure 3.7 Surface Pressure vs area per molecule  
Characteristics for a long chain fatty acid

The floating monolayer is a two-dimensional system and can be described as a two-dimensional gas obeying the equation

$$PA = kT \quad (\text{Eq 6})$$

where 'P' is the surface pressure, 'A' the effective area per molecule, 'k' the Boltzmann Constant and 'T' the thermodynamic temperature. On compressing the monolayer the surface pressure increases and three distinct phase changes are observed, from gaseous through liquid to a condensed solid phase as identified in fig 3.7. However, it must be emphasised at this stage that many materials producing stable, good quality LB films do not produce the classic, three-phase isotherms obtained for fatty acids. For example, Barraud et al<sup>22</sup> have shown that the plateau observed in the isotherms studied during their extensive analysis of TCNQ-pyridinium salts can be explained by the formation of dimers on the subphase. The studies by Lewis et al<sup>14</sup> on sulphur containing molecules have also shown non classical behaviour, in this case, the anomalies are explained by gross reorientation on the water subphase of the amphiphile during compression. Indeed, the complexity of most LB film forming materials compared to the fatty acids would lead one intuitively to such conclusions.

Extrapolation of the linear part of fig 3.7 to point 'E', as shown, characterises the area at zero pressure and is taken to be the cross-sectional area of the molecule on the water subphase. From a consideration of this limiting area per molecule and the actual form of the isotherm, important data on the behaviour and suitability of a particular molecule can be obtained. As such, an important pre-requisite to the deposition of LB films is a full characterisation of the material on the subphase.

The quality of any isotherm obtained is crucially dependent on the quality of the subphase.<sup>23</sup> The purest quality water available is generally used. Most commercial water purification systems involve distillation processes, ion-exchange stages and reverse osmosis, though the exact requirements are dependent on many factors, including local water quality. (The exact system used in this study is discussed in section 4.6).

Recently there has been interest in the use of alternative subphases, in particular the use of glycerol to study, amongst other compounds, TCNQ based molecules<sup>24</sup>. In this case the use of glycerol reduces monolayer solubility and enables the use of solvents generally prohibited due to their solubility in water.

The presence of divalent metal ions can, in many case, aid the cohesion of conventional fatty acid and other charged monolayers. The resultant structure of such layers, and the self-explanatory reason for this, is shown in fig 3.8.

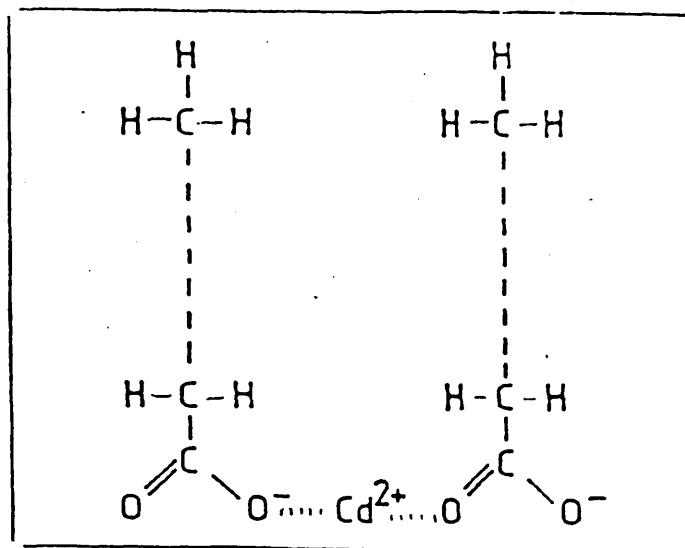


Figure 3.8 Molecular arrangement of fatty acid salts at the air-water interface

Such materials with ionisable head groups are also dependent upon the pH of the subphase - the presence of a suitable acid preventing the hydrolysis of the material. The combined effects of adding divalent metal ions and pH are shown in fig 3.9.

The quality of the monolayer is critical and it is this quality that eventually governs the properties of the film on a solid substrate. A major source of problems are the formation of molecular domains. These lead to the formation of imperfect films which, in the case of electrical applications, may not be able to withstand large electrical fields. The presence of domains can be substantially reduced if slow evaporating solvents are used to spread the material, for example mesitylene and long chain hydrocarbons.

The experimental consideration and precautions taken for producing reproducible isotherms will be discussed in greater length in Chapter 5.

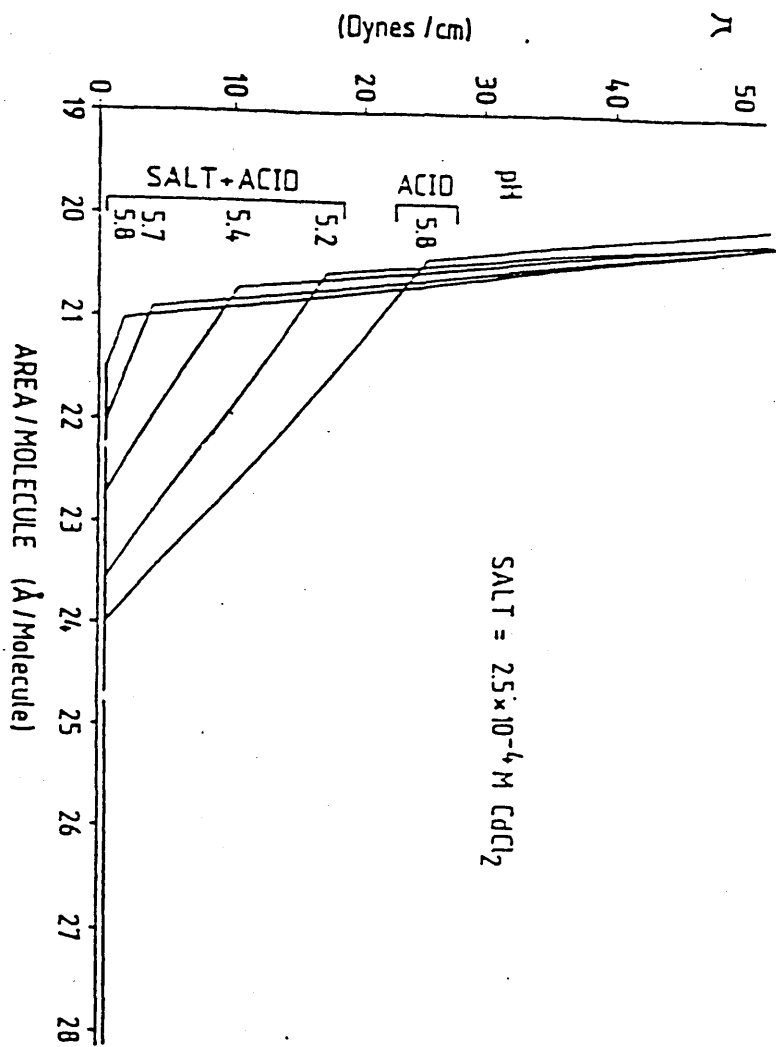


Figure 3.9 Effect of pH variation and divalent metal ion on Stearic Acid films

### 3.4 Deposition and Mono/Multilayer Assembly

The fabrication of an LB film involves the lifting of a suitable substrate vertically through a compressed monolayer, maintained at a predetermined surface pressure. Repeating this process a successive number of times produces a multilayered structure.

This vertical dipping method produces three distinct deposition modes - X, Y and Z types. The structure of these is shown in fig 3.10. As is clear, on each deposition cycle material may, or may not, be transferred to the substrate. The transference of material to the substrate manifests itself as a reduction in the area occupied by the film - the surface pressure necessarily remaining constant. Thus, the transfer ratio can be defined as:

$$\eta = \frac{\text{decrease in area of subphase covered by film}}{\text{area of substrate covered by the monolayer}}$$

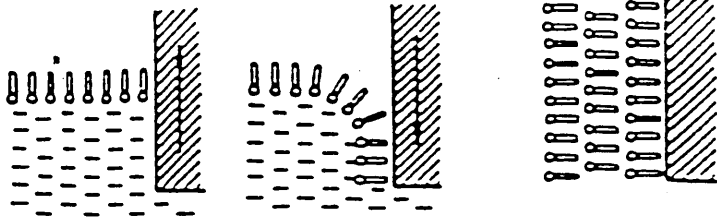
The value of  $\eta$  gives a good indication as to whether transference is occurring correctly - ideally  $\eta$  should be unity or zero. Values differing substantially may imply rearrangement of molecules or incomplete pick-up.

With reference to fig 3.10 then:

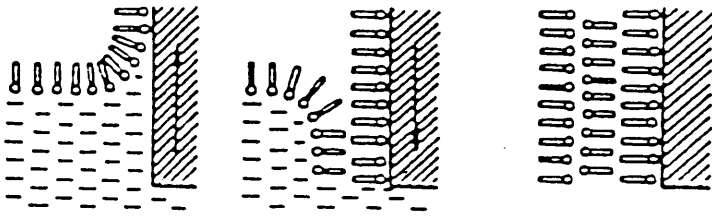
- a)  $\eta = 0$  and  $\eta = 1$ , X-type deposition
- b)  $\eta = 1$  and  $\eta = 1$ , Y-type deposition
- c)  $\eta = 1$  and  $\eta = 0$ , Z-type deposition

Notice that X- and Z-type depositions are associated with a single layer unit cell in a direction normal to the film surface, and that the Y-type is associated with a bilayer unit cell.

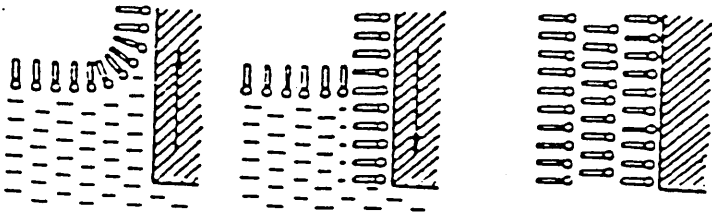
Figure 3.10 Vertical Dipping Technique



a)



b)



c)

a) X-type deposition<sup>N</sup>

b) Y-type deposition<sup>N</sup>

c) Z-type deposition<sup>N</sup>

Y-type deposition is by far the most common mode, though due to the non-centrosymmetric nature of X-type and Z-type there is considerable interest in these structures. However, as yet there is no clear understanding as to why some molecules deposit in this way.

Recently, workers have used a horizontal lifting method in order to transfer material in the gaseous and liquid monolayer states.<sup>25</sup> As its name implies, the substrate is held horizontally and lowered onto the monolayer from above, as shown in fig 3.11.

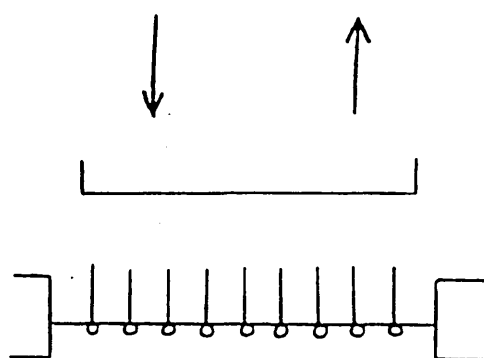


**Figure 3.11 The Horizontal Lifting Langmuir-Blodgett Technique (HLLB)**

In conclusion, therefore, the LB method for production of organised assemblies, free from vacuum processes and heating, provides a suitable mechanism for the production of very thin organic films of a defined structure and thickness.

### 3.5 Characterisation of LB Films

The methods available for the characterisation of LB films are many and varied, ranging from the very simple to the very complex. This short discussion shall start by describing the methods available for elucidating the structure of the film on the subphase and what this can tell us, proceeding then to the LB film itself - its morphology, molecular orientation, etc.

As has probably been made clear already, a great deal of information about the film forming potential of a particular molecule can be obtained simply from basic PA isotherms. These can show whether a particular molecule forms a film at the air-liquid interface at all, and if it does, whether the film is liquid, liquid-condensed, or condensed. It may also show the presence of any distinct phase changes undergone on compression. The area per molecule value can give a good indication of the molecular orientation, particularly if the value obtained is rather different from the value predicted on the basis of the known molecular structure. Whilst not in isolation offering conclusive proof, gross changes from expected PA behaviour - for example the observation of plateaus when  $P$  is essentially constant for sizable decreases in  $A$  - has led researchers to suspect that there is gross molecular reorientation occurring and some association between molecules, as discussed earlier. However, such observations could also be indicative of surface or compound contamination, and thus a certain amount of caution should be exercised.

However, for the full potential of LB films to be realised then it is the structure of the films themselves that need to be of a particular integrity, and it is the techniques used to investigate these that much of the research effort has been targeted.

Fortunately, many of the techniques available to solid state physicists, and developed over a number of years, are applicable to LB film characterisation..pa

Preliminary measurements on the thickness of the films are useful as these can tell

whether the films have been transferred with some integrity. For example, it can be shown that the molecule is lying purely perpendicular to the substrate or whether it is tilted to some degree, depending on the interlayer spacing determined. Basic optical techniques, for example Normarski microscopy<sup>26</sup> can be used in this respect. This technique is sensitive to the change in thickness either side of a step which is manifested as a phase difference in the emergent wave. Thus, as each layer will represent a "step", the thickness can be determined. Other techniques involve ellipsometry,<sup>27</sup> plasmon surface polariton field measurements,<sup>28</sup> though by far the most sensitive technique, giving the most accurate and detailed information comes from low-angle X-ray reflection.<sup>29</sup> This can determine the thickness down to a single layer with an accuracy better than 1Å. As well as giving details on the basic film structure, its technique can also be used to probe orientational changes in films when undergoing a chemical reaction. It has been particularly useful in elucidating the chemical change involved when a charge transfer salt of TCNQ, deposited as an LB film, is exposed to iodine vapour. Such salts are found to be insulating films before exposure to the iodine. On exposure, the films acquire a conductivity and shifts in X-ray peaks are indicative of changes in film thickness and an overall ordering of the film due to localisation of the iodine.

Other techniques applicable to the determination of intermolecular thickness are the variety of electron diffraction methods available. The high energy techniques are more commonly used either through the film - transmission electron diffraction (TED),<sup>30</sup> or orientated at a particular angle - reflection high-energy electron diffraction (RHEED).<sup>31</sup> These techniques are particularly useful as only the outermost layers of the films are studied and thus the technique is relatively non-destructive. Both techniques are sensitive even to a single layer. This is not to say low energy electron techniques cannot be used - indeed a single layer fatty acid film has been investigated using low energy electron diffraction (LEED).<sup>32</sup> As the wavelength of the electrons in this technique are similar to those of X-rays then

similar results could be expected to be obtained.

Study of the films by any of the techniques mentioned above will probably have revealed that the film is not perfect and that certain inhomogeneities and defects exist. So techniques are available for the examination and study of such film defects. Conventional microscopy is of some use in this area though overall its applicability is limited. Defects do not scatter light and thus observation of them with an optical microscope is apparent only by phase differences related to thickness differences between "pure" film and defect. If crystallites are present, then polarised light can be used which can deduce the birefringent character of such species.

For direct observation of the films, however, then scanning electron microscopy (SEM) is applicable.<sup>33</sup> This has even been used to observe a single layer. Though this may appear strange, because the penetrating depth of such electrons would be deep into the substrate and thus the film should be masked by this, there are differences in the secondary electrons emitted when the surface is covered with a monolayer. However, this technique has drawbacks, and a certain amount of caution should be used, particularly as to whether the film can withstand the treatment process and the high energy beams used for film visualisation.

Transmission electron microscopy (TEM)<sup>34</sup> has also been applied to this area and one great advantage of this technique is that it enables the texture of the film and the crystallographic pattern to be obtained from the same area of the sample.

Other surface investigative techniques involve Scanning Tunnelling Microscopy (STM)<sup>35</sup> often used alongside Auger analysis of the electrons emitted, thus providing comprehensive surface analysis. Recently, the powerful technique of Penning Ionisation Electron Spectroscopy (PIES)<sup>36</sup> has been applied to this field. This is a very surface sensitive technique in which the electrons do not penetrate

deep into the film.

Having obtained relevant film dimensions and an idea of the film morphology then it is clearly useful to study the film orientation. One of the most commonly used techniques is that of linear dichroism (LD).<sup>37</sup> This makes use of an anisotropic absorption of light by the film. If the electric vector of the polarised light is altered, then the absorption line will vary by an amount dependent on that electric vector and the transition dipole moment of the particular molecule. Such readings, if varied, can ultimately give rise to the various orientations of the molecule. This is clearly useful for highly polar molecules where the transition dipole moment is particularly well defined. Where the above dipole moment is not particularly defined, then the infra-red absorption bands are more commonly used as these are generally more distinct and easily categorised - though they are not as susceptible to orientational changes. Other useful techniques for studying molecular orientation are resonance Raman spectroscopy<sup>38</sup> and electron spin resonance spectroscopy<sup>39</sup> - though the latter of these techniques requires specific film requirements which must be met. Electron spin resonance is dependent upon the presence, to some degree, of free radical species and as such has been used in the study of LB film of TCNQ, and in particular conducting TCNQ/cationic films. As was discussed earlier, these systems are radical anion/cation systems.

### 3.6 Applications of LB Films

The proposed applications of LB films are many and varied and cover the range from electronics to biology. Various applications shall be discussed, though it must be stressed that there is a large amount of fundamental research needed before any real use will be found. For example, although there are many LB films that can be produced with a good deal of stability, to be able to do this reproducibly and to predict the stability of unknown materials, is still proving elusive. It is also not

certain that the technology exists to be able to fabricate the amounts of LB films needed to justify a commercial application, even if one could be proposed with confidence. However, although there is a long way to go, the number of proposed applications is numerous, and the field is expanding at such a rate as to give some cause for optimism.

To show both the fundamental and cross-disciplinary nature of LB film research, various biological film applications can be illustrated. LB multi-layers bear a striking resemblance to biological membranes. Such membranes essentially consist of fatty molecules - in fact phospholipids - together with a certain amount of carbohydrate and protein. Because such lipids are amphipathic then they tend to spontaneously orientate as an organised assembly. The structure of such an assembly is directly comparable to an LB film and Yoshikawa et al used such a film as a model system to study biological membranes.<sup>40</sup> Essentially, the system investigated attempted to "harvest" light energy which was then, by a process of many electron transfers, used to produce oxygen. The whole process was carried out at the molecular level. The light harvesting, energy transfer and subsequent reactions, were all successfully simulated artificially by using monomolecular layer assemblies. The assemblies consisted of donor and acceptor molecules interspersed with a harvester and sensitiser. Overlaps in the emission spectra of each enabled energy transfer via electron transfer to take place.

It has already been mentioned earlier that the adducts studied in this work may find uses in non-linear optical applications. The LB-film technique has prompted great interest in this area because of its ability to control (to a certain degree) the molecular orientation and structure of the films. The key to many applications in this area is the non-centrosymmetric nature of the system chosen for study. Very few single crystals satisfy this requirement and so Z or X-type LB films which are of a non-centrosymmetric nature have generated much interest. However, X or Z-

type films are generally found to be of poorer quality than Y-type structures for some reason. However, second harmonic generation has been reported in monomolecular layers<sup>42</sup> though the non-linear coefficient was not particularly large. Such observations have also been seen in non-centrosymmetric multilayers.<sup>43</sup> There have been reports of large second order coefficients using Y-type deposition. In one case the non-centrosymmetric structure results from a unique herringbone arrangement of the chromophores.<sup>44</sup> Other examples have relied on the principle of depositing alternate layers of different materials<sup>45</sup> - in this case the dipole moments of adjacent molecules would not cancel and the non-linear optical properties would be maintained.

Much work in the past has been directed towards the potential use of LB films as very thin resists.<sup>46</sup> As integrated circuit technology moved more and more to smaller and smaller circuit elements - as faster speeds and larger memories are sought - so the need for much better resolution is required. Thus, photolithographic techniques are being replaced by X-rays, electron and ion-beams. Extremely thin resists are one way in which the problem of scattering of substrate material around the point of impact when ion-beams are used can be reduced. The use of such thin resists require defect levels of negligible proportions which the LB technique has not yet shown itself to be reliably capable of.

LB films are generally excellent insulators, eg  $\text{C}_{18}$ -tricosenoic acid. They have therefore been the subject of much research towards their potential use in field effect semiconductor devices<sup>47</sup> and have been successfully used for active insulators on compound semiconductors.<sup>48</sup> However, because very many of the LB films studied have very low temperature tolerances, many manufacturers have been reluctant to use them. While there do exist films with very high temperature tolerances - for example aromatic or polymeric based materials - these are often films of much poorer quality, and so once again there appears to be the unfortunate

"trade-off" between film stability and quality.

However, there are grounds for optimism in the future of LB film research. Whilst admittedly there is no tangible evidence of electronic application after substantial funding and effort during the past few years, the unique ability to exercise a degree of control over the film development using this technique is encouraging.

Certainly, the scope for producing suitable organic amphiphiles is endless and so it can only be a matter of time before the molecule is found that can provide the easily transferred, defect-free, stable film sought.

Papers presented at the bi-annual conferences on Langmuir-Blodgett films have to date been published as special volumes of Thin Solid Films. The proceedings of the last conference in France<sup>49</sup> brings the reader up-to-date with the current state of the art.

### 3.7 REFERENCES

- 1 G G Roberts, *Adv Phys*, 34, 475, (1985)
- 2 I R Peterson, *J Phys D Appl Phys*, 23, 379, (1990)
- 3 D Tafor, *J Colloid Interface Sci*, 75, 240, (1980)
- 4 T Terada, R Yamamoto and T Watanabe, *Sci Pap Inst Phys Chem Res Jpn*, 23, 173, (1934)
- 5 B Franklin, *Phil Trans R Soc*, 64, 445, (1774)
- 6 Lord Rayleigh, *Proc R Soc*, 47, 364, (1890)
- 7 A Pockels, *Nature*, 43, 437, (1891)
- 8 I Langmuir, *J Am Chem Soc*, 39, 1848, (1917)
- 9 K B Blodgett, *J Am Chem Soc*, 57, 1007, (1935)
- 10 H Kuhn, D Möbius and H Bucher, *Physical Methods in Chemistry*, 1, 577, (1972)
- 11 A Barraud, C Rosilio and A Ruaudel-Teixier, *J Colloid Interface Sci*, 62, 509, (1977)
- 12 B Tieke, G Wegner, D Naegele, and H Ringsdorf, *Angew Chem, Int Ed Engl*, 15, 764, (1976)
- 13 M F Daniels, O C Lettington, and S M Small, *Thin Solid Films*, 99, 61, (1983)
- 14 T J Lewis, D M Taylor, J P Llewellyn, S Salvagno and C J M Stirling, *Thin Solid Films*, 133, 243, (1985)
- 15 G L Gaines, *Insoluble Monolayers at Liquid-Gas Interfaces*, Interscience, New York, (1966)
- 16 R H Tredgold, *Thin Solid Films*, 152, 223, (1987)
- 17 A Barraud, P Lesieur, A Ruaudel-Teixier and M Vandevyver, *Thin Solid Films*, 133, 125, (1985)
- 18 M Fujiki and H Tabei, *Synthetic Metals*, 18, 815, (1987)
- 19 S Baker, M G Petty, G G Roberts and M V Twigg, *Thin Solid Films*, 99, 53, (1982)
- 20 R H Tredgold, S D Evans, P Hodge, R Jones, M G Stocks and M C J Young, *Brit Polym J*, 19, 397, (1987)
- 21 P S Vincett, W A Barlow, F T Boyle, J A Finney and G G Roberts, *Thin Solid Films*, 60, 265, (1979)

- 22 A Barraud, M Florsheimer, H Mohwald, J Richard, A Ruaudel-Teixier and M Vandevyver, *J Colloid Interface Sci*, 121, 491, (1988)
- 23 O Albrecht, *Thin Solid Films*, 178, 563, (1989)
- 24 T Nakamura, M Matsumoto, F Tahei, M Tanaka, T Sehiguchi, E Manda and Y Kawabata, *Chem Lett*, 709, (1986)
- 25 K Fukuda, H Nakahara and T Uato, *J Colloid Interface Sci*, 54, 430, (1976)
- 26 M Francon, *Rev Opt* 2 (1952)
- 27 J O Birzer and H J Schulzer, *J Colloid Polym-Sci*, 264, 642, (1986)
- 28 B Rothenhansler, C Duschl and W Knoll, *Thin Solid Films*, 159, 323, (1988)
- 29 M Pomerantz and A Segmuller, *Thin Solid Films*, 68, 33, (1980)
- 30 I R Peterson, G J Russell and G G Roberts, *Thin Solid Films*, 109, 34, (1983)
- 31 I R Peterson, G J Russell, D B Neal, M C Petty, G G Roberts and T Ginnais, *Philos Mag B*, 54, 71, (1986)
- 32 V Vogel and C Woll, *J Chem Phys*, 84, 5208, (1986)
- 33 J B Lando and J E Hansen, *Thin Solid Films*, 180, 141, (1989)
- 34 R A Hann, S K Gupta, J R Fryer and B L Eyres, *Thin Solid Films*, 134, 35, (1985)
- 35 J H Coombes, J B Pethica, M E Welland, *Thin Solid Films*, 159, 293, (1985)
- 36 Y Harada, *Surf Sci*, 158, 2455, (1985); H Ozaki, Y Harada, K Nishiyama and M Fujihara, *J Am Chem Soc*, 109, 950, (1987)
- 37 K Ogawa, H Yonehara and E Maekawa, *Thin Solid Film*, 210, 535, (1992)
- 38 M Vandevyver, A Ruaudel-Teixier, L Brehamet and A Barraud, *Thin Solid Films*, 99, 41, (1983)
- 39 M Vandevyver, A Barraud, A Ruaudel-Teixier, P Maillard and C Gianotti, *J Colloid Interface Sci*, 85, 571, (1982)
- 40 K Yoshikawa, M Mahino, S Nakata and T Ishii, *Thin Solid Films*, 180, 117, (1989)
- 41 M Fujihira, M Sakomura, T Kamei, *Thin Solid Films*, 180, 43, (1989)
- 42 I R Girling, N A Cade, P V Kolinsky and C M Montgomery, *Electronics Letts*, 21, 169, (1985)
- 43 I R Girling, N A Cade, P V Kolinsky, J D Earls, G H Cross and I R Peterson, *Thin Solid Films*, 132, 101 (1985)

- 44 G Decher, B Tieke, C Bossard and P Günther, J Chem Soc Chem Commun, 933, (1988)
- 45 I Ledoux, D Joise, P Frenaux, J P Piel, G Post, J Zyss  
T McClean, R A Hann, P F Gordon and S Allen, Thin Solid Films, 160, 217, (1988)
- 46 M Vekita, H Awaji, M Murata and S Mizuuma, Thin Solid Films, 180, 271, (1989); H Kato, M Tawata, S Morita and S Hattori, Thin Solid Films, 180, 299, (1989)
- 47 G L Larkins Jr, C D Fung and S E Richert, Thin Solid Films, 180, 217, (1989)
- 48 J P Lloyd, M C Petty, G G Roberts, P G Lecomber and W E Spear, Thin Solid Films, 99, 297, (1982)
- 49 Thin Solid Films, Vols 210 - 211, (1992)

This chapter discusses the design and operation of the Langmuir trough used in this work. The more esoteric experimental considerations regarding isotherm recording, film stability, etc are discussed in Chapter 5.

### 4.1 The Joyce - Loebel Monolayer Coating Unit

This commercially available trough is of proven design and was originally developed by scientists at ICI and Durham University based on the idea of Blight et al<sup>1</sup>. It is used successfully by many academic and industrial research groups throughout the world.

The two essential features necessary in the operation of a Langmuir Trough - isotherm recording and monolayer removal - are fully automated. All mechanical units are made from corrosion resistant material. The main features of this, and indeed any other Langmuir Trough, are shown schematically in fig 4.1.

### 4.2 The Compression System

Traditionally, the container holding the liquid subphase forms an integral part of the compression system. In such a system, it acts as part of the boundary between the floating monolayer on the subphase and the clean water (monolayer free) beyond. Consequently, there is the need for incorporation of a suitable seal to limit any potential film leakage.

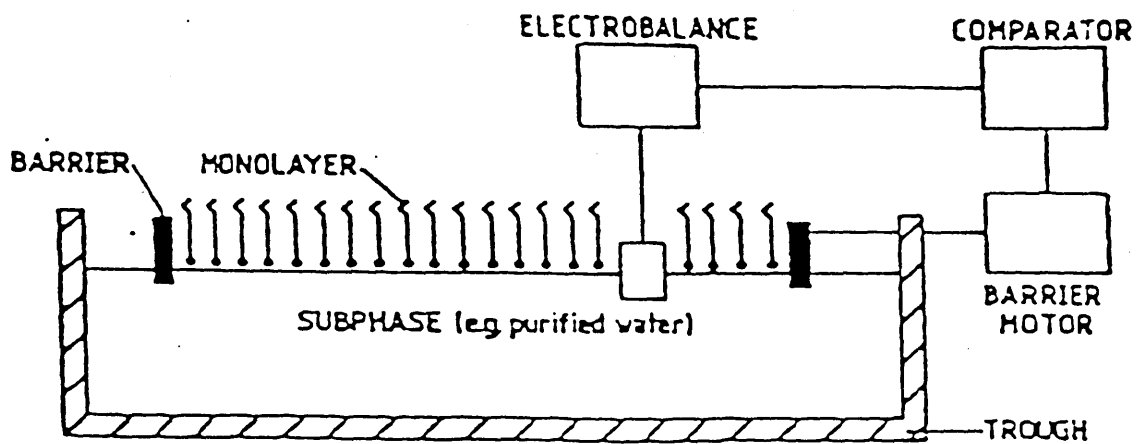


Figure 4.1 Schematic diagram of the essential features of a Langmuir Trough

An important feature of the Joyce - Loebel trough is the incorporation of a constant perimeter PTFE coated glass fibre barrier to define the working area. This system keeps the problems of film leakage (mentioned above) and contamination to a minimum. The design of the barrier is outlined in fig 4.2.

The compression barrier is a belt of width 2cm, and is held in place by a system of six PTFE rollers which are in turn secured by two mobile overarms. By means of a highly geared motor the mobile overarms are moved symmetrically inwards or outwards. At all times the barrier is kept taut and thus the size of the film area can be carefully controlled. The study of the film in both compression and expansion mode is possible at a range of speeds.

#### 4.3 Surface Pressure Measurement

The Wilhelmy Plate technique used to monitor the surface pressure is very reliable and can be used accurately for a range of surface pressures. A sensitive microbalance attached to a sensor (typically a piece of Whatman Grade 1 chromatography paper) in the subphase measures the differential pressure. This is shown schematically in fig 4.3.

As is shown, the plate is semi-immersed in the subphase and is attached to a microbalance directly above it via a thread. Hence, counterbalancing forces on the microbalance can be directly linked to the surface pressure provided the microbalance is sensitive enough to cope with the small forces involved.

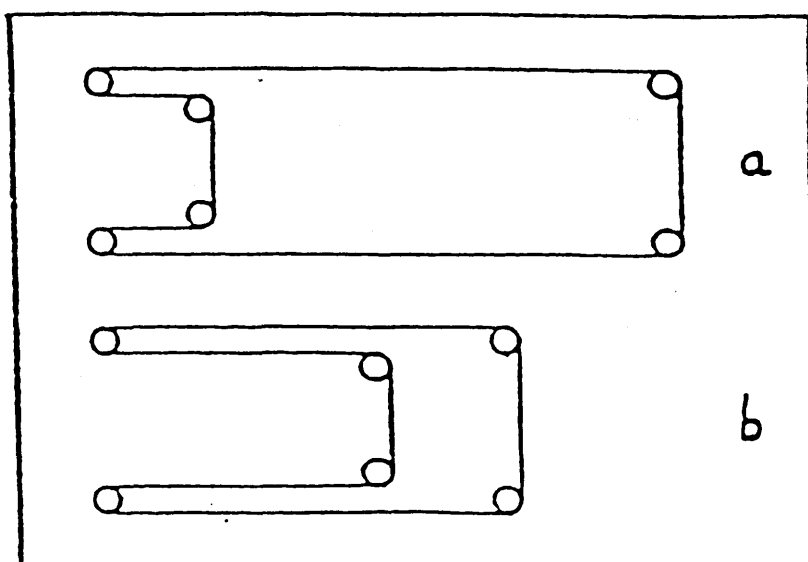


**Figure 4.2** Molecules deposited within an area defined by PTFE barrier as shown

- a) Maximum Area
- b) Minimum Area

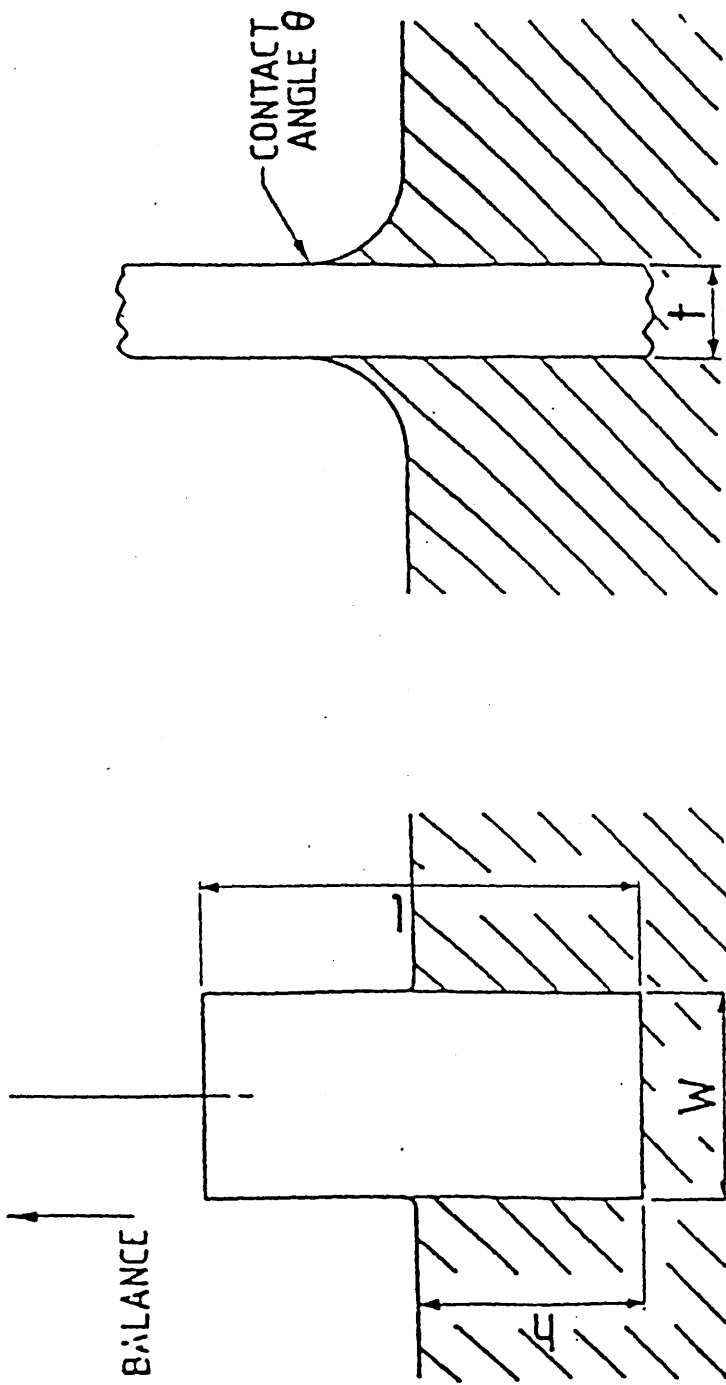


Figure 4.3 Representation of Surface Pressure Measurement

The forces acting on the plate are gravity and surface tension downwards, and buoyancy due to displaced water upwards. Thus, for a plate of the dimensions shown - length 'l', width 'w' and thickness 't', immersed to a depth 'h' with a contact angle  $\theta$  (fig 4.3), the net downward force is given by

$$F = \rho_p g l w t - \rho_o g l w h + 2 \gamma (t + w) \cos \theta \quad \text{Eq (7)}$$

where  $\gamma$  is the surface tension; 'g' the gravitational constant and ' $\rho$ ' is the density ( $\rho_p$  = paper density;  $\rho_o$  = subphase density). The surface pressure ' $\pi$ ' is regarded as being the reduction in surface tension occurring when the subphase is covered by a monolayer - ie it is the expanding pressure of the monolayer opposing the natural contracting tension of the subphase surface.

Thus,

$$\begin{aligned} \pi &= \gamma_o - \gamma_1 \\ &= \Delta \gamma \end{aligned}$$

where  $\gamma_o$  = surface tension of the clean liquid,  $\gamma_1$  = surface tension of the subphase covered with a monolayer.

Hence

$$F = 2(\gamma_o - \gamma_1)(t + w) \quad \text{Eq (8)}$$

assuming that the contact angle,  $\theta$ , is zero (ie  $\cos \theta = 1$ ).

Thus, if the plate is of negligible thickness and width 1cm and ignoring the upward force due to the displaced monolayer, then

$$F = 2 \Delta \gamma \quad \text{Eq (9)}$$

ie, the weight measured in mg is equal to twice the surface pressure measured in  $\text{mN}\cdot\text{m}^{-1}$ .

#### 4.4 Trough Operation

The detail given below is quite general, and is not specific to any one material or indeed any subphase.

##### 4.4.1 Cleanliness

The need for scrupulous cleanliness has already been shown and its importance cannot be stressed too highly. Many of the problems encountered in monolayer work are due to the presence of impurities and other "surface active" contaminants. Rigorous cleaning procedures and the use of highest purity solvents available are essential, as well as carrying out experiments in the cleanest environment possible.

The trough was cleaned at least three times weekly using alternate washings of dichloromethane or chloroform, iso-propyl alcohol and high purity water. The barrier and rollers were also cleaned at the same time, using the same procedure. Although the system incorporated a fan to presumably keep the air around the water subphase circulating, it was found that this introduced severe turbulence on the water subphase and consequently was not used. Indeed, the whole working system was mounted on an anti-vibration table.

#### 4.4.2 Trough Calibration

Before use, all separate instruments - pH meter, microbalance and chart recorder were calibrated in accordance with their respective manufacturers instructions, and recalibrated at regular intervals.

##### 4.4.2.1 Calibration of Surface Area

For reproducible, accurate isotherms to be obtained then the abscissa of the X-Y chart recorder must be calibrated. To do this, knowledge of the maximum and minimum areas within the constant perimeter barrier is required. The approximate values of these are 1000cm<sup>2</sup> and 100cm<sup>2</sup>, though all researchers should determine the exact value of these for themselves. Because the speed at which the barrier is moving prior to attaining the maximum and minimum areas affects exactly when the microswitches trip, the speed used for area calibrations should be that at which the isotherm measurement takes place.

##### 4.4.2.2 Calibration of Surface Pressure

When the microbalance has been correctly calibrated by the use of standard weights, then the surface pressure is directly related to the dimensions of the Wilhelmy plate as discussed previously at 4.3. Thus, the ordinate of the X-Y recorder can be most readily calibrated by the addition of known weights to the microbalance.

#### 4.5 The Subphase

Most of the work carried out on Langmuir Troughs requires an aqueous subphase. The purest quality water available is used. In this work a Millipore "Milli-Q" water purification unit was employed feeding water of  $18\text{m}\Omega$  resistance directly into the trough as and when required. This system makes use of an initial reverse osmosis stage followed by a system of "polishing" filters which ultimately remove contaminants at the biological level. When adding divalent metal ions to the subphase (to aid certain film stability, and discussed earlier), then these must also be of the purest grade available. Similarly with the addition of acid or alkali to raise or lower the subphase pH. It is advisable to change the water - cleaning the trough at the same time - at least every other day, and certainly after the weekend, or whenever the system may not have been used for some time.

#### 4.6 Subphase Surface Cleaning

Obviously, for reproducible results to be obtained, then the level of surface contamination should be kept to an absolute minimum. It is therefore necessary to clean the subphase surface prior to the spreading of the monolayer material. Such cleaning is routinely done by attaching a clean glass pasteur pipette (preferably new) to a suitable suction pump and then sucking the surface clean. Depending on the mains pressure then a simple water pump will suffice, or if this is not available then a pump capable of taking a mixture of both air and water is necessary. Once the surface has been cleaned then its quality must be checked. Checking for the degree of contamination present is easier if the surface is cleaned at minimum area (ie fully closed), then opening the barrier and closing slowly. Any appreciable increase in the surface pressure is indicative of surface contamination and the process should be repeated. Ideally, if the subphase is totally clean then there will be a zero increase in the surface pressure.

This technique has recently been criticised by Albrecht<sup>2</sup> who pointed out that any system where the barrier cannot close to give an absolute zero, will still have an appreciable area left which, on compression, could show surface contamination. The way to overcome this may be to spread and compress a well characterised amphiphile (for example, stearic acid) and observe any deviations from the standard isotherm.

#### 4.7 Monolayer Material Preparation and Spreading

A standard solution (known concentration) of the desired material must first be produced in a suitable solvent. Solvents commonly used in Langmuir-Blodgett work are shown in Table 4.1

SOLVENT	Mpt (°C)	Bpt (°C)	SOLUBILITY g/1000g H <sub>2</sub> O
n-hexane	- 94	69	0.01
cyclohexane	6.5	81	0.07
benzene	5.5	80	1.8
chloroform	- 64	61	8
diethyl ether	- 116	35	75

**Table 4.1 Common solvents, with relevant data, for Langmuir-Blodgett film preparation**

The minute volumes of material in solution needed, can be deposited onto the subphase by means of a micrometer syringe - of which several commercial varieties are available. On occasion mixed solvent systems are used, particularly where one solvent "spreads" differently from the other.

When producing such solutions, extreme accuracy is required in order to obtain reproducible results - the mass of adduct dissolved in the solvent was in this work measured to one hundredth of a milligram. The amount of solvent used was typically one millilitre - delivered by a Gilson pipette. The amount of solution then deposited onto the subphase was known to the nearest ten microlitres. The amount of material deposited on the subphase should be calculated to give a compressed monolayer when the barrier is half-closed between the minimum and maximum areas. The material is added dropwise with the syringe tip head just above the subphase. Once deposited, then time is allowed for any excess solvent to evaporate - approximately 5 minutes is generally enough.

#### **4.8 Temperature of the Subphase**

Changes in the properties of a monolayer forming material can be due to increasing or decreasing the temperature of the subphase. The temperature can be altered by incorporating a heat exchanger into the trough, and measuring the temperature with a suitable probe. It must again be stressed that the heat exchanger and temperature probe should be thoroughly checked for cleanliness if they are to come into contact with the subphase.

#### **4.9 Compression of the Monolayer**

Before the compression of the monolayer can begin, the microbalance must be zeroed. It is routinely straight forward to do this by adding or removing weights from the microbalance pan to give a coarse zero and then finalising with the zero control key. Cleaning the subphase will change any zero reading obtained as it removes water from the trough, so all cleaning should be carried out before the system is zeroed. It is more usual for the compression to be carried out slowly - the

typical time scale for an isotherm measurement being about 15 - 20 minutes. Once the essential features of the isotherm have been recorded, the barrier is returned to its original open position. This avoids the collapse of the monolayer if it is compressed too far. However, when studying a novel material for the first time, the collapse pressure is usually recorded.

#### 4.10 Control of Surface Pressure

To facilitate monolayer removal to the substrate, it is useful to be able to control the surface pressure of the monolayer. A negative feedback loop provides the facility to maintain the system at a constant pressure - compensating for removal of material by closing the barrier by an appropriate amount. A feedback time constant puts additional damping into the feedback loop and can thus change the response time of the system.

#### 4.11 Transfer of Monolayer

Much of the details of the monolayer removal - in particular the various ways in which a materials may be deposited on a monolayer - have been mentioned in the previous chapter. The number of layers that may be required to be deposited, the drying time between successive layers, the speed of the deposition and the depth can all be selected and controlled using this system. During the deposition process, all vibrations should be kept to an absolute minimum and the system is often mounted on an anti-vibration chamber, and preferably in a basement room.

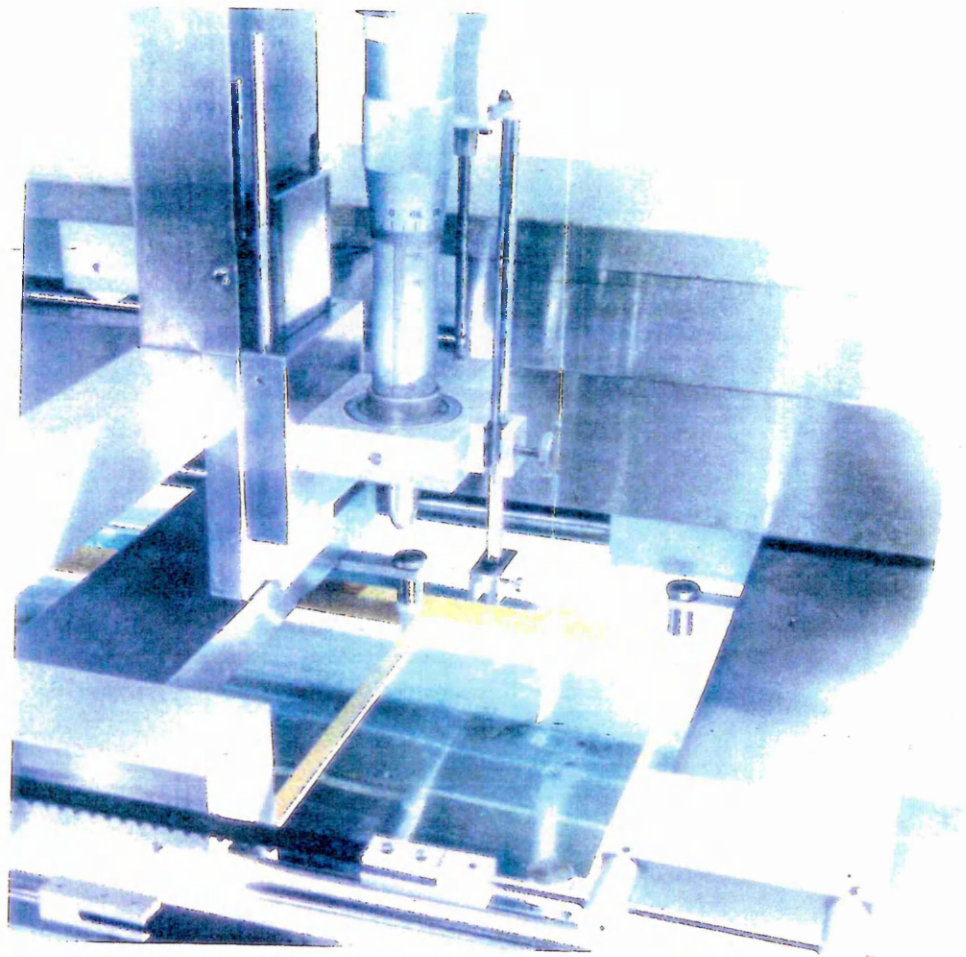
The deposition process is most conveniently monitored using a two-channel recorder to measure both the surface pressure and surface area against time. If the system is behaving correctly, then a decrease in area should be observed as material

is being removed from the subphase, due to the negative feedback loop maintaining the surface pressure at the predetermined value. If the area remains steady then this would indicate that there is no material being transferred.

Photographs 1 and 2 show various features of the Langmuir Trough used in this work, and the layout of the Langmuir-Blodgett laboratory at the Health and Safety Executive.



Photograph 1 : The Langmuir-Blodgett Laboratory



Photograph 2 : Details of the Compression System and  
Dipping Head.

#### 4.12 REFERENCES

- 1 L Blight, C W N Campbell and V J Kyte; *J Colloid Sci*, 20, 393, (1965)
- 2 O Albrecht, *Thin Solid Films*, 178, 563, (1989)

## CHAPTER 5: LANGMUIR - BLODGETT FILMS - RESULTS AND DISCUSSION

A systematic study of the film forming potential of the donor- $\pi$ -acceptor zwitterionic adducts was carried out in collaboration with scientists at the Health and Safety Executive Research and Laboratory Services Division in Sheffield. Very briefly, the study concentrated on three main areas:

- a) The behaviour of the materials on the water subphase
- b) The deposition of the materials as LB films
- c) The characterisation of the films by ultraviolet/visible spectroscopy

The results and discussion of each of these areas are discussed in turn below.

### 5.1 Langmuir Film Studies on R(4)Q3CNQ

The molecular structure of such donor- $\pi$ -acceptor adducts leads one to suspect that they may form an insoluble, monomolecular film at the air water interface. The fact that these adducts are sparingly soluble in many organic solvents, and that many such solvents are not suitable for spreading on water, was not a serious problem as the materials are soluble in dichloromethane. Thus, solutions of the materials could be prepared by weighing out the appropriate adduct and then dissolving in an appropriate amount of solvent delivered by a Gilson pipette. The concentration of the resultant solution was typically  $1\text{mg ml}^{-1}$ . All glassware and the spatula were thoroughly cleaned beforehand and a new pipette was used each time in order to keep any external contamination to a minimum.

An appropriate volume of the solution was then delivered to the water subphase, dropwise, by means of a micrometer syringe. Between each drop time was allowed for the solvent to evaporate and for the materials to achieve free association with the

subphase. Once all the solvent had been added and allowed to evaporate - typically after a period of ten minutes - the monolayer was compressed and the surface pressure vs area per molecule characteristics were studied.

The Joyce-Loebl Langmuir Trough 4 System will calculate the area per molecule if certain parameters are known. These are the maximum and minimum areas enclosed by the barrier, which are set internally during the calibration routines. The concentration of the solution added to the subphase is also calculated, knowing the volume of solution added to the subphase. Thus the area occupied per molecule can be calculated.

The shape and form of the isotherms for the range of materials studied are shown in figures 5.1 to 5.8. The scale of the area per molecule axis is chosen by the instrument software, explaining certain of the anomalies in scaling along the area axis. Table 5.1 shows the values of the area molecule for each adduct at  $25 \text{ mNm}^{-1}$ . It was noted that there was a definite change in molecular arrangement occurring at the alkyl chain lengths greater than 15 carbon atoms as is clear from the sudden increase in the area per molecule. In view of the molecular geometry of the adduct, the area values are quite small and a more detailed discussion of the structure of the Langmuir films is offered later in the chapter.

Figures 5.9 and 5.10 show successive compressions and expansions of the Langmuir film and it can be seen that the degree of hysteresis on successive compression and expansion is minimal. The problem of film hysteresis has been acknowledged for some time.<sup>1</sup> Very simply, if the molecule is compressed and then expanded, then in a fully dynamic system, it would be expected that there would be no change in the pressure/area profile.

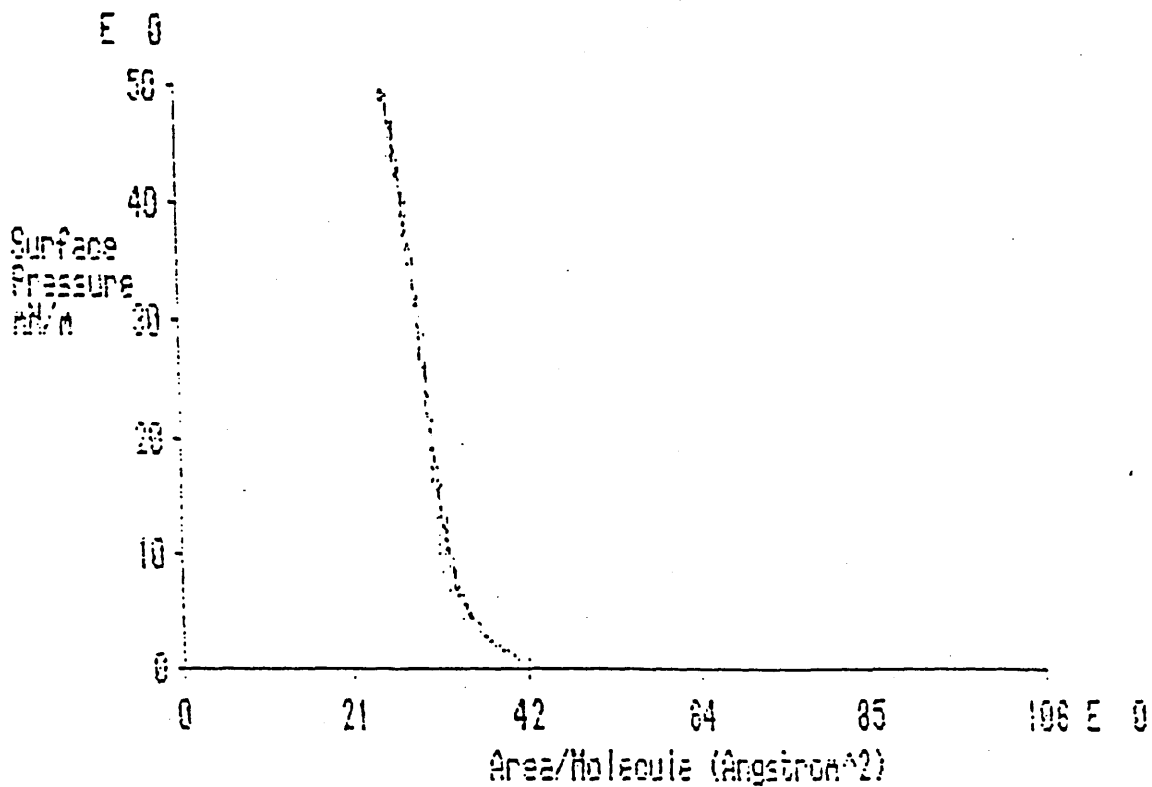


Figure 5.1 Isotherm showing change in surface pressure ( $\text{mNm}^{-1}$ ) against Area per molecule ( $\text{\AA}^2$ ) for C8(4)Q3CNQ

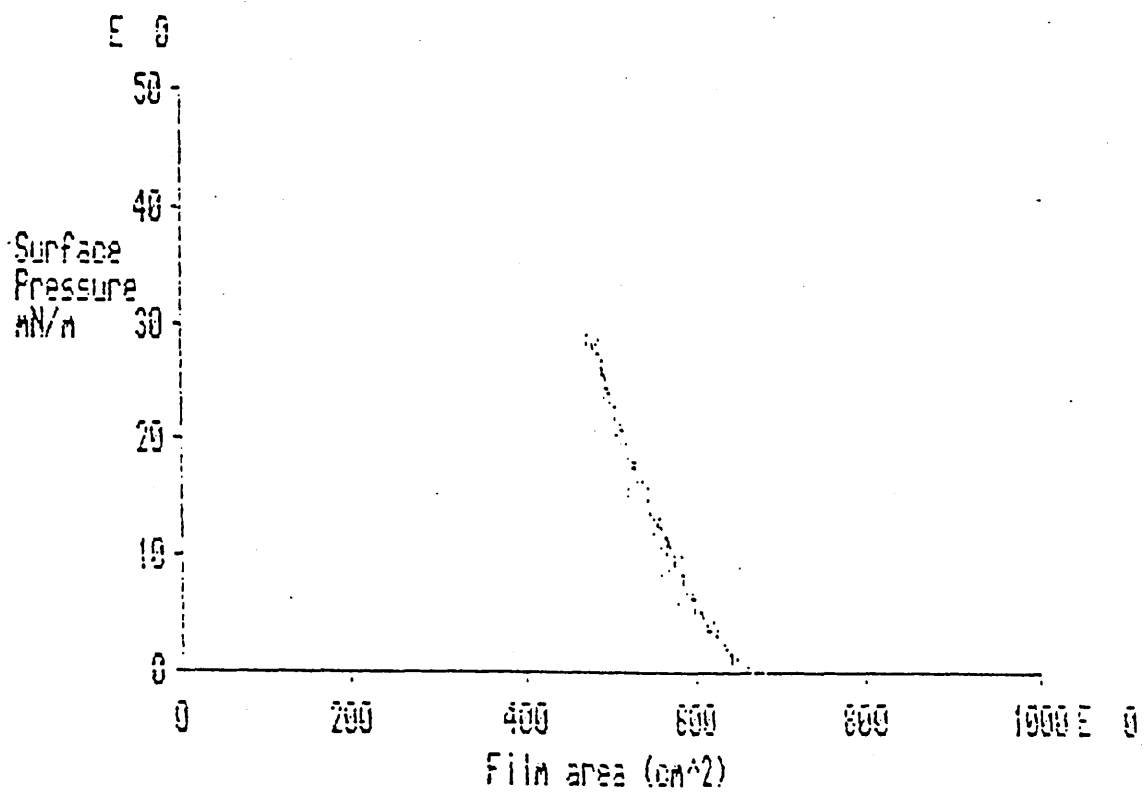


Figure 5.2 Isotherm showing change in surface pressure ( $\text{mNm}^{-1}$ ) against Area per molecule ( $\text{\AA}^2$ ) for C9(4)Q3CNQ

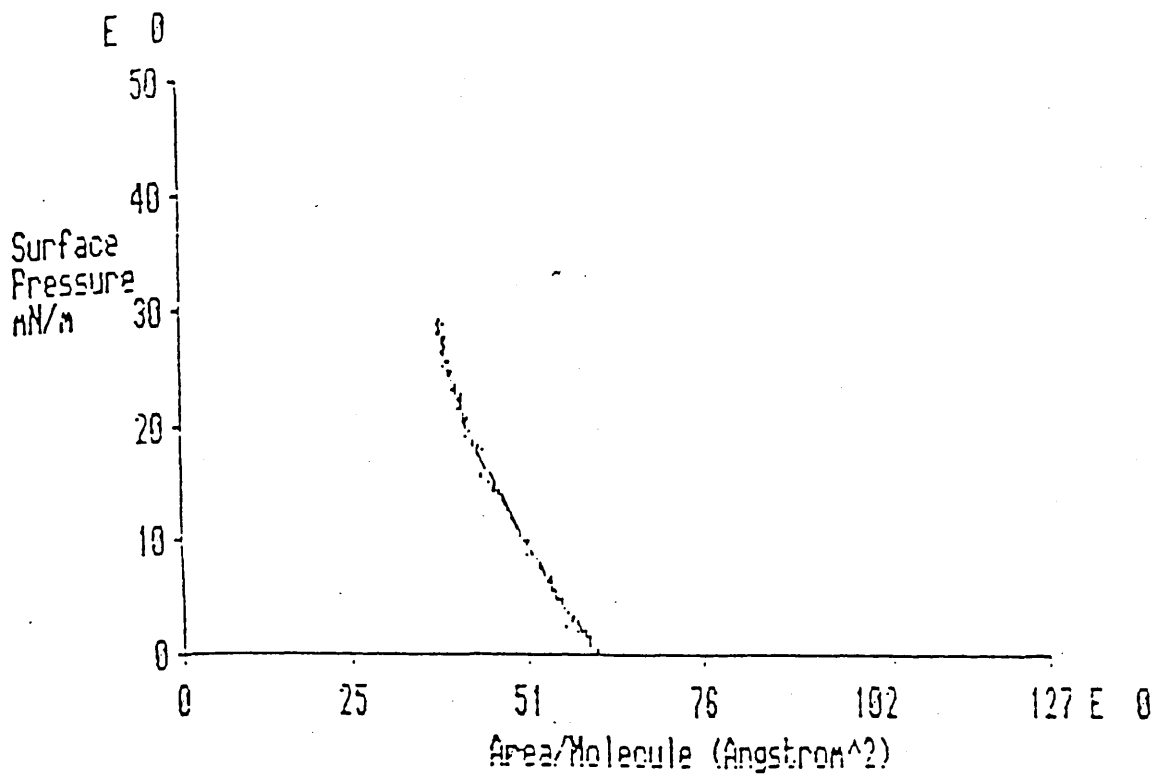


Figure 5.3 Isotherm showing change in surface pressure ( $\text{mNm}^{-1}$ ) against Area per molecule ( $\text{\AA}^2$ ) for C11(4)Q3CNQ

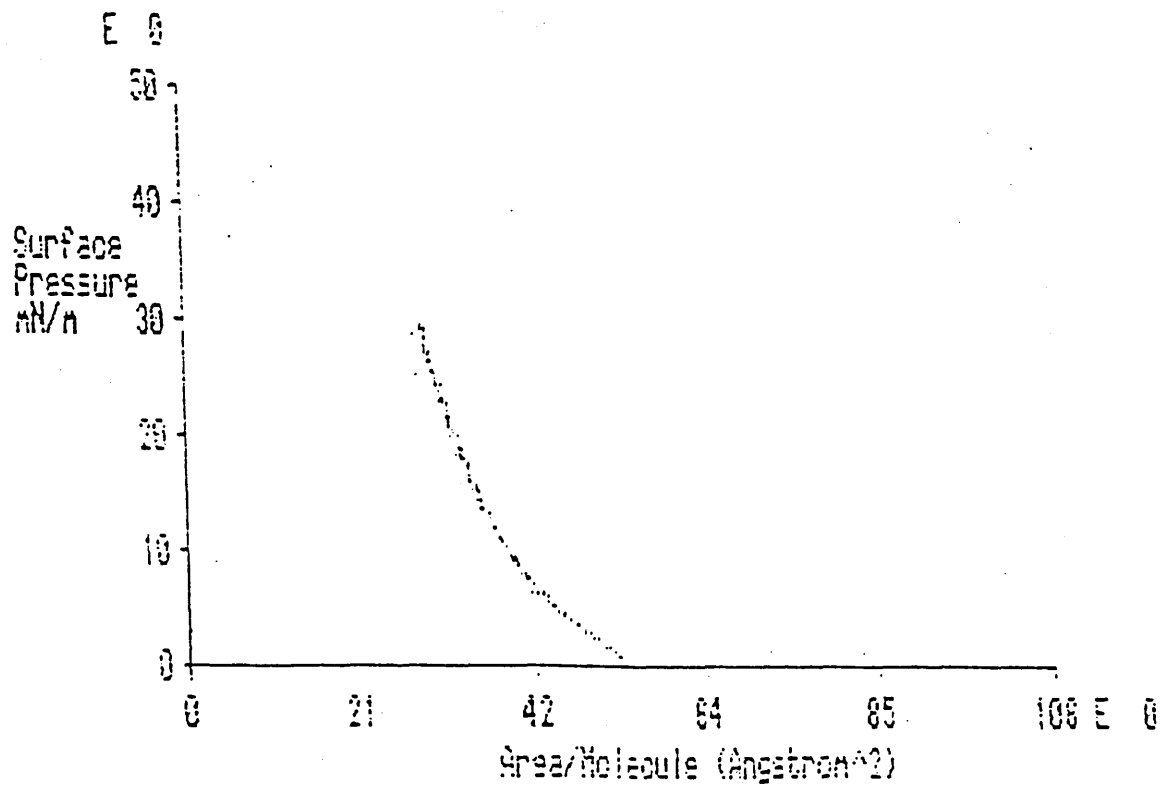


Figure 5.4 Isotherm showing change in surface pressure ( $\text{mNm}^{-1}$ ) against Area per molecule ( $\text{\AA}^2$ ) for C13(4)Q3CNQ

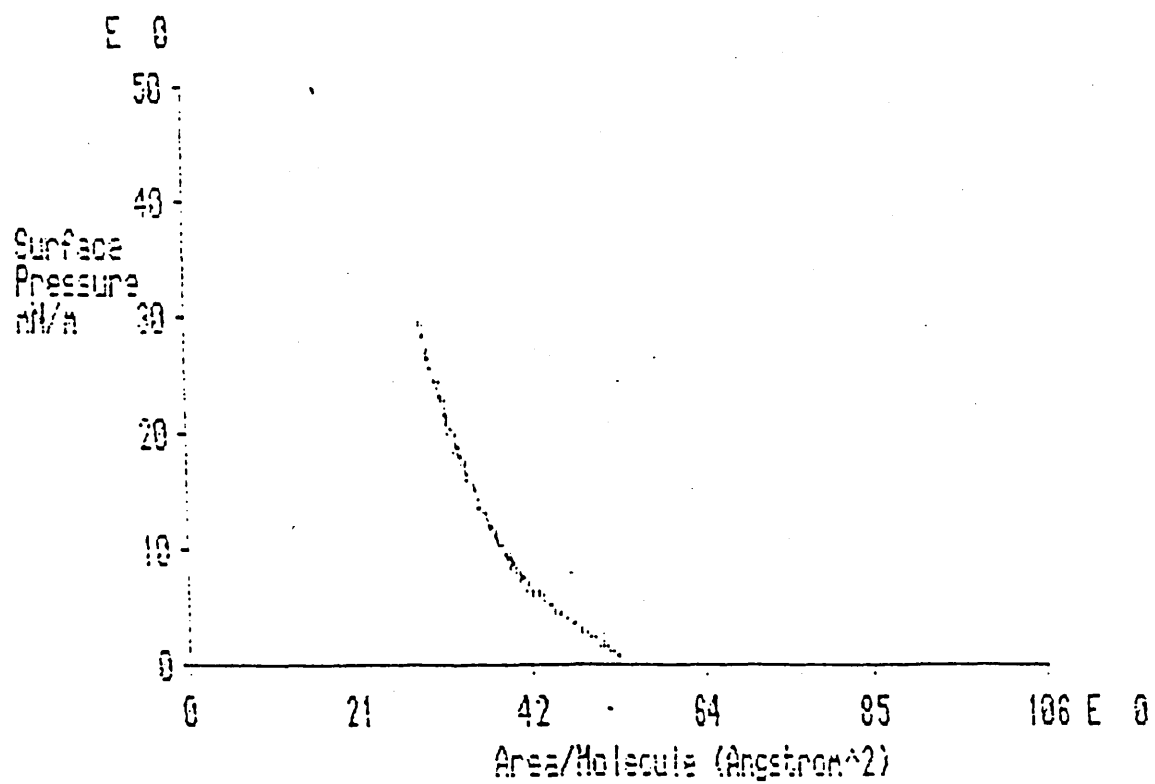


Figure 5.5 Isotherm showing change in surface pressure ( $\text{mNm}^{-1}$ ) against Area per molecule ( $\text{\AA}^2$ ) for C14(4)Q3CNQ

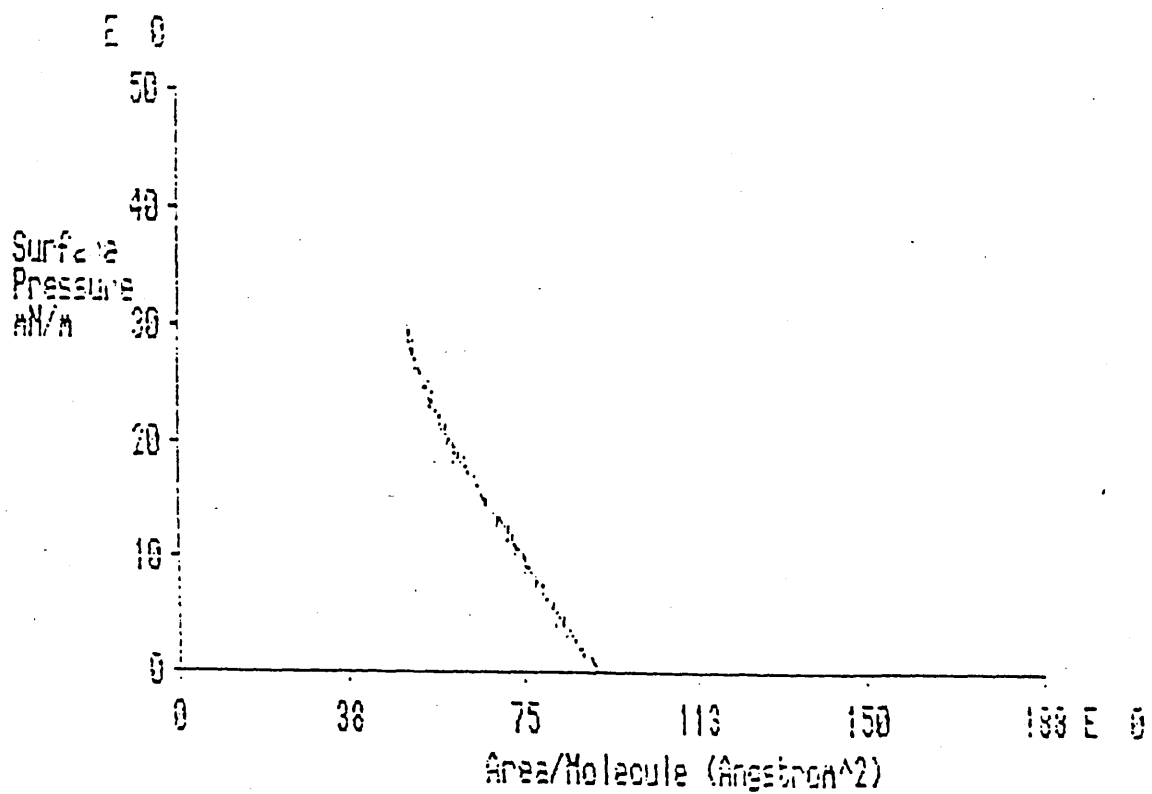


Figure 5.6 Isotherm showing change in surface pressure ( $\text{mNm}^{-1}$ ) against Area per molecule ( $\text{\AA}^2$ ) for C15(4)Q3CNQ

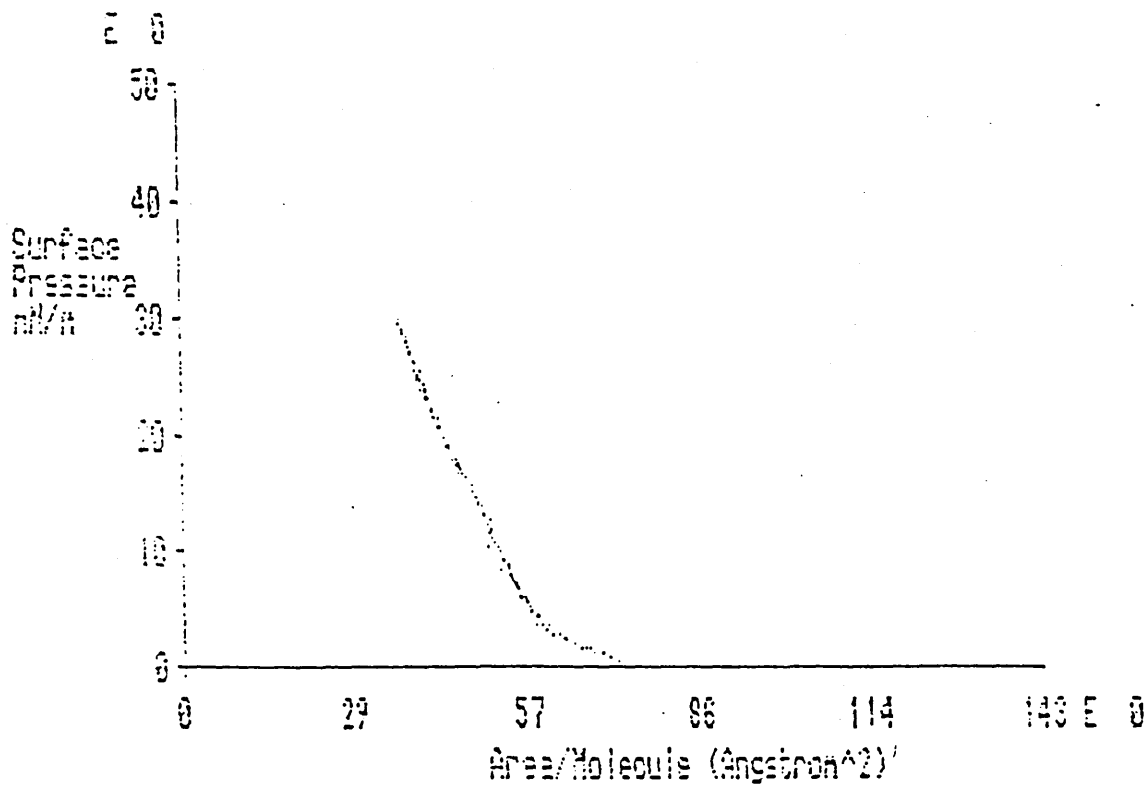


Figure 5.7 Isotherm showing change in surface pressure ( $\text{mNm}^{-1}$ ) against Area per molecule ( $\text{\AA}^2$ ) for C16(4)Q3CNQ

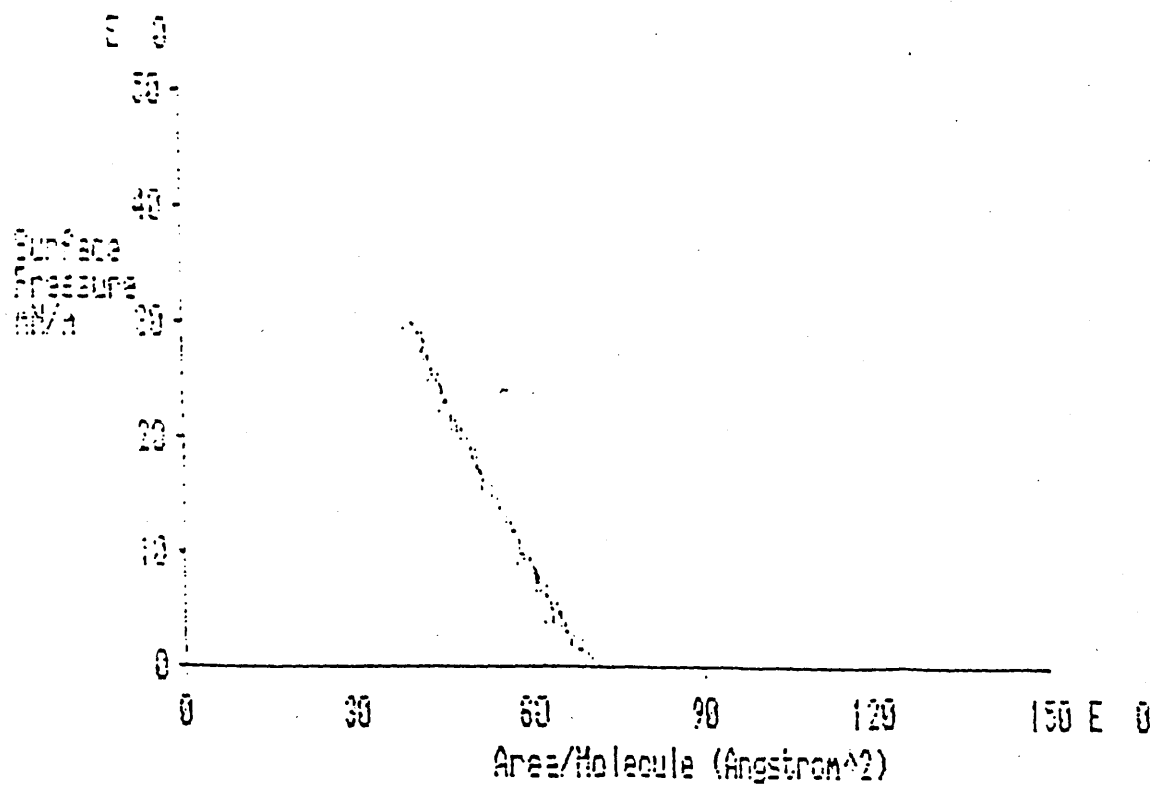
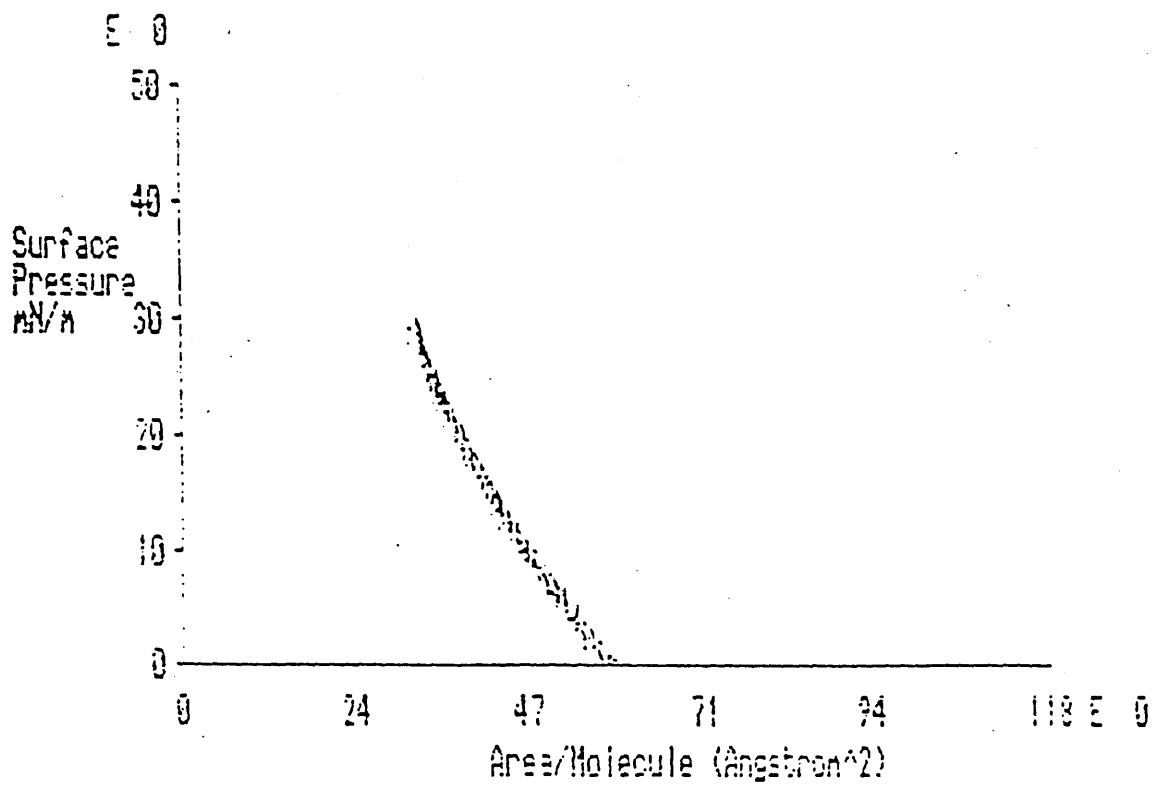


Figure 5.8 Isotherm showing change in surface pressure (mNm<sup>-1</sup>) against Area per molecule (Å<sup>2</sup>) for C20(4)Q3CNQ



**Figure 5.9** Four successive compression/expansion cycles showing negligible film hysteresis - C11(4)Q3CNQ

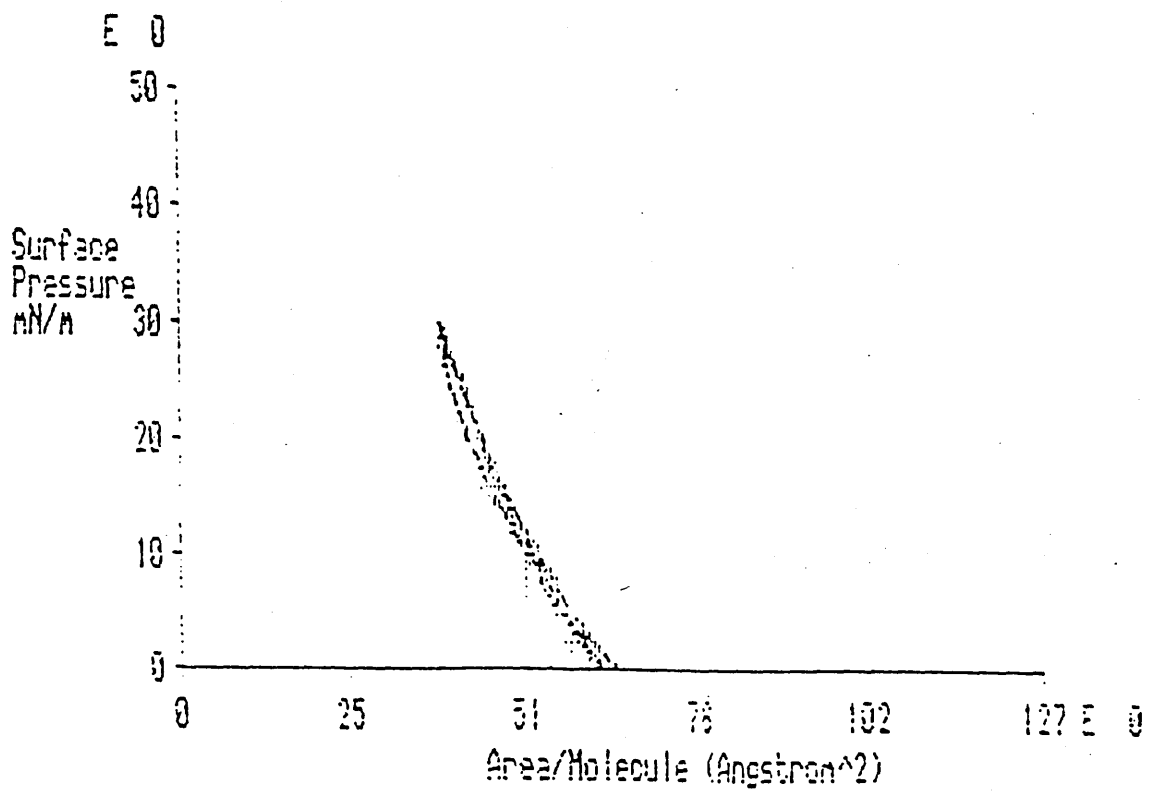


Figure 5.10 Further compression/expansion cycles showing negligible film hysteresis - C16(4)Q3CNQ

R (No. of carbon atoms)	AREA PER MOLECULE ( $\text{\AA}^2$ )
C8	32
C9	30
C10	34
C11	30
C12	30
C13	31
C14	31
C15	40
C16	44
C18	42
C20	48

Table 5.1 Area per molecule data for R(4)Q3CNQ adducts at  $25 \text{ mNm}^{-1}$

This is because, on compression, each molecule would be expected to organise into its preferred orientation and on expansion to return to a state equivalent to its original integrity. While molecules can obtain a preferred orientation on compression, they can be preferentially influenced by neighbouring molecules on successive expansions and compressions and thus retain an aggregated state. A routine compression/expansion experiment of this type was therefore carried out on each zwitterion to see whether such aggregation is present.

If the materials are to be successfully transferred to a solid substrate and fabricated as LB films then the compressed monolayer should be stable at the chosen deposition pressure. Thus, the barrier can be held at a particular surface pressure and the film area monitored with time. If the material is undergoing structural reorientation or if the film is collapsing and dissolving into the subphase then a decrease in the film area will be observed as a consequence of the feedback system maintaining the surface pressure at the predetermined value. Figures 5.11 to 5.13 show that the films are stable, with a 0.1% decrease in film area occurring over a period of one hour.

This work has shown that these materials form monomolecular layers at the air-water interface. The isotherms obtained are not of the classic three phase shape shown in fig 4.3 which is normal for long chain stearic and other fatty acids, though this is not really surprising. The molecular features - long alkyl chain and small, typically carboxyl, head groups - which often lead to defined phase changes in more condensed films, are almost all missing in long chain adducts of R(4)Q3CNQ. For example, such a bulky head group does not tend to favour efficient packing and maximum cohesion between hydrocarbon tails, nor is the presence of two polar moieties in the chromophore favourable. Also, the attraction of one polar group for the aqueous subphase would have to be overcome before the most stable state is reached. This would be a slow process and distinct gaseous-liquid-solid phase

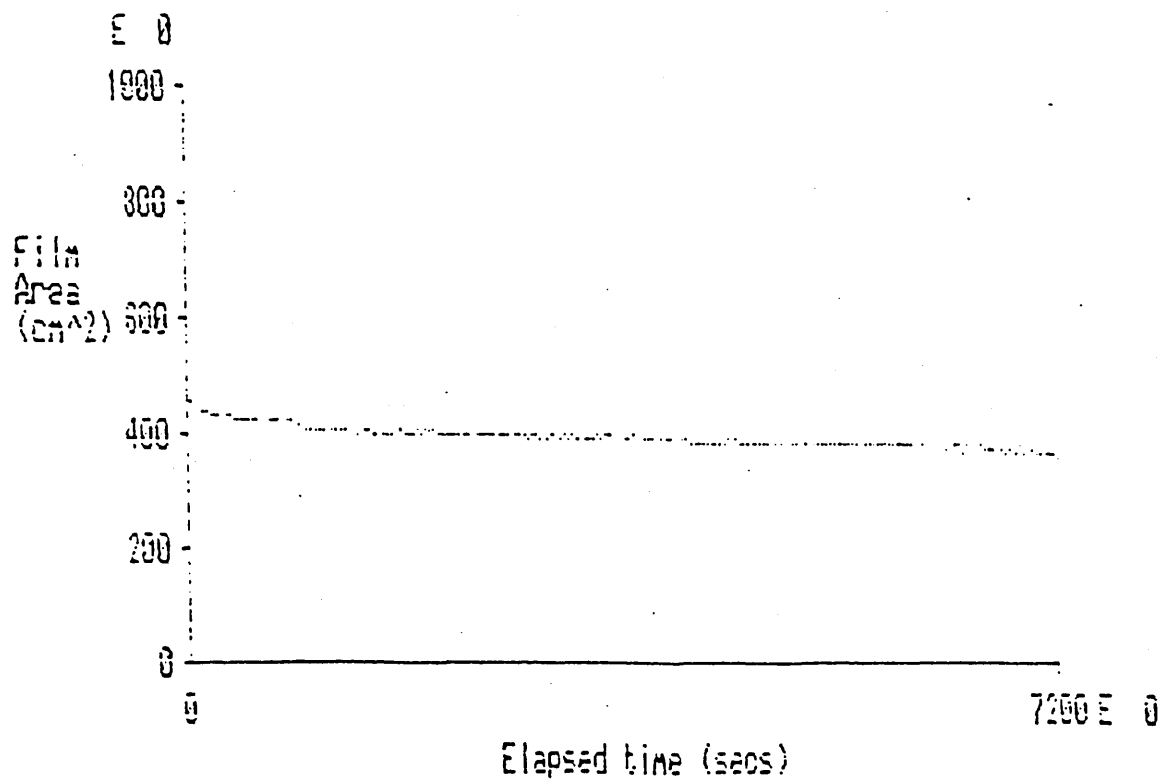


Figure 5.11 Stability of C8(4)Q3CNQ film at 25 mNm<sup>-1</sup>

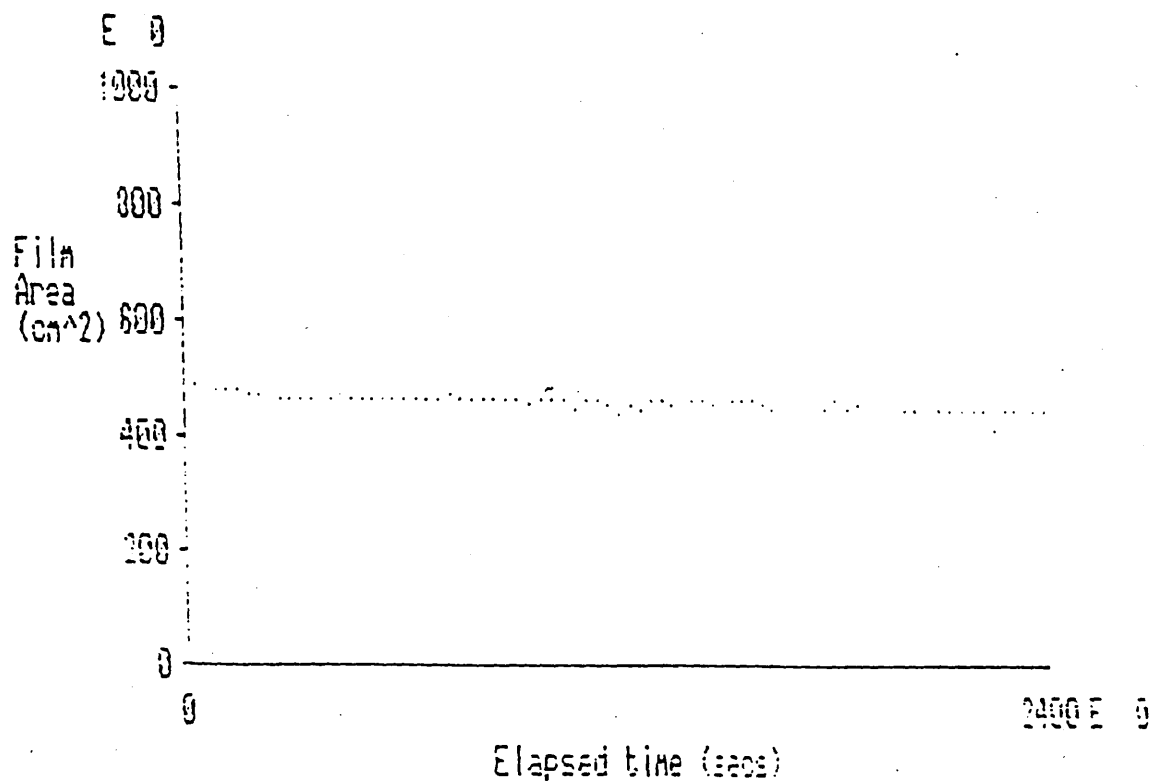


Figure 5.12 Stability of C16(4)Q3CNQ film at 25 mNm<sup>-1</sup>

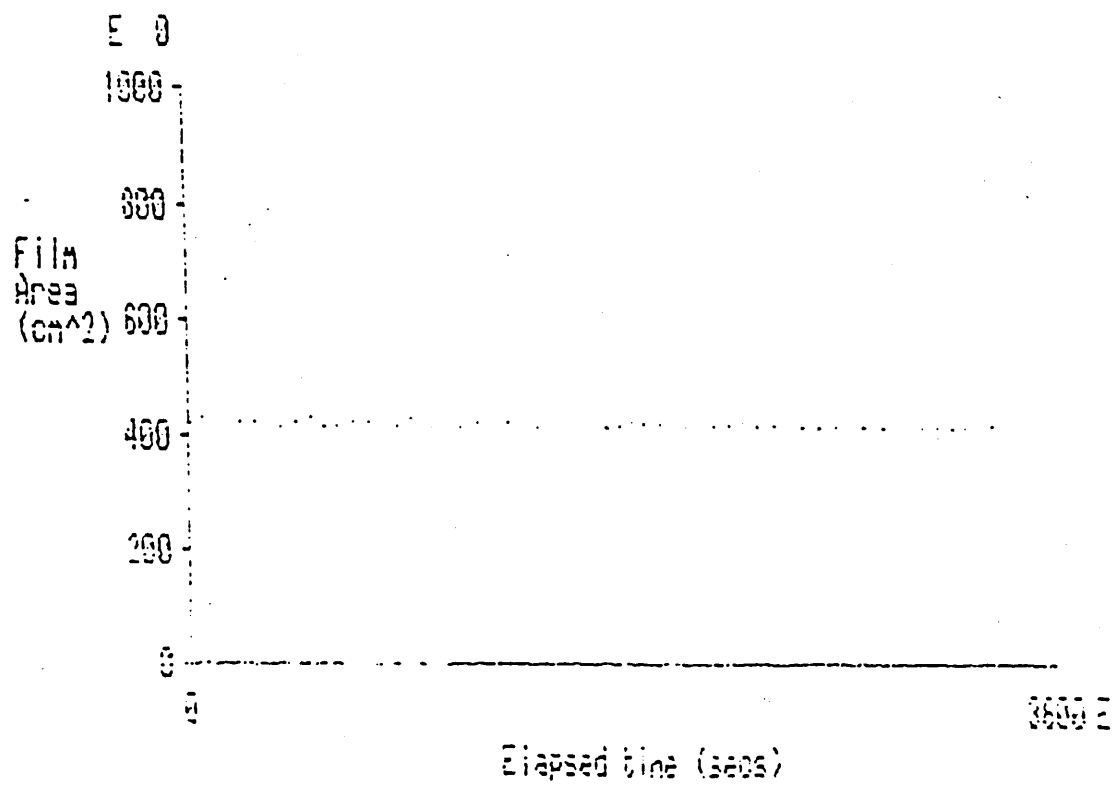


Figure 5.13 Stability of C11(4)Q3CNQ film at 25 mNm<sup>-1</sup>

changes would not be expected to be observed.

The effect of pH and added salt (say  $\text{Cd}^{2+}$ ) was also found to be minimal. The change in film characteristics on changing the pH is again more prevalent in more "conventional" films as is the effect of adding a divalent metal ion to aid the film cohesion.

## 5.2 Langmuir-Blodgett Films of R(4)Q3CNQ adducts

The transference of material from the condensed monolayer to a suitable substrate can be attempted once a knowledge of the materials' behaviour outlined in 5.1 has been fully investigated. The mechanics of the LB technique have been fully described previously.

The adducts were deposited onto glass (silica) substrates which had been treated to render the surface hydrophilic. This was done by the following technique involving several successive washes in water (18 M $\Omega$  milli-Q), iso-propylalcohol and dichloromethane. The slides were then left to soak overnight in a concentrated solution of sodium hydroxide. Before use, each freshly prepared slide was (always handling with tweezers) washed in copious quantities of ultra pure water and blown dry with filtered nitrogen ("white spot").

The condensed film was held at 25 mNm $^{-1}$  and the slide, held in the dipping head (shown in photograph 2, Chapter 4) was passed vertically through the subphase from air to liquid, at a rate of 5 mm/min $^{-1}$ . After travelling a predetermined distance into the subphase, the slide was then removed at the same rate. This procedure was then repeated several times, thus forming a stable film on the slide.

As described in section 4.4, the transfer ratio ' $\eta$ ' can be determined to establish whether the resultant film is X, Y or Z-type. Each stroke down or up constitutes one possible layer transferred. Selected transfer ratios and deposition profiles are

shown in table 5.2 and 5.3 and these results are shown in bar graphs 5.14 and 5.15. It is clear that neither pure X, Y or Z-type deposition occurs, rather that the films are predominantly Y-type with material being transferred on both the up and down stroke. As a consequence of the hydrophilically treated slide, no material is transferred on the first downstroke. This is because the surface of the substrate, being hydrophilic, attracts water, and the first immersion of the slide into the subphase results only in the wetting of the slide (fig 5.16(a)). On removal, the hydrophilic head is deposited on the slide as a consequence of the water substrate attraction shown (fig 5.16(b)). The substrate surface is then rendered hydrophobic and thus on the next immersion the hydrophobic tails will be attracted to the substrate. This leads, after successive passages through the subphase, to a head-to-head, tail-to-tail structure. Thus, films can be produced with a certain degree of order.

The next portion of the work involved the further characterisation and study of the films by a variety of techniques with a view to establishing their structure more fully.

### 5.3 Characterisation of LB films of R(4)Q3CNQ adducts

It has already been shown that the transfer ratio can give some indication as to whether or not one monolayer at a time is being transferred. The integrity of the films can be assessed in other ways as mentioned in chapter 3 and, to illustrate one method, an absorbance vs number of layers plot for C15(4)Q3CNQ is shown in fig 5.17. This essentially straight line plot is indicative of good, reproducible monolayer transference.

Layer Number	Transfer Ratio ( $\eta$ )
1	0
2	1.09
3	0.76
4	1.09
5	0.76
6	1.06
7	0.76
8	1.04
9	0.82
10	0.99
11	0.76
12	0.99
13	0.99
14	1.00
15	0.99

**Table 5.2 Selected transfer ratios for C16(4)Q3CNQ**

Layer Number	Transfer Ratio ( $\eta$ )
1	0
2	0.6
3	1.1
4	0.6
5	0.6
6	1.1
7	0.6
8	0.6
9	1.1
10	0.6
11	1.1
12	0.6

**Table 5.3 Selected transfer ratios for C14(4)Q3CNQ**

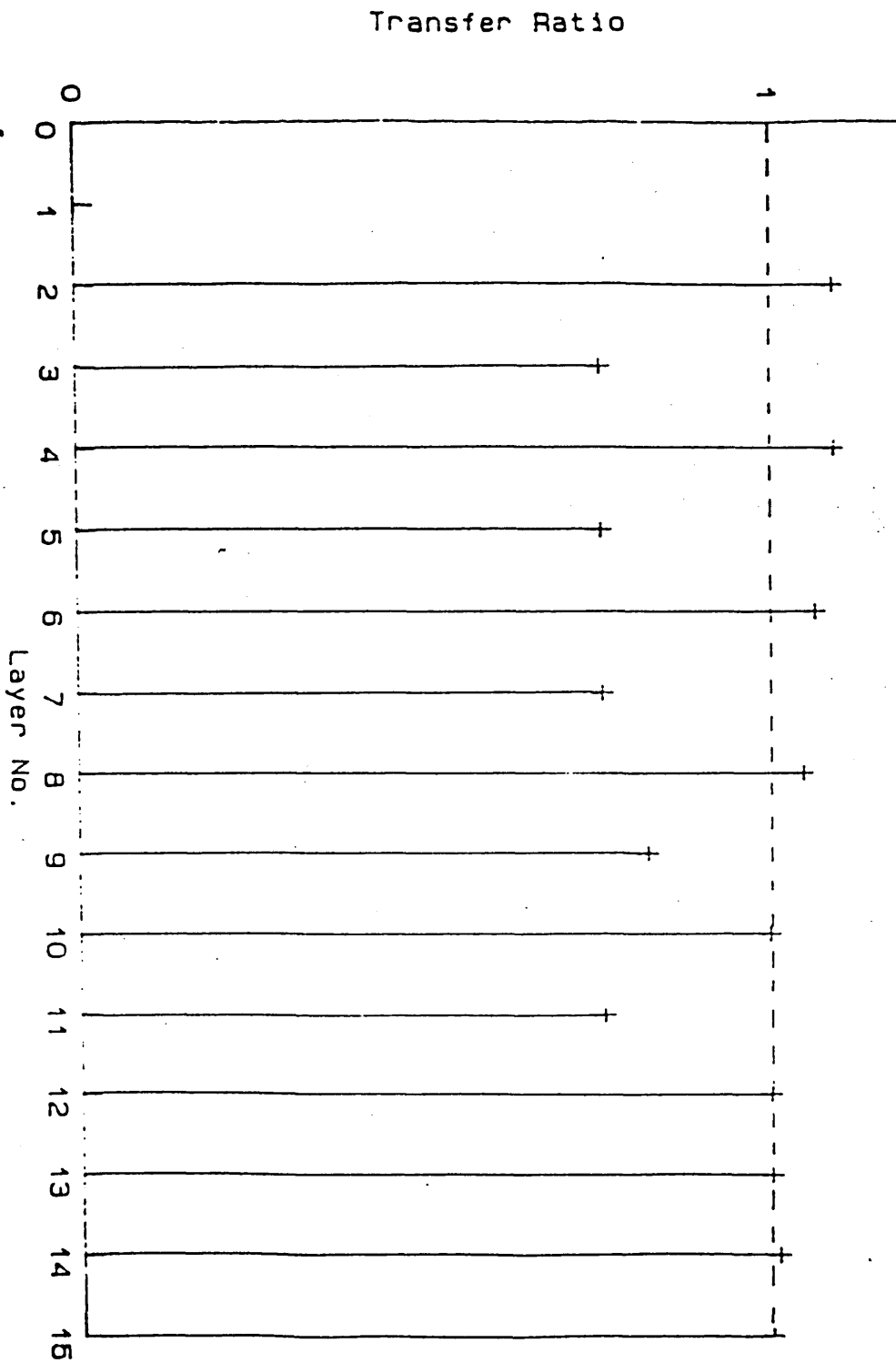


Figure 5.15 Computed transfer ratios for C16(4)Q3CNO

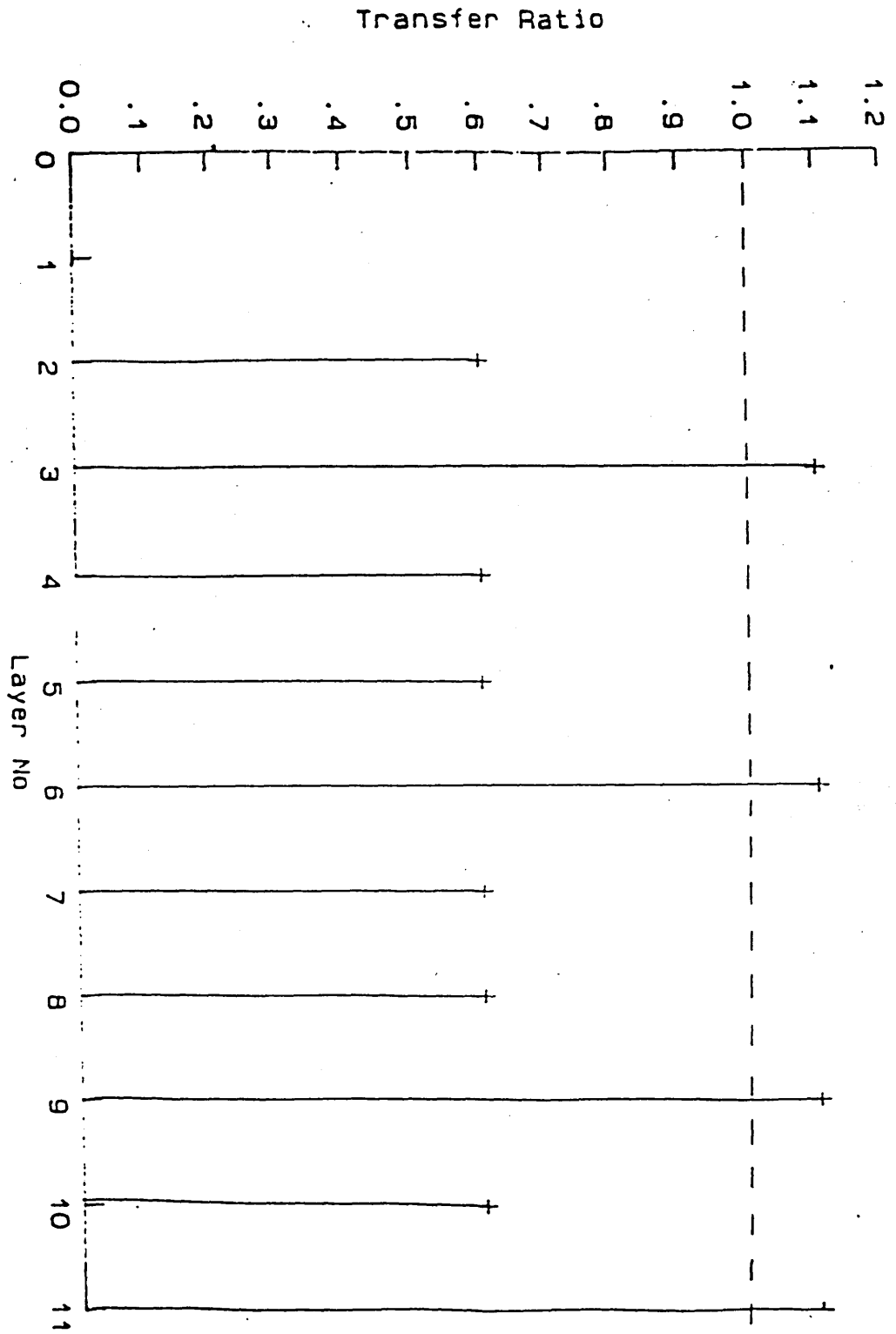


Figure 5.14 Computed transfer ratios for C14(4)Q3CNQ

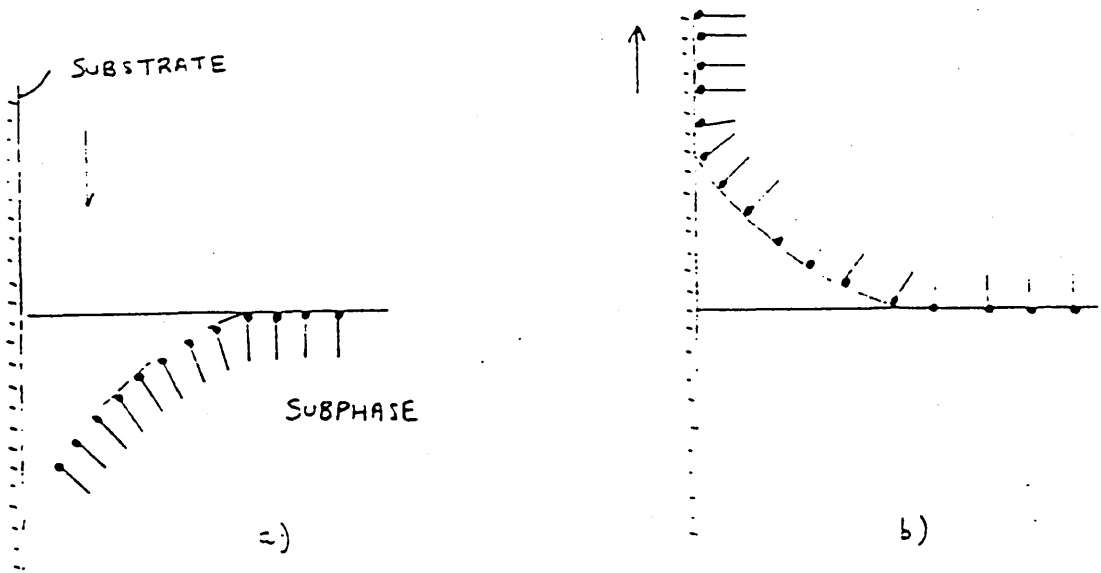


Figure 5.16 Deposition process showing:

- a) 1st downstroke (no transfer)
- b) 1st upstroke (transfer)

The resultant substrate surface is hydrophilic

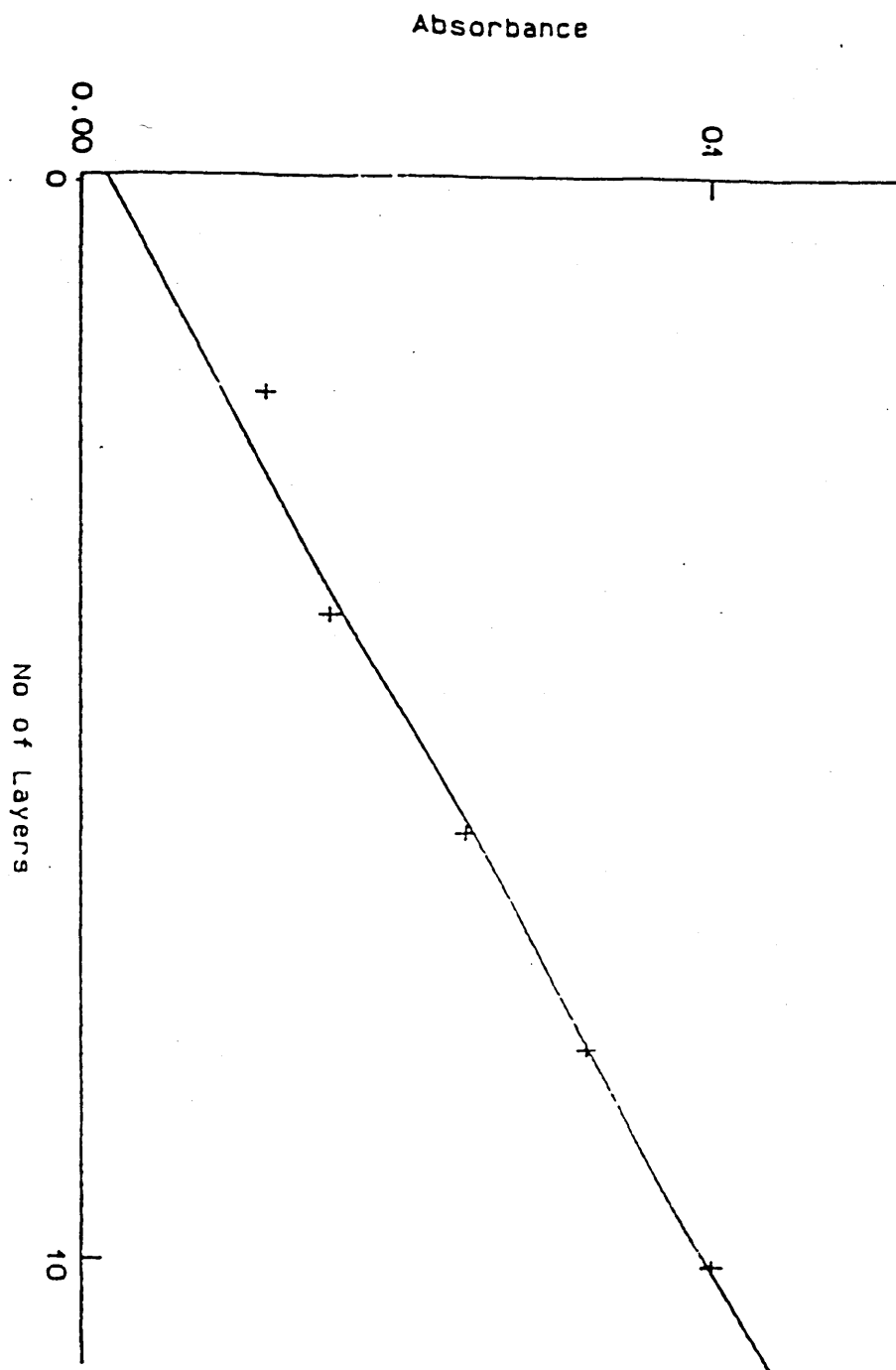


Figure 5.17 Absorbance vs No of layers for C15(4)Q3CNQ

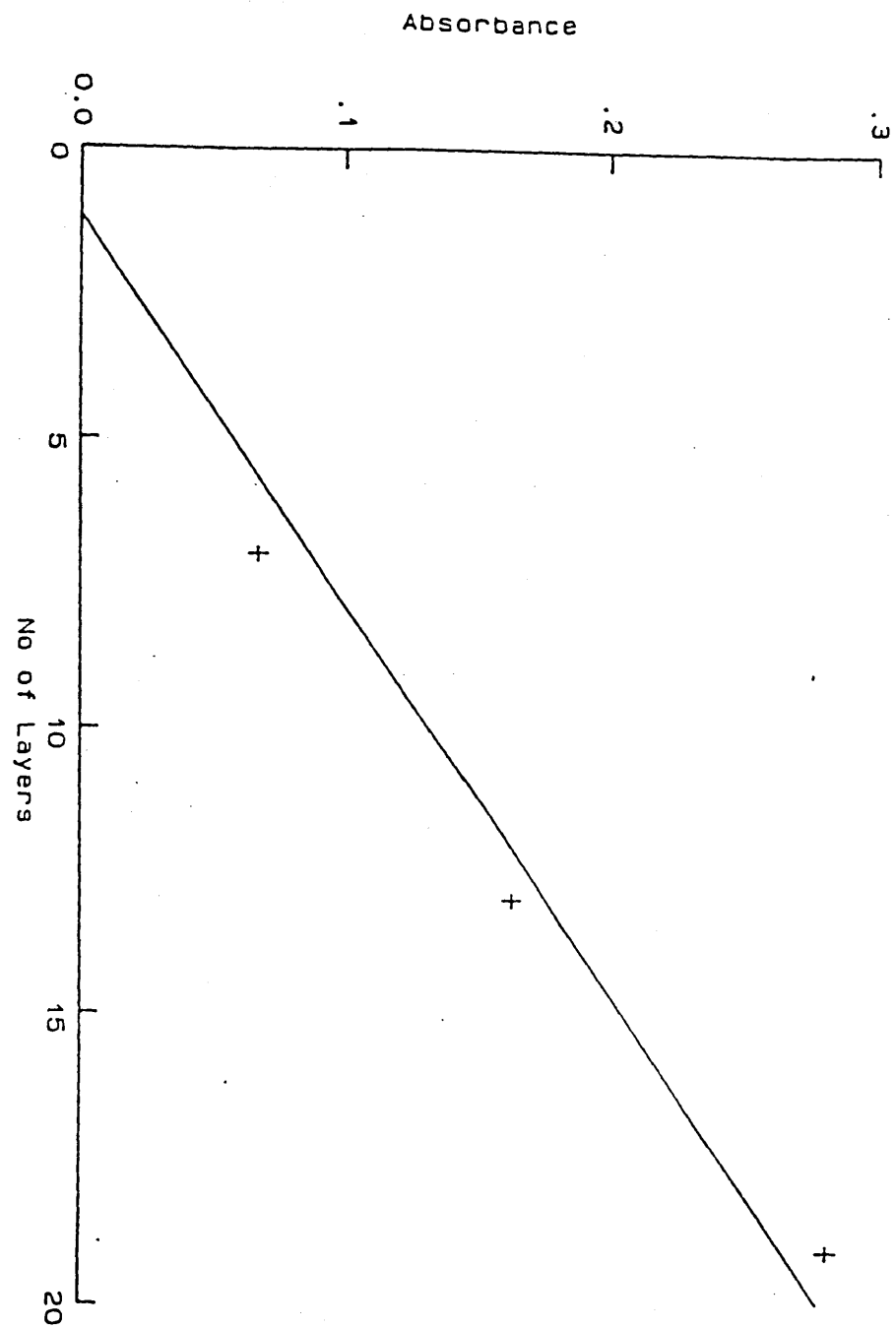


Figure 5.17 Continued... Absorbance vs No of layers for C14(4)Q3CNQ

The films were also studied using uv/vis spectroscopy. Selected spectra are shown in figures 5.18 to 5.26. It is apparent that the band is considerably sharpened as compared to the solution spectra and shifted to shorter wavelength, with a further shift to shorter wavelengths as the chain length increases. The measured  $\lambda_{\text{max}}$  (nm) values are shown in table 5.4. A fuller discussion as to why this should be observed is given in the later part of this chapter.

A study of the film morphology and structure was made using Transmission Electron Microscopy (TEM). The procedure used to study the films was that first described by Zingsheim<sup>2</sup>, and which has been used by many researchers since then<sup>3</sup>. This particular microscopic technique is used because TEM requires the use of very thin substrates. The particular material is deposited as an LB film onto a glass slide coated with  $\text{Al}_2\text{O}_3$  (ie aluminium which has been allowed to slowly oxidise in air). The film is then "flashed" with carbon, thus enabling the area covered by the LB film to be visualised. Once this has been done, the slide is then lowered into a solution of mercury (II) chloride by some suitable instrument. It is critically important when carrying out this stage that the slide is lowered into the mercury solution at the correct angle to ensure the solution attacks the aluminium and does not attack the film through the carbon. The LB film can then be transferred to microscope grids and is then ready for examination. The advantage of studying these films by TEM is that the transmission electron microscope allows electron diffraction patterns to be obtained from the same area that is under observation. Thus, the film texture and the underlying crystallographic pattern can be obtained from the same part of the film.

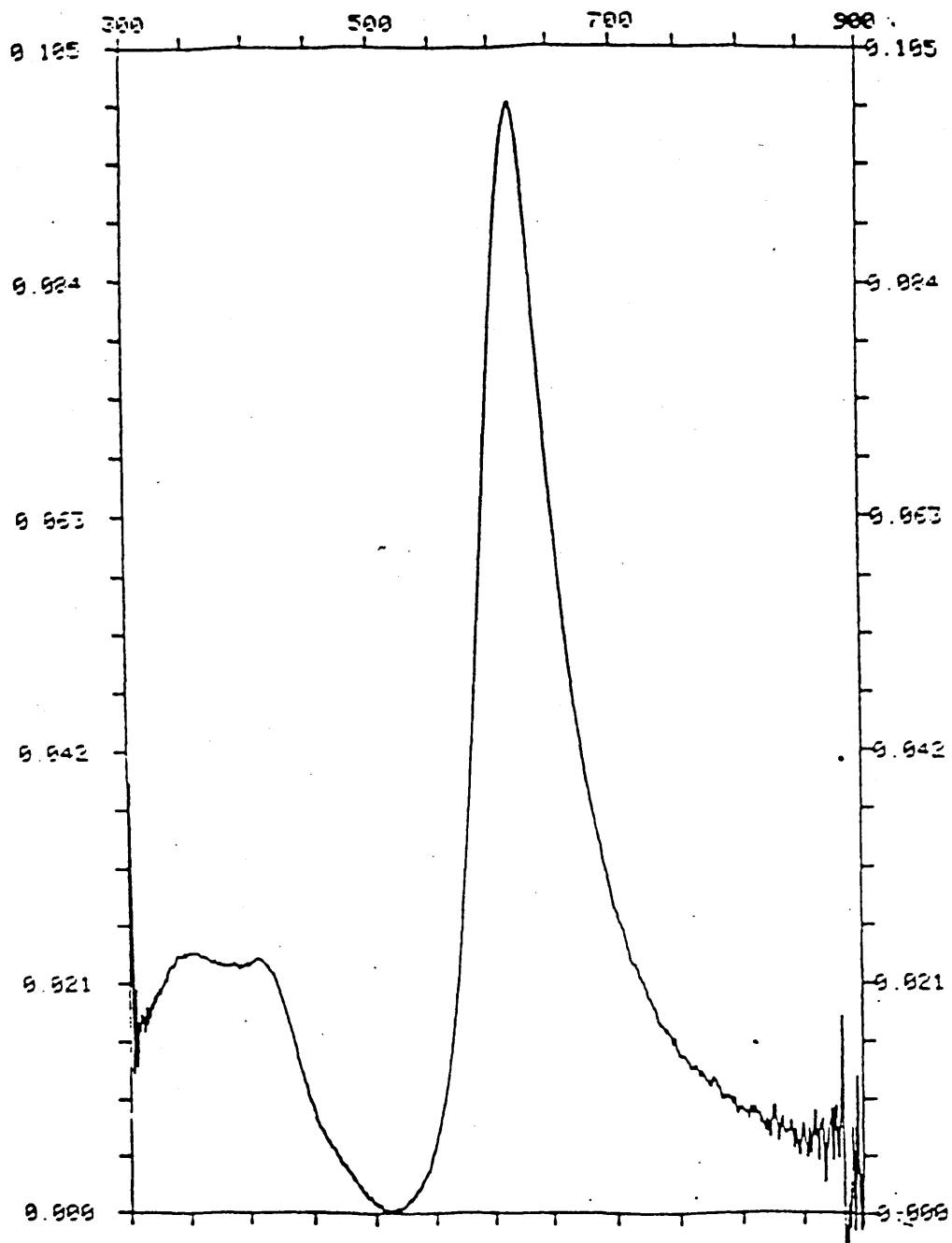


Figure 5.18 UV/VIS spectra for a 6-layer LB film of C8(4)Q3CNQ

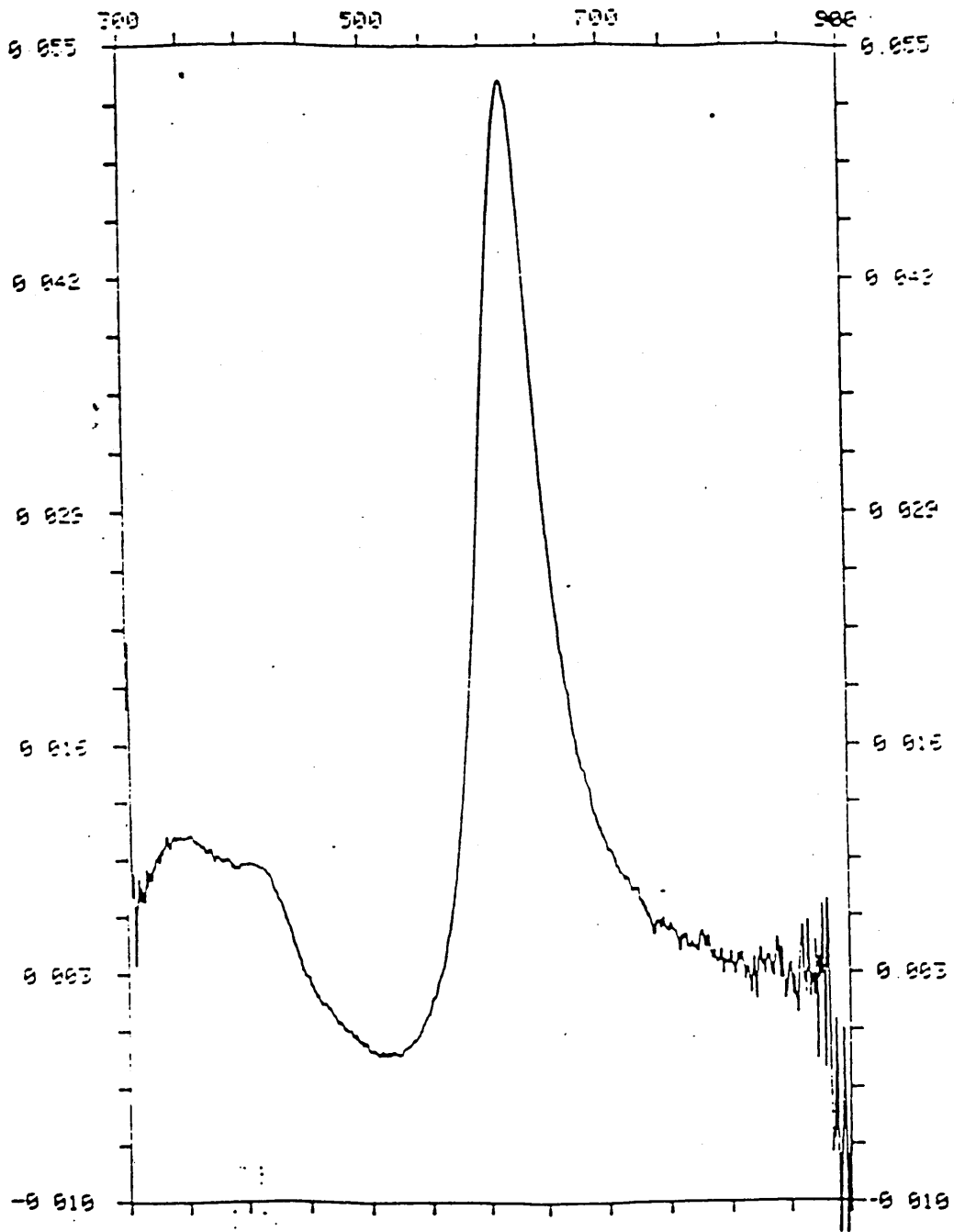


Figure 5.19 UV/VIS spectra for a 3-layer LB film of C9(4)Q3CNQ



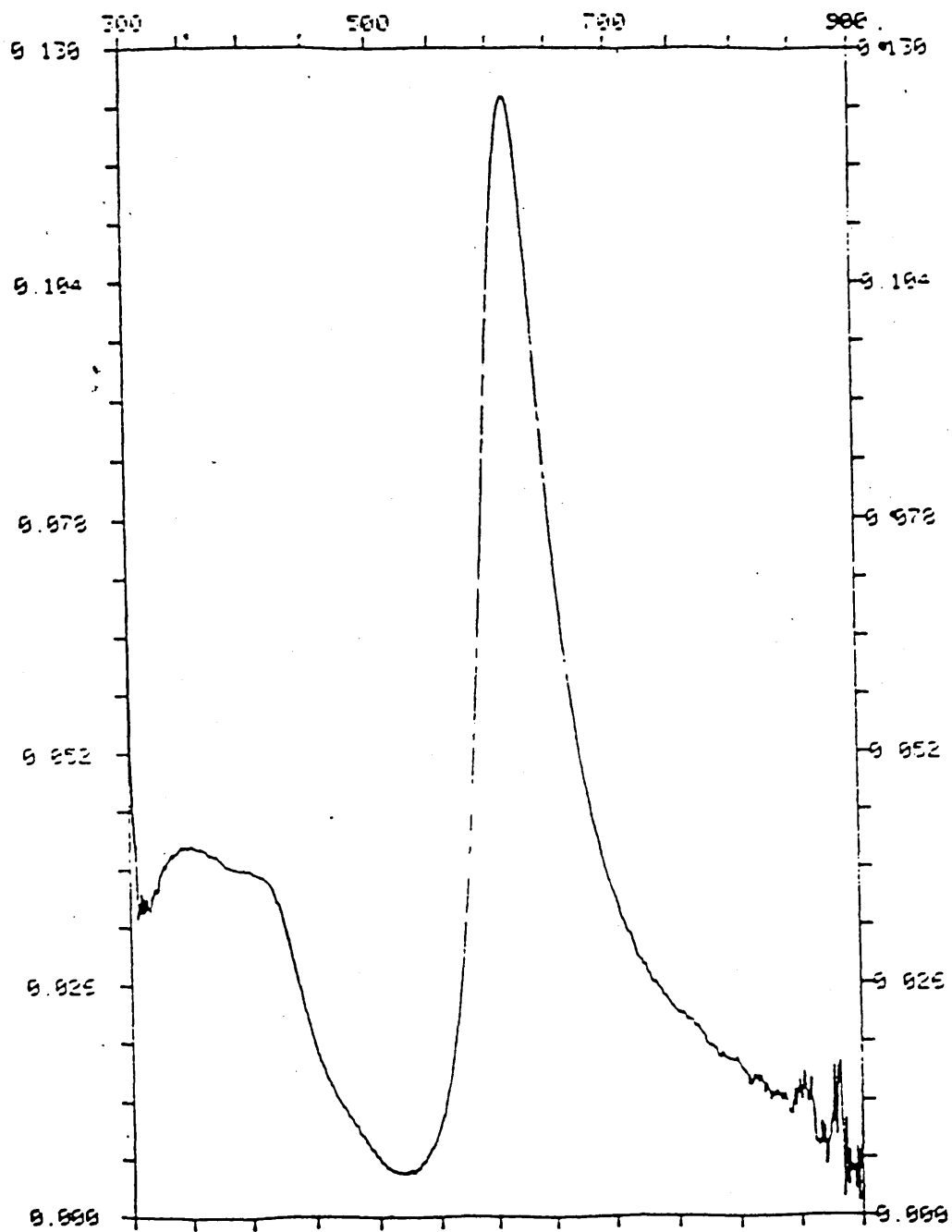


Figure 5.21 UV/VIS spectra for an 8-layer LB film of C12(4)Q3CNQ

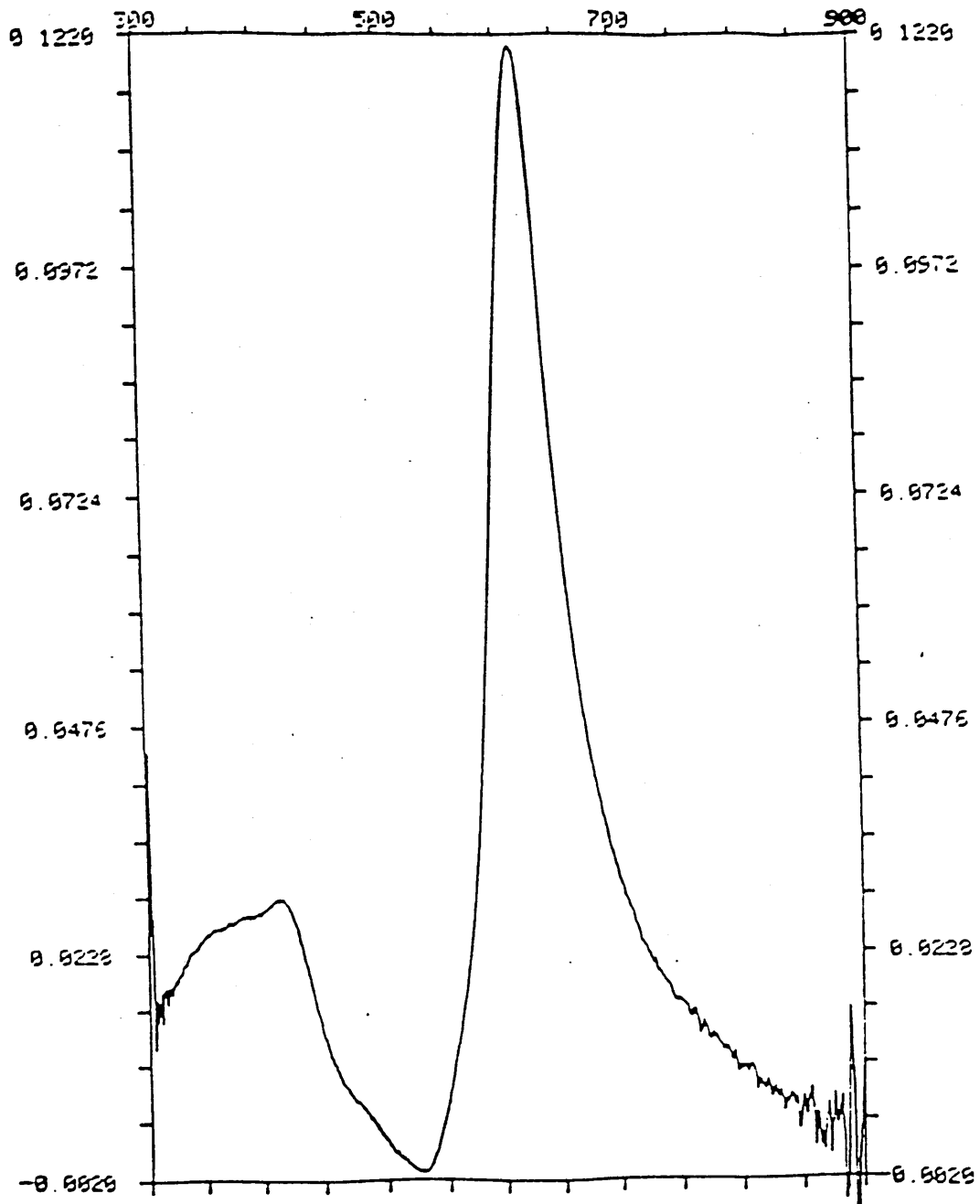


Figure 5.22 UV/VIS spectra for a 5-layer LB film of C13(4)Q3CNQ

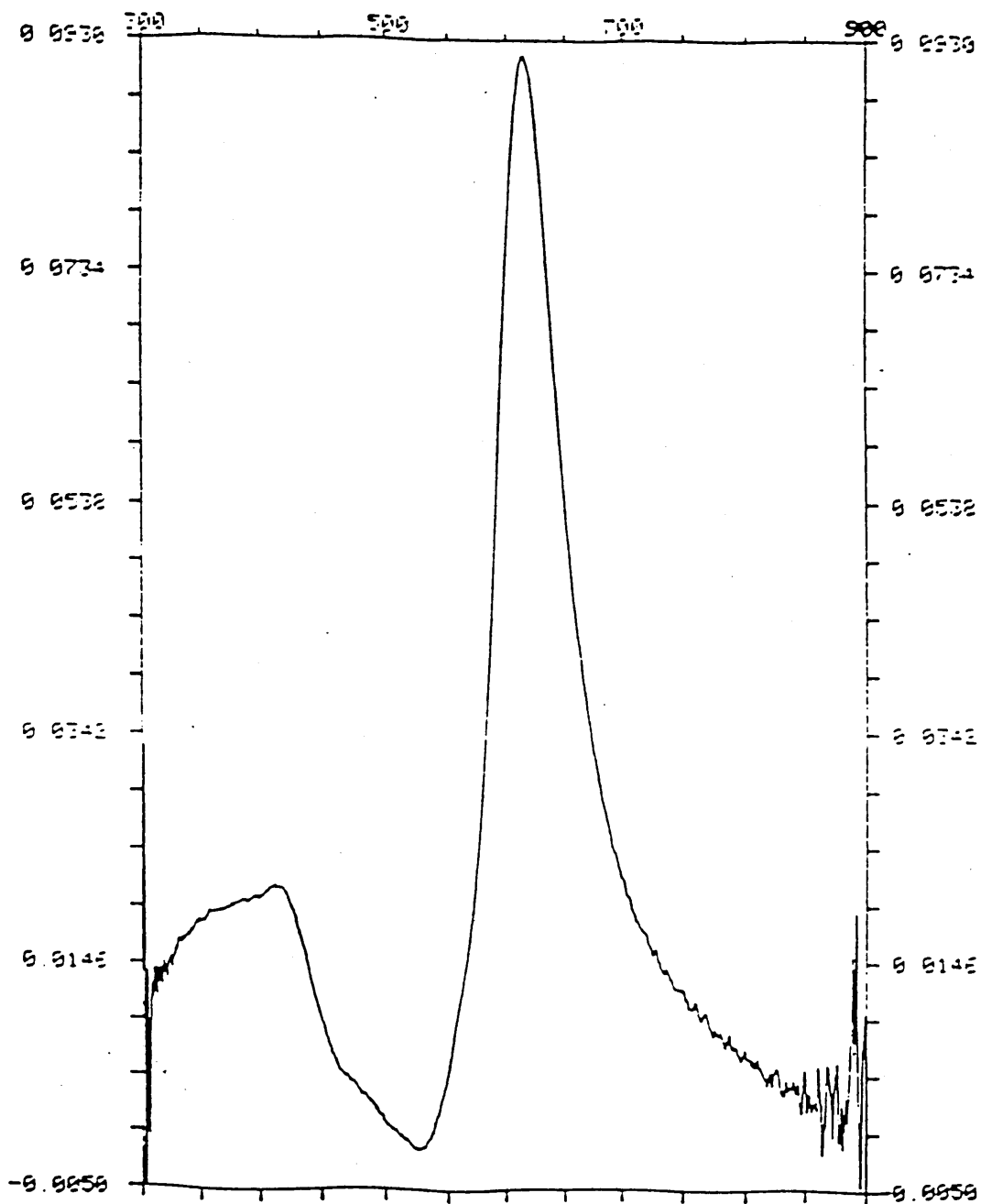


Figure 5.23 UV/VIS spectra for a 4-layer LB film of C14(4)Q3CNQ

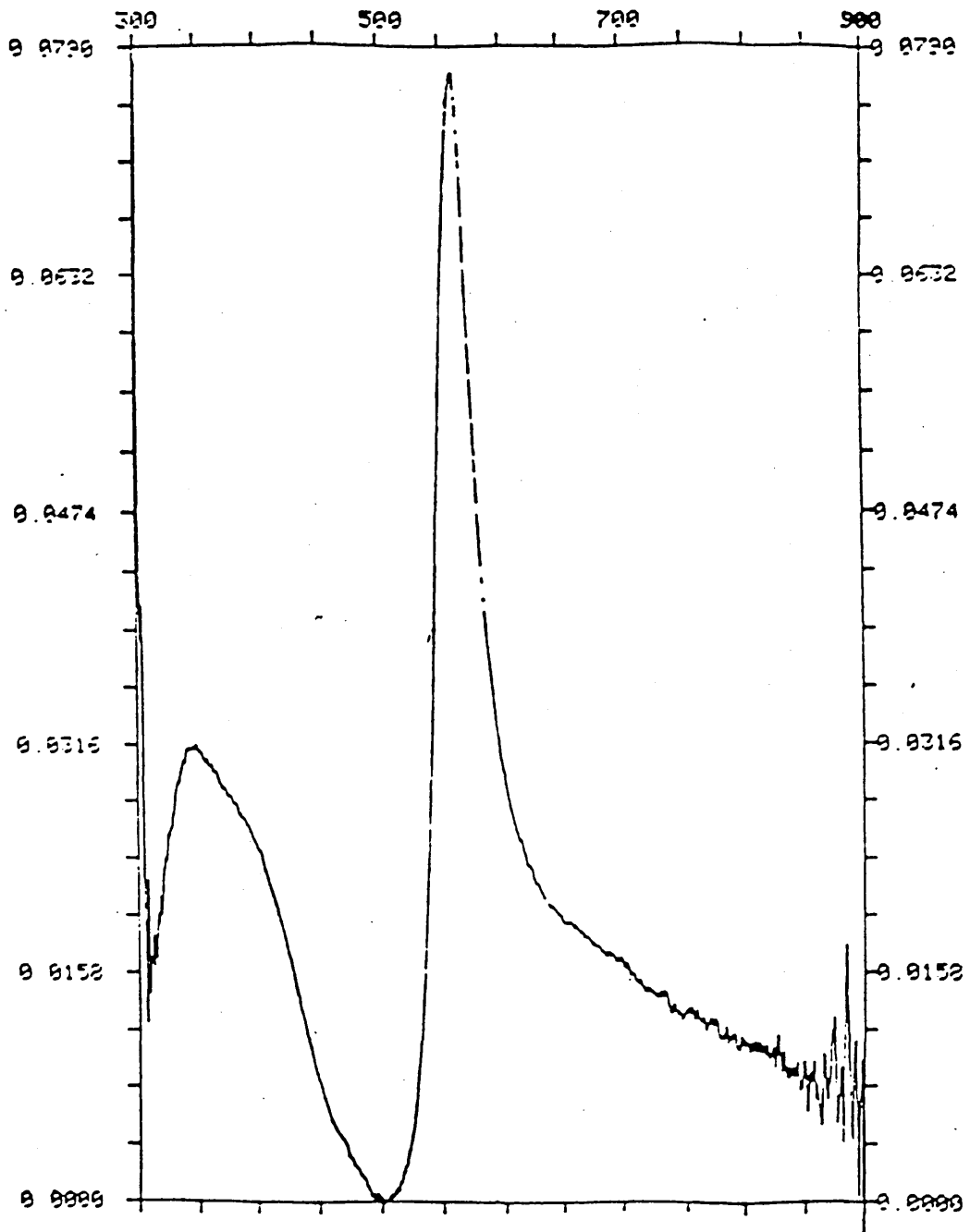


Figure 5.24 UV/VIS spectra for a 5-layer LB film of C15(4)Q3CNQ

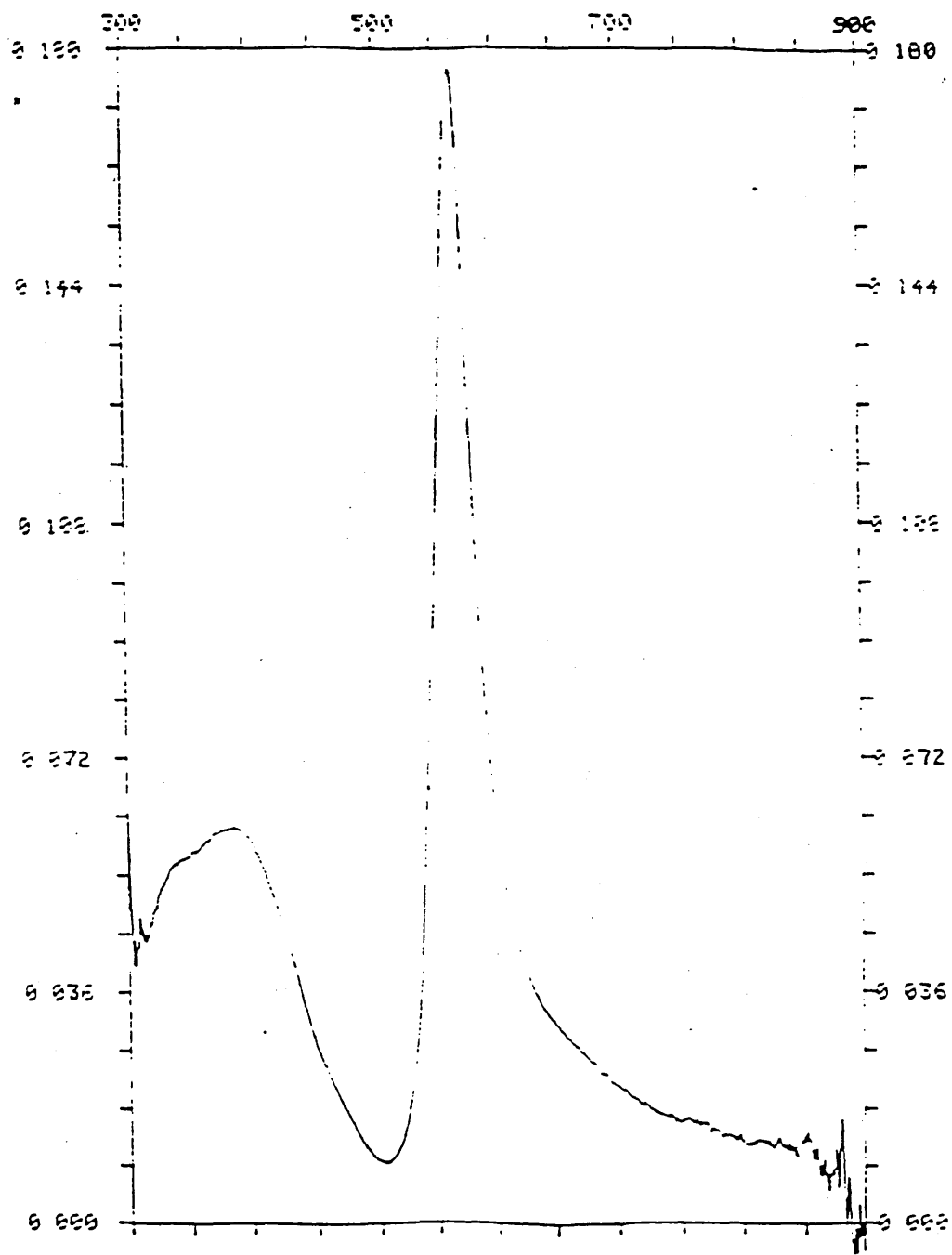


Figure 5.25 UV/VIS spectra for an 8-layer LB film of C16(4)Q3CNQ

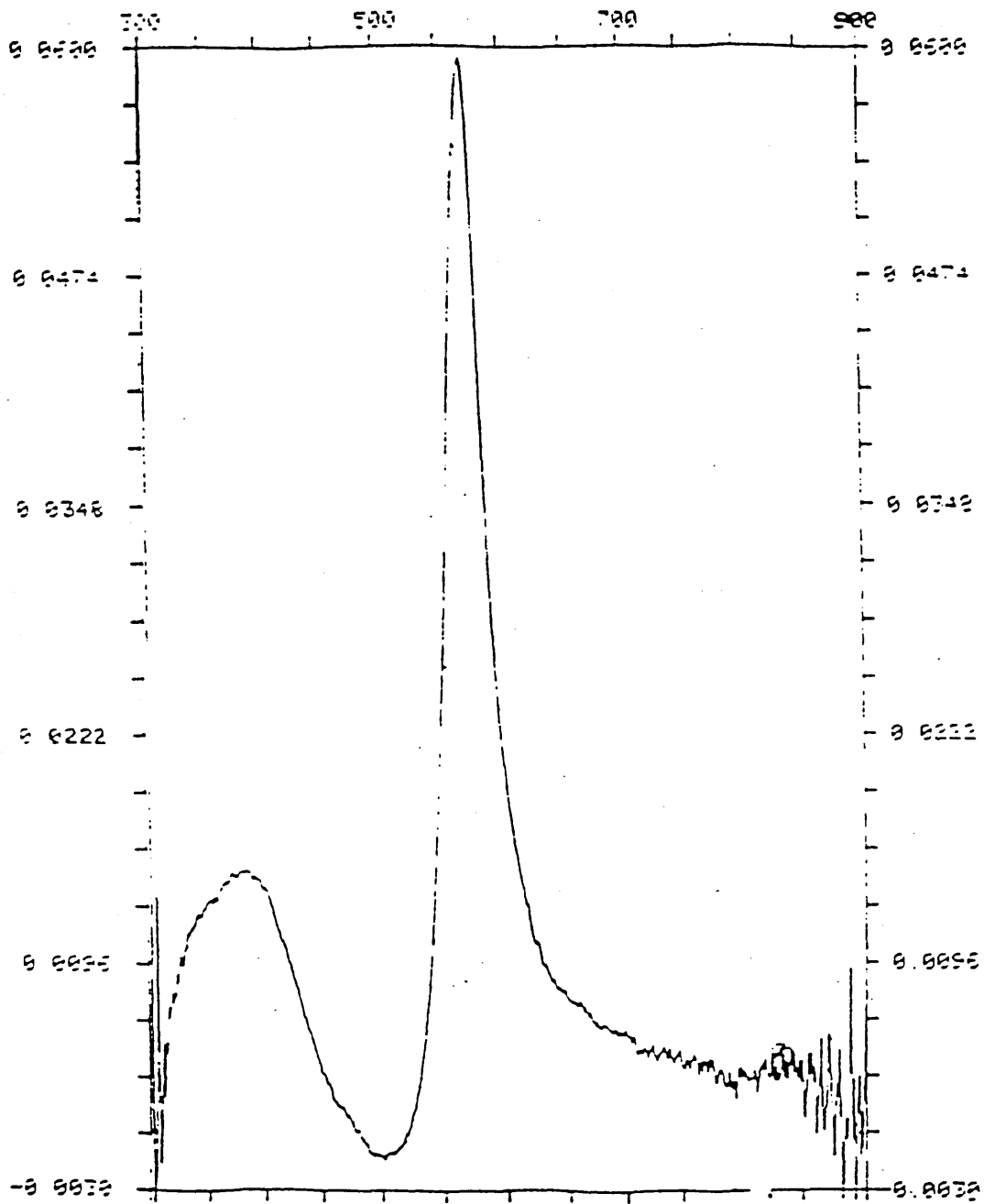


Figure 5.26 UV/VIS spectra for a 4-layer LB film of C20(4)Q3CNQ

R(No. of carbon atoms)	$\lambda_{\text{max}}$ (nm)
C8	616
C9	617
C10	616
C11	616
C12	613
C13	615
C14	615
C15	561
C16	565
C18	565
C20	568

Table 5.4 Variation in  $\lambda_{\text{max}}$  for LB films of R(4)Q3CNQ adducts

Using a 100 KeV microscope the film morphology and corresponding diffraction patterns were observed. These are shown in figures 5.27 to 5.29. This data is for an 8-layer film of C16(4)Q3CNQ. The diffraction patterns are very encouraging, showing, as they do, excellent structural order. Such hexagonal patterns are characteristic of the head-to-head, tail-to-tail, etc structure proposed on the basis of the observed predominantly Y-type deposition. There is also a certain degree of "twinning" of the diffraction pattern. This would appear to suggest that there is a separate orientational regime for the "head" as opposed to the "tail" - this is expanded in the next section in which a more detailed description of the film structure is proposed and described. Examination of the X-ray spectrum of each area studied (Figs 5.30 and 5.31) showed that there was no contamination beyond that which would be expected from the preparative technique used to observe the films. Whilst further study is certainly needed in this area, these results do appear to confirm that the materials can be fabricated as LB films of some structural integrity, and suggest that the films can be prepared with some degree of confidence.

#### 5.4 General Discussion

A detailed study of Langmuir (ie those films on the water surface) and Langmuir-Blodgett films of Zwitterionic adducts of TCNQ - general formula R(4)Q3CNQ, where R is an alkyl chain of 8 carbon atoms or greater - has been carried out. The study concentrated on quinolinium adducts rather than picolinium adducts because it was felt that the extra aromatic ring of the quinolinium part of the 'head' group would enable shorter chain adducts to be fabricated as LB films. The ability to fabricate LB films of anthracene with hydrophobic 'tail' groups as short as 4 carbon atoms was first shown by workers at Durham University and ICI in the late 1970's and was discussed in Chapter 3. The structural formula of anthracene is that of 3 fused benzene rings, and this factor was proposed as being the reason why shorter

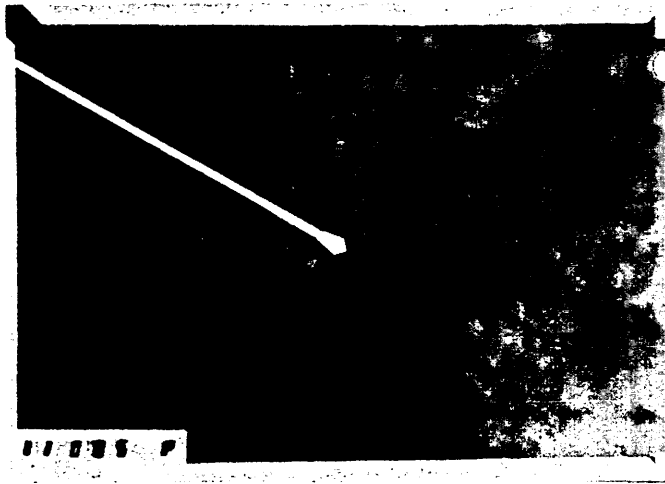


Fig 5.27 : Film Morphology of an 8-layer  
LB film of C16(4)Q3CNQ

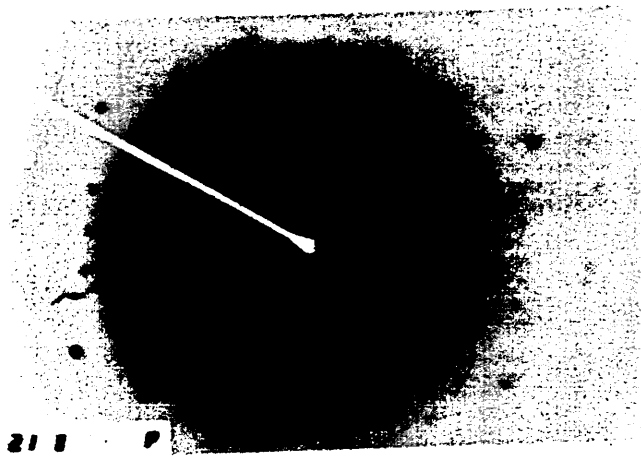
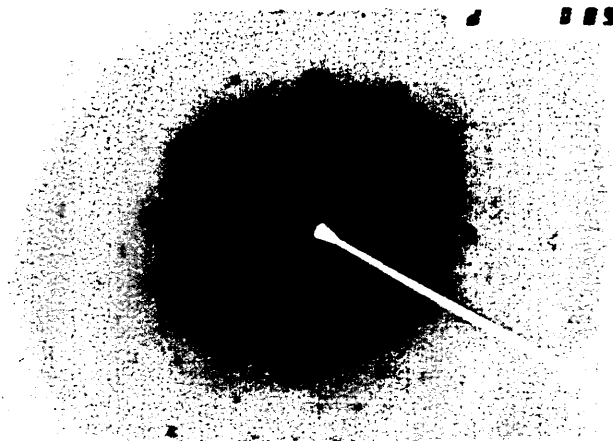


Fig 5.28 : Diffraction Patterns of an 8-layer  
LB film of C16(4)Q3CNQ

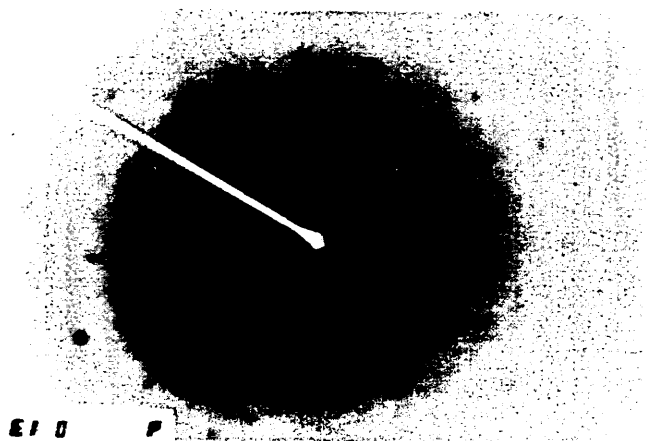


Fig 5.29 : Diffraction Pattern of an 8-layer  
LB film of C16(4)Q3CNQ

27 CNT

1K FS: A

10200 EV

20 EV/CHAN

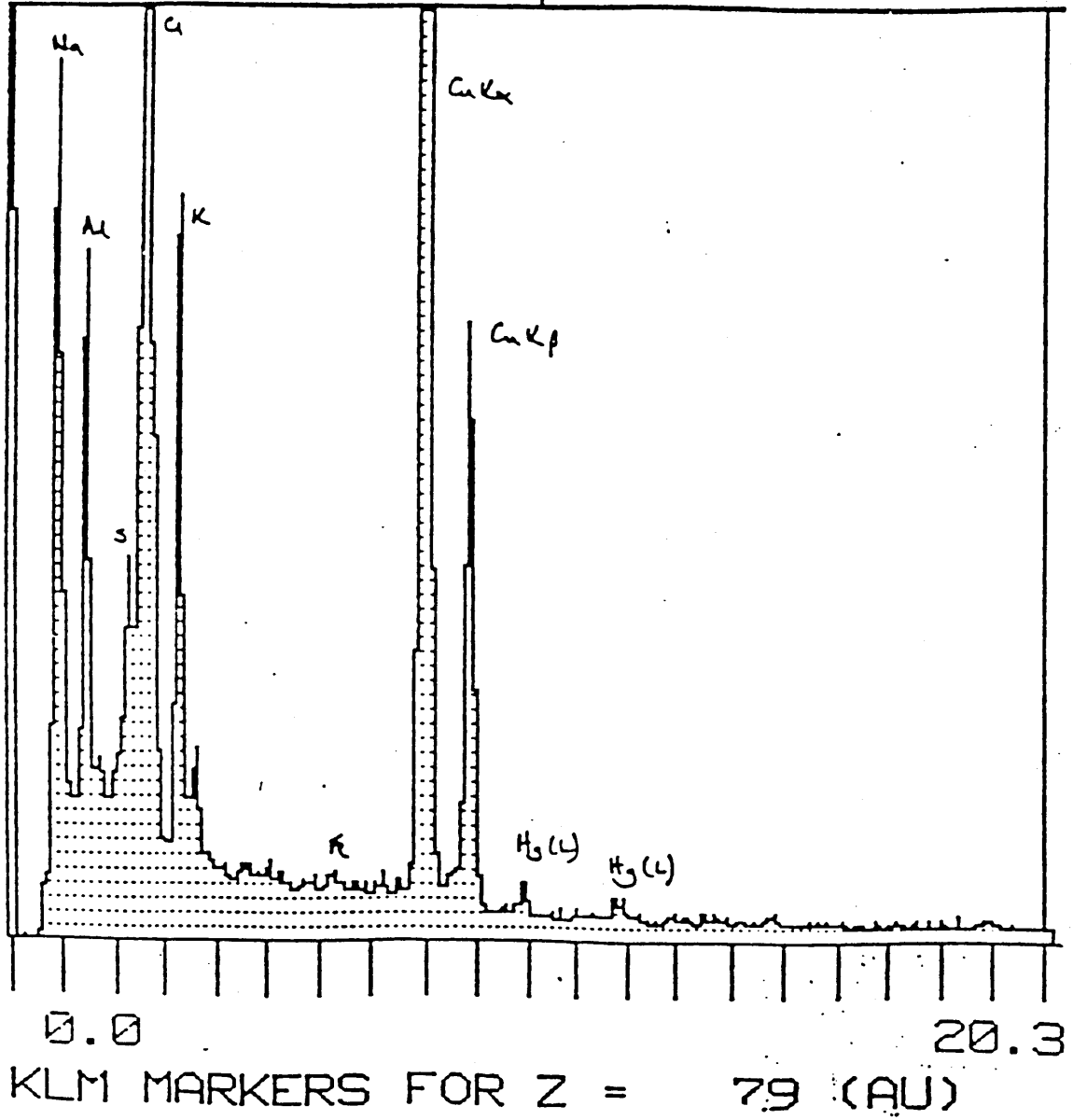


Figure 5.30 X-ray spectra of films of C16(4)Q3CNQ showing no contamination beyond which would be expected

26 CNT

1K FS: A

10200 EV

20 EV/CHAN

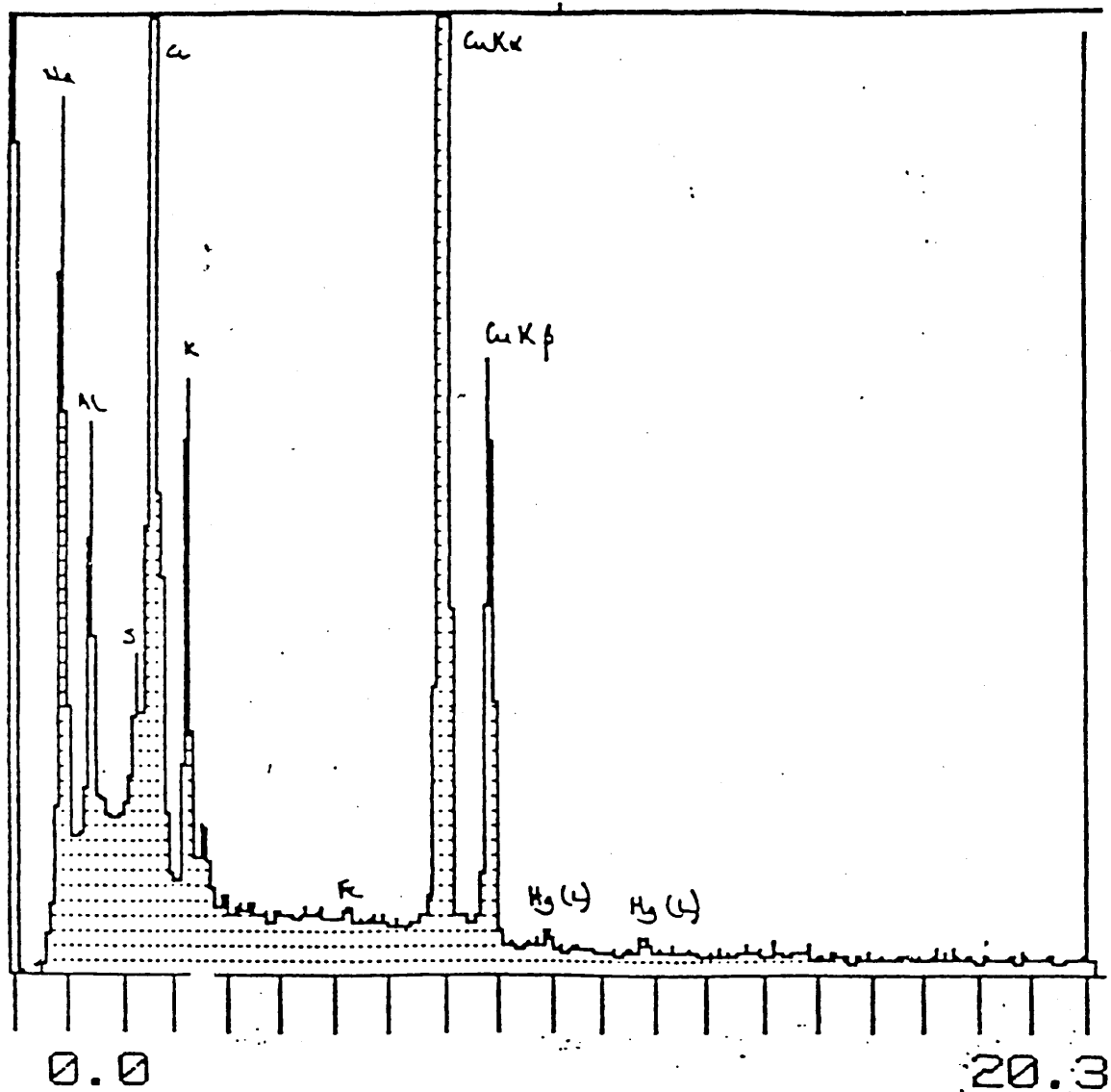


Figure 5.31 Further X-ray spectra of C16(4)Q3CNQ LB films

hydrophobic tails than those commonly used could be incorporated.

Before discussing in detail mechanisms that may be occurring in the films as the alkyl chain length is increased, a summary of the results obtained is given.

- (i) For alkyl chains < 15 carbon atoms, the area per molecule of R(4)Q3CNQ adducts on the water surface is  $32 \pm 2 \text{ \AA}^2$ .
- (ii) For alkyl chains > 15 carbon atoms, the area per molecule of R(4)Q3CNQ adducts is  $44 \pm 4 \text{ \AA}^2$ .
- (iii) For alkyl chains < 15 carbon atoms, the resultant LB films are green, with  $613 \pm 3 \text{ nm}$ .
- (iv) For alkyl chains > 15 carbon atoms, the resultant LB films are purple with  $565 \pm 4 \text{ nm}$ .

In addition, the shorter chain adducts show a relatively broader transition (HWHM =  $37 \pm 2 \text{ nm}$ ) compared to the longer chain adducts HWHM =  $22 \pm 1 \text{ nm}$ , in this case).

Clearly, on the basis of the differing area per molecule values, it can be postulated that a change in molecular orientation or alignment occurs on the water subphase, once the alkyl chain length is > 15 carbon atoms.

Fig 5.32 shows the possible ways in which the limiting areas of these materials may alter on compression. Fig 5.32(a) and 5.32(b) show that the limiting cross-sectional area 'A' can be reduced or increased by reducing or increasing the degree of overlap between the chromophores. Fig 5.32(c) shows an alternative where the

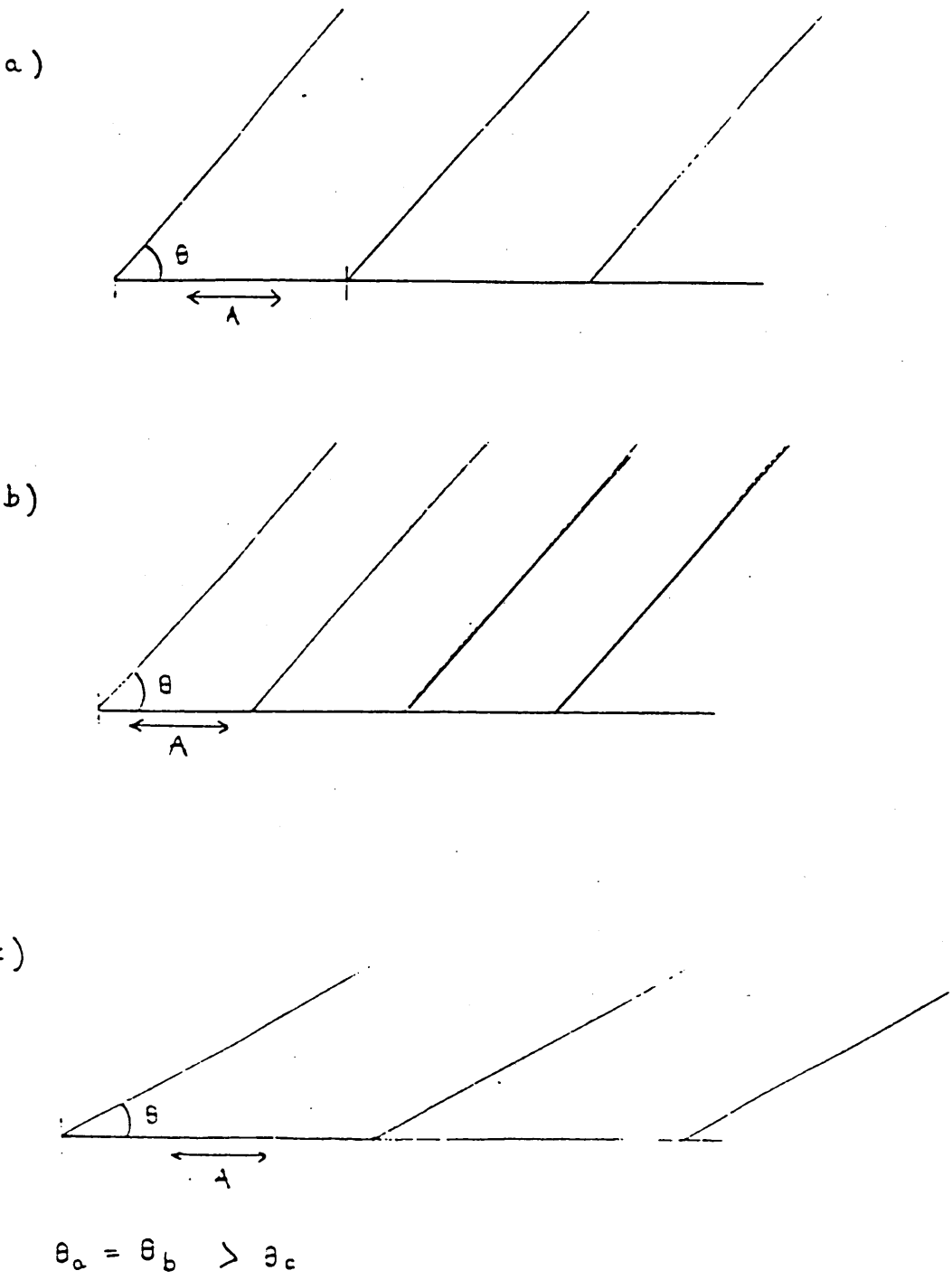


Figure 5.32 Representation of the ways in which the area per molecule, 'A', can change

angle of tilt of the chromophore,  $\theta$ , is reduced, though the degree of overlap remains the same.

Examination of figures 5.32 and 5.33 shows that perhaps the most reasonable explanation is that there is a decrease in the value of  $\theta$  so that this leads to a more favourable electrostatic orientation. Implicit in this model is the requirement that the cationic portion of the chromophore lies directly above the anionic portion of the adjacent molecule. This assumption is made purely on the basis of the fact that it is in this orientation that repulsive electrostatic interactions are minimised.

It is obvious from the values of the area per molecule that the chromophore is tilted. The face area is about  $144\text{\AA}^2$  and the area of the terminal  $-\text{C}(\text{CN})_2$  "butterfly" is about  $24\text{\AA}^2$ . As the measured values of the area per molecule lies between these two extreme positions, then the chromophore must be tilted to some degree. The value of  $\theta$ , and thus the orientation of the chromophore, can be calculated as shown below.

The tilt angle in question,  $\theta$ , is the angle between the plane of the subphase and the long axis of the chromophore. Assuming that the molecules are orientated as shown in figure 5.34, with  $\theta$  in this case purely arbitrary, the parameters needed to calculate  $\theta$  are:

- a) the length (long axis) of the chromophore;
- b) the width of the chromophore on its widest part;
- c) the face area of the chromophore.

Therefore, from fig 5.34, the length of the chromophore is 'm', the width at its widest part is 'n' which can be calculated knowing 'm' and the face area. If the area per molecule (A) is known, then 'l' can be calculated as  $l = \frac{A}{n}$ . Then the

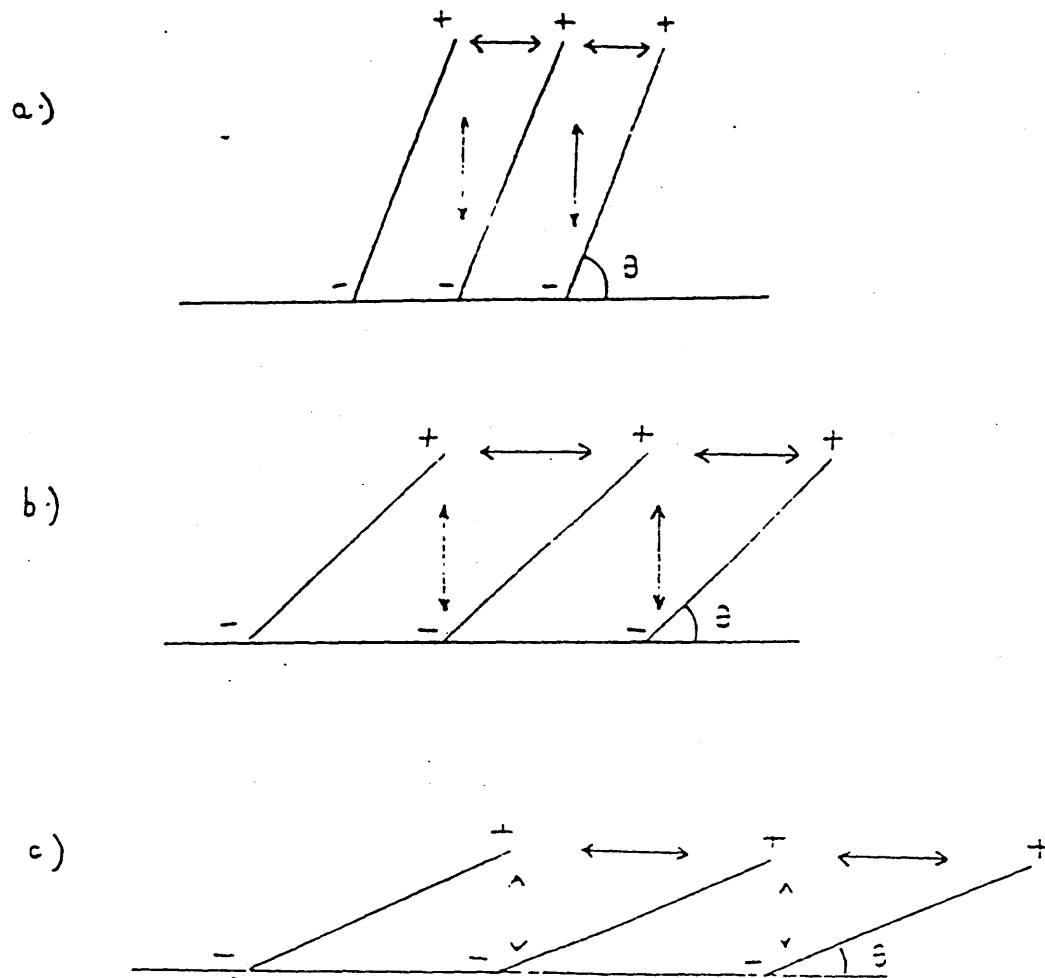


**Figure 5.33** Electrostatic interactions on altering the tilt angle  $\theta$

ie: as  $\theta$  decreases, so attractive forces increase and repulsive forces decrease

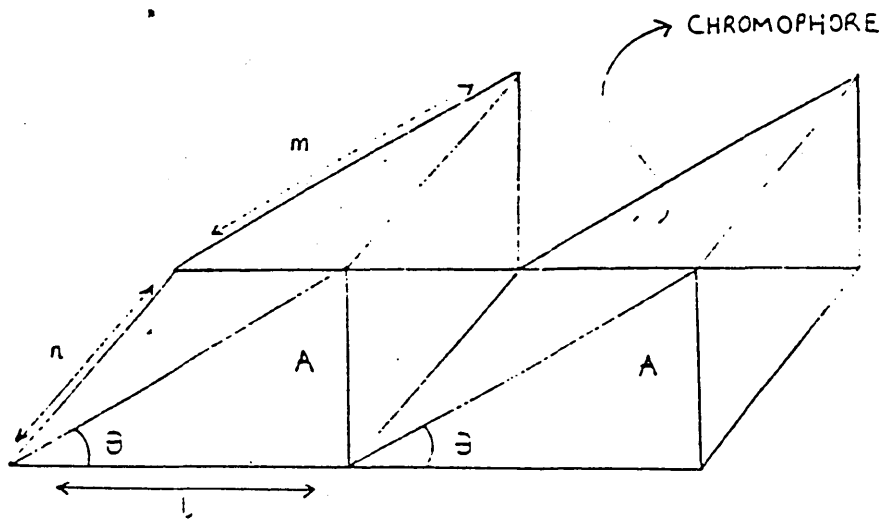


Figure 5.34 Schematic diagram showing the parameters needed to calculate  $\theta$

value of  $\theta$  is found as  $\cos \theta = 1/m$ . For the range of adducts studied, the values of  $\theta$  are shown in table 5.5.

The cross-sectional area occupied by a long hydrocarbon chain is about  $19\text{\AA}^2$ . For conformational circumstances it is preferable that the long chains align themselves vertically and parallel as at the orientation the "zig-zag" chains interlock exactly. For area per molecule values greater than  $19\text{\AA}^2$  then the chains will tilt to try and adopt the preferred orientation. Using the model shown in figure 5.35, knowing the area per molecule of both the chains and the chromophore, the tilt angle of the chains,  $\phi$ , can be calculated. The values are shown in table 5.6.

R (no. of carbon atoms)	$\theta$ °
C8	73
C9	75
C10	72
C11	75
C12	75
C13	74
C14	74
C15	69
C16	67
C18	68
C20	65

**Table 5.5** The variation in the tilt of the R(4)Q3CNQ chromophore with change in hydrophobic chain length

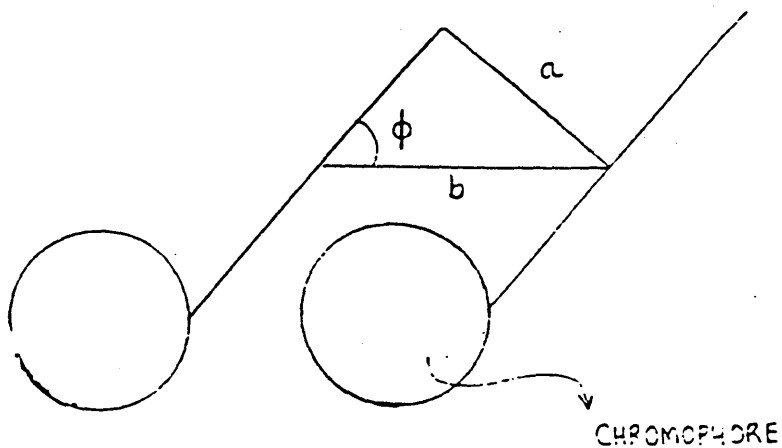


Figure 5.35 Schematic diagram showing the parameters needed to calculate  $\phi$

- 'a' = area occupied by closely packed alkyl chains
- 'b' = area per molecule on water subphase
- $\phi$  = resultant tilt angle of the alkyl chains

R (no. of carbon atoms)	$\phi$ °
c8	36
c9	39
c10	34
c11	39
c12	39
c13	38
c14	38
<hr style="border-top: 1px dashed black;"/>	
c15	28
c16	25
c18	27
c20	23

**Table 5.6** The variation in the tilt of the hydrocarbon chains as the chain length increases for R(4)Q3CNQ adducts

Electrostatic interactions have been postulated a number of times<sup>5</sup> as the main (or at least one) factor governing the orientation of zwitterionic amphipathic molecules at the air-water interface. It is known that an array of parallel dipoles orientated perpendicular to the water subphase would induce a repulsive interaction. The alternative attractive interactions would occur when the molecular dipoles are aligned parallel. The sign and magnitude of any resultant interaction is governed by the relative orientation of the molecule.

Thus, as a first approximation, it is reasonable to assume that the molecules are orientated as shown in the model, thus minimising repulsive electrostatic interactions. The validity of this approximation could be checked by modelling the monolayer by using energy minimisation techniques.<sup>6</sup> The effects of these electrostatic interactions and other dispersion interactions within the molecule could then be studied for the range of adducts of increasing alkyl chain length. Other techniques could also be used to probe the changes occurring in the subphase surface. For example, grazing - angle fluorescence spectroscopy<sup>7</sup> could give information on the molecular orientation at the air-water interface, or indeed any aggregation of the molecules that may or may not be present. It is very likely that should aggregation be occurring, then changes in the area per molecule would be observed. Thus, an alternative explanation to the observed phenomena involves the preferential organisation of the molecules into dimers/trimers/tetramers, etc. This proposal is expanded on in more detail later in this chapter.

What is clearly very interesting in this study is the observed change in film behaviour that occurs as the alkyl chain length is increased. It is also noted that this change is abrupt and therefore cannot be put down to gradual orientational changes due to subtle hydrophobic/hydrophilic interactions. Very little work in this field systematically looks at altering the alkyl chain length for a common head group, and observing the effect that this has on film formation - both on the water subphase and

solid supports. Data of this type was carried out on fatty acid derivatives early in the century and is documented in the classic text by Adam<sup>4</sup>. It appears not to be done to any great extent these days though this work appears to show that there is much use in carrying out such studies whenever a new molecule is investigated. Such information can then be used to decide on the optimum conditions for films formation. Notice that in doing this, we are including molecular geometry as well as more generally acknowledged factors such as compression rates, pH, etc in our analysis.

To recap therefore, for  $C < 15$ , the area per molecule values are smaller than for  $C > 15$ . This is certainly a true phenomenon as can be seen by the  $\lambda_{\text{max}}$  (nm) values of the resultant LB films shown previously at table 5.2. There is a clear shift in the characteristic absorption bands.

Notice also that the absorption line is broader for short chains than for long.

A number of reasons can be proposed as to why there is also a change in  $\lambda_{\text{max}}$  (nm) of the films with changing alkyl chain length.

The first point that can be made is that the colour of the compressed films on the water subphase is the same as the colour of the resultant LB films. This can be taken as evidence that the structural orientation of the Langmuir films is maintained through to the LB films. If this is the case, then one possible explanation is that the electronic transition changes from, primarily, an intermolecular to an intramolecular charge transfer process, as follows. For shorter chain analogues ( $R < 15$  carbon atoms) then the chromophore is tilted more away from the plane of the subphase; for longer chain analogues, ( $R > 15$  carbon atoms) the chromophore is tilted more towards the subphase plane. This same alignment is then maintained in the LB film. Thus, for short adducts, the intramolecular charge transfer transition moment and the electric field vector are aligned in a more parallel arrangement, and

thus the resulting transition is primarily an intermolecular process. For long chain adducts the converse is the case. Here, the intermolecular charge transfer transition moment and the electric vector are aligned more parallel and hence the resultant transition is primarily an intramolecular process.

The assignment of the transitions in this way is consistent with the work of Akhtar et al<sup>8</sup> (see Chapter 1) who assigned the lower energy transition, ie longer wavelength, to an intermolecular transition in their analysis of the solid state spectra of adducts of this type. Although the energy of the transition in the LB films is considerably shifted from that of the single crystal spectra they studied, this may well be due to preferential alignment in the crystal (ie head-to-tail) not wholly observed in the LB film.

Because the make up of the chromophore is constant throughout the series of adducts studied during this work, then the changes in area per molecule of adducts observed during the study,  $\lambda$  max and shape of the absorption line are probably a function of changing the alkyl chain length. The change in the parameters occurs at an alkyl chain length of fifteen carbon atoms, and it may be significant that the length of a fifteen carbon alkyl chain is the same as the long axis of the TCNQ quinolinium chromophore. Thus, if it is assumed that there is a subtle interplay between electrostatic and amphipathic balances, then for alkyl chains less than 15 carbon atoms the hydrophilic moiety is longer than the hydrophobic moiety and for chains greater than 15 carbon atoms the hydrophilic portion is shorter.

It is also possible that steric factors cause the shifts in area per molecule and corresponding change in spectra, for example, shorter chain analogues (<C15), adopting the orientational characteristics of long chain analogues -  $\theta \approx 65^\circ$  and  $\phi \approx 23^\circ$  - would experience some degree of steric hindrance as shown in figure 5.36.

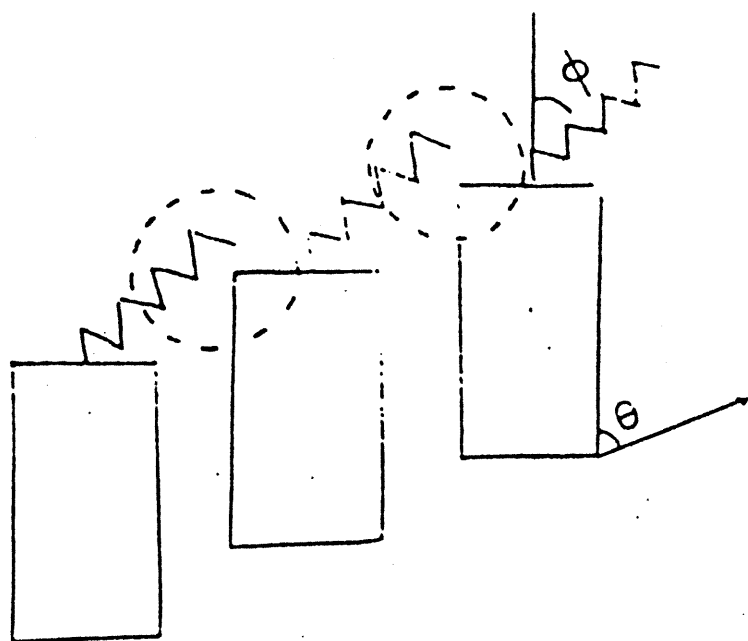


Figure 5.36 Steric interactions between the chromophore and hydrocarbon chains arising from change in tilt angles ' $\theta$ ' and ' $\phi$ '

Thus, because the colour of LB films is the same as the colour of the compressed Langmuir film on the surface, it is proposed that the colour arises because the same molecular orientation is present in both films. Spectroscopic data has already been shown in table 5.4 and for full comparison the collected data in Table 5.7 shows the dramatic change in the phenomena with increasing chain length. Hence the observed change in the values of  $\theta$ ,  $\phi$ ,  $\lambda_{\text{max}}$  (nm) and Area per molecule ( $\text{\AA}^2$ ) in LB and Langmuir films respectively and the shift and change in shape of the absorption band must be a consequence of this observed change in the film structure. Comparison with the solution spectra shows that the predominant band is considerably shifted to shorter wavelength and is much narrower. On the basis of the more random nature of solution compared to the relatively ordered regime of the LB film, it would be expected that the transition would be considerably altered.

However, an alternative explanation to those already proposed, and briefly mentioned earlier is that there is some form of aggregation taking place between molecules. It is very well documented that many classes of dyes exhibit colour changes due to environmental effects<sup>9</sup>. These colour changes and spectral shifts can be split into two categories:

- (a) colour shifts due to isomerism
- (b) colour shifts due to changes in the environment.

Colour shifts due to isomerism usually involve two distinct species each with their own particular absorption wavelength. Colour shifts due to changes in the environment are usually applicable to a single chromophore, and involve steric interactions, solvent induced shifts or the influence of neighbouring molecules-the well documented H-and-aggregation phenomena.<sup>10</sup> If indeed any aggregation is occurring, then the shifts observed in this work are undoubtedly environment induced,

R (no. of carbon atoms)		A.Mol <sup>-1</sup> (Å <sup>2</sup> )	λ max (nm)	
C8	73	32	616	HWHM = 37 ± 2nm
C9	75	30	617	
C10	72	34	616	
C11	75	30	616	
C12	75	30	613	
C13	74	31	615	
C14	74	31	615	
C15	69	40	561	HWHM = 22 ± 1nm
C16	67	44	565	
C18	68	42	565	
C20	65	48	568	

**Table 5.7 Change in parameters with increasing chain length for R(4)Q3CNQ adducts**

and are probably due to the influence of neighbouring molecules. Indeed, the classic documentation of steric factors influencing spectroscopic transitions was a study of quinolinium type dyes.<sup>11</sup> It is unlikely however that steric factors alone are causing the shifts shown in this work - 1,4 - substitution is the least likely substitution to lead to steric hindrance. Certainly it would be expected that long chain substitution in the 1,2 - position would have a greater effect.

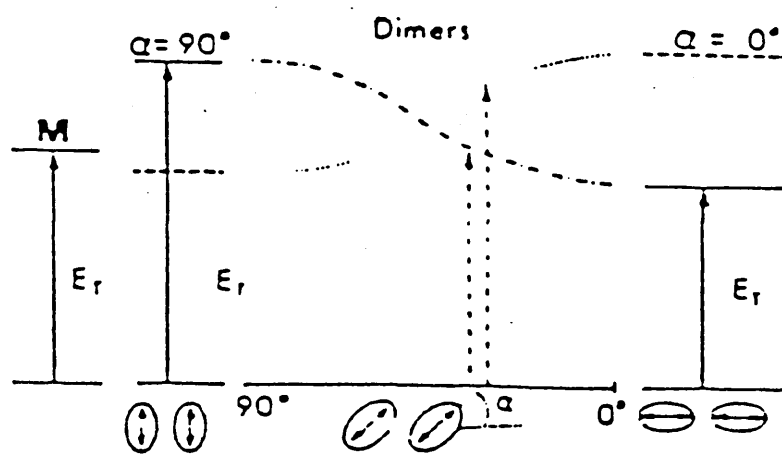
Interactions between neighbouring dye molecules produce spectral shifts and very definite changes in the band shape. The absorption maxima can shift to shorter wavelength (H - aggregation) or to longer wavelength (J -aggregation).

As well as generally being identifiable from the changes in the energy of the charge transfer band, other features are common to H or J aggregates. For example, H aggregates are favoured by an increase in the alkyl chain length<sup>12</sup>. This is interesting when one considers the shifts observed in this work. The longer chain adducts show an abrupt shift to shorter wavelength at  $R > C15$ . It is characteristic of H and J aggregation that the observed shifts occur abruptly. Thus, there is evidence, albeit tentative, from the results obtained here for H aggregation - where longer chains show a shift to shorter wavelength. While generally H aggregated bands are broad<sup>13</sup>, there are examples of very sharp bands of this type<sup>12</sup>.

For dipolar molecules such as the ones studied in this work, the position of allowed electronic transition is a function of the angle  $\alpha$  as shown in figure 5.37.

The angle  $\alpha$  is that between the transition moment - in this case the long axis of the zwitterion - and a line joining the centres of the molecules. Dipole - dipole interactions suggest that the lowest energy transition will be allowed for  $\alpha \rightarrow 0^\circ$  and the higher energy transition for  $\alpha \rightarrow 90^\circ$ . At intermediate angles and less ideal dipole arrangements, more than one transition may occur and the band may be split

Figure 5.37 Allowed electronic transitions as a function of the angle ' $\alpha$ '



- the so called Davydov splitting. It should therefore be expected that the transition is considerably shifted to higher energy (ie shorter wavelength) in the LB film of zwitterionic adducts in view of the calculated values of the tilt angle assuming that the LB films are produced with a certain degree of structure.

This discussion has highlighted possible explanations for the observed changes in film behaviour with increasing chain length. However, further work is needed to fully elucidate the nature of these changes. The possibilities for further work are many, though all would involve more intensive investigation of film structure. For example, low-angle x-ray diffraction would enable accurate determination of the interlayer spacings within the LB film. Such information would enable us to conclude whether or not the tilt angles calculated in this work are accurate. It would also give data on the specific orientation of the molecules - though this can be determined more accurately from the polarised uv-vis or ir-spectra of the molecules. Very simply, as the spectra are determined by interaction of a molecular transition moment with the electric field vector of the incident radiation, then systematic orientation of the LB films, at angles to the incident radiation, can give by analysis of the spectra, accurate determination of the molecular orientation. For example, if the electric field vector and the molecular transition dipole are orthogonal, then no, or very weak, spectral bands will be observed.

Thus, a combination of microscopy, diffraction and spectroscopy could probe the structural changes taking place. Because, such a change in the film structure leads to quite large changes in the resultant uv spectra, then for some potential applications this could be a possible advantage of these materials over others. For example, for photochromic devices, mixed monolayers could be produced between long chain and short chain adducts with the resultant overlap in the uv spectra giving a tunable response compared to simple monolayers of only long or short chains. Similarly, such tunable responses would be useful for any optical second

harmonic generation applications.

There is much scope for the synthesis of derivatives of this one general type of zwitterionic adduct. Long chain adducts of  $\alpha$ -rather than  $\gamma$ -substituted quinoline could be attempted, as could  $\alpha$ - or  $\gamma$ -substituted picoline adducts. There is also scope for fluorination of the alkyl chains as well as using derivatives of TCNQ, eg TCNQF<sub>4</sub>. The extent to which adducts of these types show similar changes in film behaviour over a homologous series could then be studied, as well as any advantages/disadvantages in film stability.

However, to conclude this portion of the discussion therefore, it is postulated that the structure of the films is governed primarily by electrostatic interactions within the head groups. The chromophore is orientated intermediate between an arrangement parallel and perpendicular to the subphase and support. As the hydrophobic nature of the material increases, the molecule undergoes another rearrangement. The hydrophobic chains do not lie perpendicular to the plane of the film, rather they are tilted towards the plane. The tilt angles of the chromophore,  $\theta$ , and the hydrocarbon chain,  $\phi$ , are slightly different which results in a slight herringbone arrangement. The proposed film structure is shown in fig 5.38. The absorption band of this film is shifted considerably to shorter wavelength possibly due to aggregation and the dipole - dipole interactions resulting between neighbours, or a change from an inter- to an intra-molecular charge transfer. These tentative explanations are worthy of further work in this area.

## 5.5 Change in Film structure and absorbance bands with time

The area per molecule values quoted are obtained when the film is deposited and compressed immediately. In this case, "immediately" implies as soon as the usual period of time has elapsed between deposition of material onto the subphase and

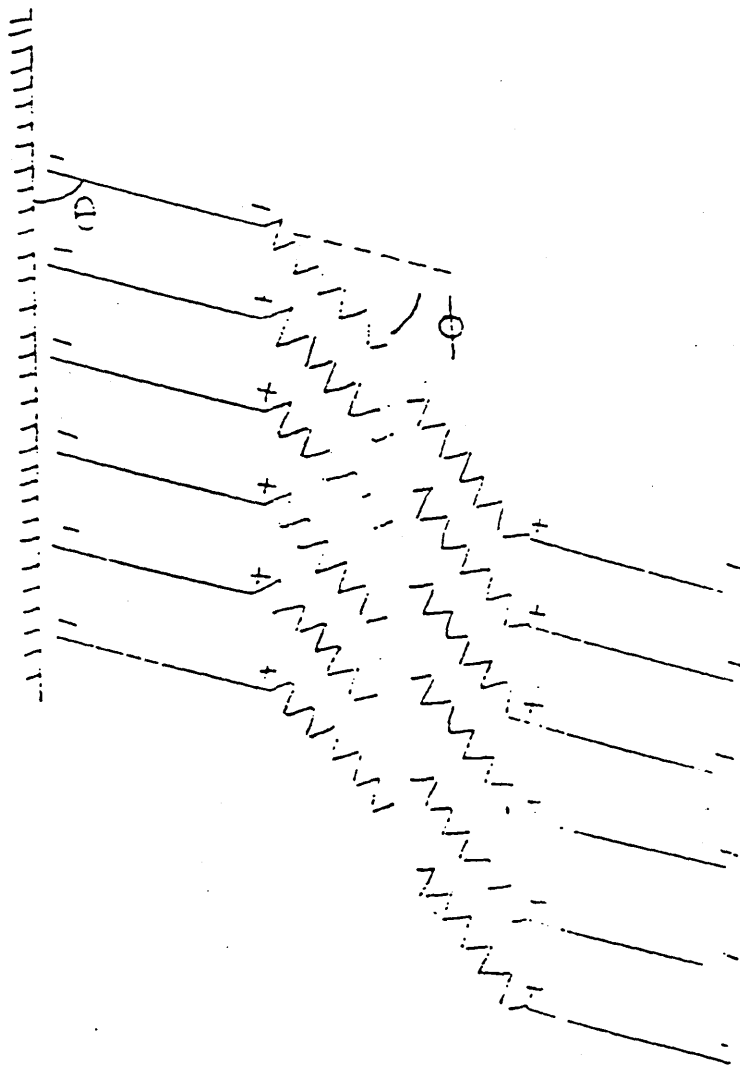


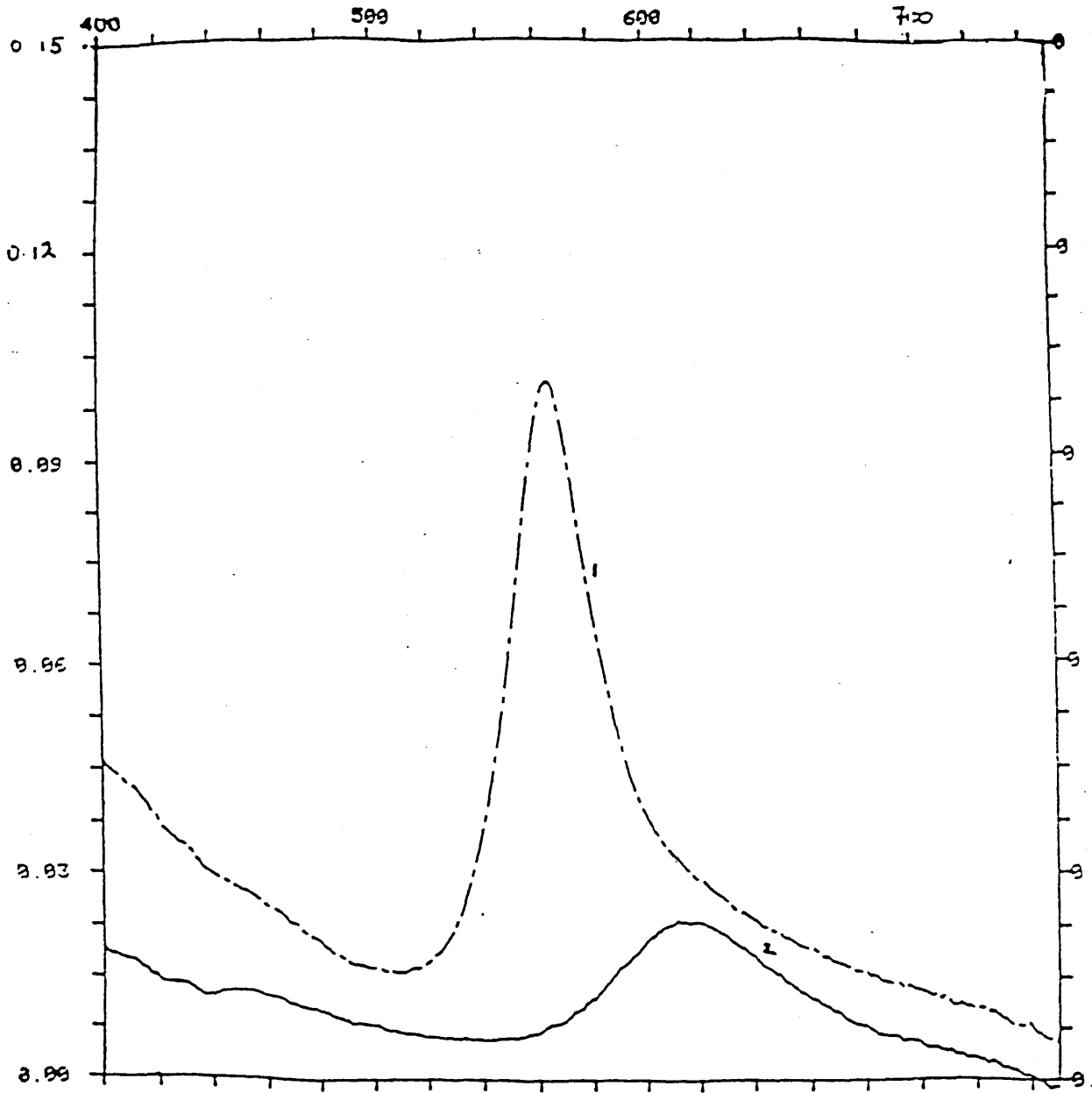
**Figure 5.38** Proposed structure of the fabricated LB film of long chain analogues of the zwitterion R(4)Q3CNQ - particular tilt angles applicable to C11(4)Q3CNQ

then allowing time for the material to evaporate. If, however, the film is deposited and then left for increasing periods of time, then the area per molecule can increase dramatically. This is shown for various adducts in table 5.8. The resultant shifts occurring in the spectra of the LB film deposited after these time periods is shown in fig 5.39. From the previous discussion, it could be concluded that the molecules are tilted further and further towards the subphase, and preserving this structure within the LB film as a consequence. Thus, the tilt angle  $\Theta$  decreases to a value of  $\sim 28^\circ$  with a corresponding decrease in the tilt of the hydrocarbon chains. Such a tilt angle ( $\alpha \rightarrow 0$ ), from the previous argument) would be expected to lead to shifts to longer wavelengths.

However, it is known that these materials are photochromic and a one other plausible explanation is that the gross reorientation that appears to be occurring at the subphase is due to a photochromic reaction causing gross molecular rearrangement within the chromophore. Alternatively, further aggregation of the H- or J-types in films is occurring - it is clear that further work is needed in this area also.

Figure 5.39 Change in UV/VIS spectra with time for C16(4)Q3CNQ

- 1 Compressed immediately
- 2 Compressed after 2½ hours



ADDUCT	AREA PER MOLECULE <sup>-1</sup> (Å <sup>2</sup> )
C11 (4) Q3CNQ Immediate 2½ hours	  26 45
C15 (4) Q3CNQ Immediate 2½ hours	  40 62

**Table 5.8 Change in Area Per Molecule  
with time for C11 (4) Q3CNQ and C15 (4) Q3CNQ**

## 5.6 REFERENCES

- 1 G L Gaines, "Insoluble Monolayers at Liquid - Gas Interfaces", New York, Interscience, (1966)
- 2 H P Zingsheim, Scanning Electron Microsc., 1, 357, (1977)
- 3 See for example, R A Hann, S K Gupta, J R Fryer and B L Evers, Thin Solid Films, 134, 35, (1985)
- 4 N K Adam, "The Physics and Chemistry of Surfaces", Oxford University Press
- 5 P J Bowen and T J Lewis, Thin Solid Films, 99, 157, (1983)  
D A Cadenhead, R J Demchak and M C Phillips, Kolloid-ZZ-für Polymere, 220, 63, (1967)
- 6 A Ulman, S D Evans and R G Snyder, Thin Solid Films, 210, 806, (1992)
- 7 R Linton, V Guarisco, J J Lee, B Hagenhoff and A Benninghoven, Thin Solid Films, 210, 565, (1992)
- 8 S Akhtar, J Tanaka, R M Metzger and G J Ashwell, Mol Cryst Liq Cryst, 139, 353, (1986)
- 9 The Theory of the Photographic Process (4 ed), Ed T H James, Macmillan Publishing, New York, (1977)
- 10 H Bucher and H Kuhn, Chem Phys Lett, 6, 183, (1970)
- 11 L G S Brooker, F L White, R H Sprague, S G Dent Jnr and G Van Zandt, Chem Rev, 41, 325, (1947)
- 12 A H Herz, Photograph Sci Eng, 18, 323, (1974)
- 13 W West, S P Lovell and W Cooper, Photograph Sci Eng, 14, 52, (1970)

## ACKNOWLEDGEMENTS

I would like to express my warmest thanks to Dr Norman Bell of the Department of Applied Chemistry and Professor John Brooks of the Materials Research Institute, Sheffield Hallam University, for all their support and encouragement throughout this work. I also thank all the staff in the Environment Sensing Systems Section of the Health and Safety Executive's Research Laboratories in Sheffield - in particular Dr Stephen Thorpe without whose support much of this work would have been impossible.

Thanks are also due to Dr Marek Szeblewski for many valuable discussions and loan of materials, and also Dr Ian Sandy for providing me with the materials used in the early part of the work. I would also like to thank Dr Tom Maclean of ICI and Drs Graham Cross, Ian Girling and Ian Peterson, late of the long range research group at the GEC Hirst Laboratories, for advice in establishing the Langmuir-Blodgett film laboratory and allowing me to spend time at their laboratories. For helpful discussions on interfacial phenomena I would like to thank Dr Malcolm Macdonald and, for help in the interpretation of the mass spectra, Dr John Little, both of Sheffield Hallam University.

I would also like to thank all the technical staff at Sheffield Hallam University and the other postgraduate students from both the Department of Chemistry and Applied Physics; Mrs Suzanne Wragg for typing the work; my family for putting up with someone who refused to foresake the life of a student until the age of twenty-five, and Curtise Monk for her support.

Finally, I would like to pay tribute to the late Dr Alwyn Jones of the Health and Safety Executive, Sheffield, who shared in the supervision of this work, and whose unerring support through the often frustrating times of developing the Langmuir-Blodgett laboratory was invaluable. As well as being a much respected scientist, he was a man of great warmth, and those who had known and worked with him would, I think, say it was a pleasure that they had done so.